Validation of Travel- and Exposure-Time Based Nonlinear Reactive Transport Models

Dissertation

der Mathematisch-Naturwissenschaftlichen Fakultät

der Eberhard Karls Universität Tübingen

zur Erlangung des Grades eines

Doktors der Naturwissenchaften

(Dr. rer. nat.)

vorgelegt von

MSc. Alicia Sanz Prat

aus Zaragoza

Tübingen

2016

Gedruckt mit Genehmigung der Mathematisch-Naturwissenschaftlichen Fakultät der Eberhard Karls Univesität Tübingen.

Tag der mündlichen Qualifikation:
Dekan: Prof. Dr. Wolfgang Rosenstiel
1. Berichterstatter: Prof. Dr.-Ing. Olaf A. Cirpka
2. Berichterstatter: Prof. David Blowes
3. Berichterstatter: Dr. Chuanhe Lu

Acknowledgments

This dissertation is the result of the collaboration between several individuals, whose contribution, guidance and support during the last years made possible the completion of this work.

Firstly, I would like to thank my supervisor Prof. Dr.-Ing. Olaf Cirpka the opportunity to become PhD candidate in the Hydrogeology Work Group in the Eberhard Karls University of Tübingen. His scientific inspiration, ideas and fruitful discussions are manifested in this dissertation. I am very grateful for everything I learned from Dr. Chuanhe Lu, whose dedication, sound scientific criteria and great willingness to seek solutions improved and facilitate my research work. I am also grateful for having worked with Dr. Michael Finkel for his good advice and relevant comments. The Research Fellowship gave me the opportunity to meet and work with Dr. David Blowes (University of Waterloo) and Dr. Richard Amos (Carleton University). I want to special thank both for their support and wise advice during the months that I spent in Canada.

I should like to mention to several kind researchers that I had the chance to meet during these years: Dr. R.G. McLaren (University of Waterloo) and Dr. René Therrien (Université Laval), who took the time to increase my understanding on the reactive transport simulations in HydroGeoSphere; Dr. Tim Ginn (Washington State University), whose enthusiasm for travel and exposure time models and willingness to teach led to fruitful conversations and inspiring suggestions; Dr. Ulrich Maier (Georg-August-Universität Göttingen), Dr.-Ing. Nico Trauth (Helmholtz-Zentrum für Umweltforschung) and our conversations regarding reactive transport modelling.

The collages of the Hydrogeology Group and the International Research Training Group are also responsible of the enjoyable work environment built by means of multiple travels, dinners and coffee-breaks.

Special thanks for my family and close friends that encouraged me to enjoy and take profit of this adventure. In particular to my parents, Francisco Sanz and Gloria Prat for their unconditional love and support, as well as for being an example of self-commitment and integrity; to my brother Javier, for being the best fellow and an example of enthusiastic and hard worker. To Yolanda, Álvaro and Oscar for the countless joyful moments we spent together, or via videoconference.

This research work was possible by the funds of the German Research Foundation (Deutsche Forschungsgemeinschaft, DFG) granted to the International Research Training Group of the "Integrated Hydrosystem Modelling".

Abstract

Groundwater resources are very important to guarantee sufficient fresh water supply worldwide. To ensure its quality, which is often endangered by natural and anthropogenic hazards, existing risks and possible protection measures need to be adequately evaluated. Mathematical models describing the transport of reactive solutes in groundwater are the key tool for this evaluation. The models help to understand the complex system of coupled physical and biogeochemical processes in the subsurface at different time and spatial scales. The parameterization and operation of such models may raise difficulties as subsurface properties are typically uncertain and computational costs for three-dimensional simulations might be immense. The travel-time based models simplify the description of reactive transport by replacing the spatial coordinates with the groundwater travel time, posing a quasi-one-dimensional (1-D) problem and potentially rendering the determination of multidimensional parameter fields unnecessary. This alternative approach is based on the assumption that the location of stationary reactive fronts i.e. concentration profiles correspond to certain groundwater isochrones which can be truth for ideal conditions that avoid solute and groundwater mixing processes: stationary flow, constant and uniform penetration of the groundwater and dissolved reactant across the entire inlet boundary, and uniform spatial distribution of the biogeochemical parameters within the domain. Travel time is defined as the time that a particle spent to achieve an observation point from the inlet boundary and it is numerically measurable through the seepage velocity field and conservative transport simulation. The stochastic behaviour of the flow field and the diffusive-dispersive transport mechanisms confer random properties to the travel time, which are expressed by local travel time probability density functions, $pdf(\tau)$, at each location. The corresponding mean travel time are commonly used as the independent variable in travel-time based models. The main hypothesis of this thesis is that the chemical-compound concentrations as function of time and travel time at each location can be a good approximation to the spatially-explicit concentrations, even when non-ideal conditions may affect the reactive behaviour. To test the validity of this hypothesis, several representative test cases are considered in this work. These test cases are inspired by real-world observations of surface water-groundwater interactions in the hyporheic zone, where dissolved organic carbon, oxygen and nitrate infiltrate into the groundwater and trigger aerobic and anaerobic degradation of organic matter by aerobic and denitrifying bacteria. In a first study, six scenarios are analysed which are differing in the variance of log-hydraulic aquifer conductivity and in the inflow boundary conditions. The results show that the conceptualization of nonlinear bioreactive transport in complex multidimensional domains by quasi 1-D travel-time models is valid for steady-state flow fields if the reactants are introduced over a wide cross-section, and dispersive mixing is adequately parameterized. Results from a second series of test cases focussing on transient time-periodic flow show that a modified version of travel-time based reactive transport models is valid if only the magnitude of the velocity fluctuates, whereas its spatial orientation remains constant. Finally, in a third study, the model is used to simulate reactive transport in geochemical and geophysical heterogeneous porous media, which request the use of the exposure time, equivalent to the time of reaction between two or more reactants, instead of travel time. The results show that the exposure-time models are able to provide good approximation of nonlinear reactive transport problems when transverse mixing is not the controlling process of the reactive system.

Kurzfassung

Grundwasser ist eine bedeutende Frischwasser-Ressource weltweit. Um seine Qualität, die durch natürliche und anthropogene Gefahren vielerorts gefährdet ist, sicherzustellen, müssen die bestehenden Risiken und mögliche Schutzmaßnahmen angemessen bewertet werden. Ein wichtiges Instrument für diese Bewertung sind mathematische Modelle, mit welchen der Transport von reaktiven gelösten Stoffen im Grundwasser beschrieben werden kann. Die Modelle helfen, das komplexe System von gekoppelten physikalischen und biogeochemischen Prozessen im Untergrund in unterschiedlichen zeitlichen und räumlichen Skalen zu verstehen. Die Parametrisierung und Anwendung solcher Modelle ist mitunter schwierig, weil die Untergrundeigenschaften nicht vollständig bekannt sind und Rechenzeiten für dreidimensionale Simulationen immens sein können. Verweilzeit-basierte Modelle vereinfachen die Beschreibung des reaktiven Stofftransports, indem die Raumkoordinaten durch die Verweilzeit des Grundwassers ersetzt werden. Dadurch ergibt sich ein quasi-eindimensionales (1-D) Problem, das fallweise auch ohne die Bestimmung multidimensionaler Parameterfelder gelöst werden kann. Dieser alternative Ansatz beruht auf der Annahme, dass sich stationäre Reaktionsfronten, d.h. Konzentrationsprofile entlang bestimmter Isochronen der Grundwasserfließzeit ausbilden. Dies gilt unter idealisierten Bedingungen, d.h. wenn Mischungsprozesse des Grundwassers und darin gelöster Stoffe vernachlässigbar sind, die Grundwasserströmung stationär ist, der Stoffeintrag konstant und uniform ist, und die biogeochemischen Parameter innerhalb des Modellraums räumlich konstant sind. Die Verweilzeit ist definiert als die Zeit, die ein Wasserpartikel benötigt, um von seinem Eintragspunkt am Modellrand den jeweiligen Beobachtungspunkt im Modellraum zu erreichen. Sie kann mit Hilfe des Geschwindigkeitsfelds und einer konservativen Transportsimulation numerisch leicht bestimmt werden. Aufgrund des stochastischen Verhaltens des Strömungsfeldes und diffusiv-dispersiver Transportprozesse ist die Verweilzeit als Zufallsvariable aufzufassen, die durch lokale Wahrscheinlichkeitsdichtefunktionen der Verweilzeit, pdf(τ) beschrieben werden kann. Die aus diesen Funktionen abgeleitete mittlere Verweilzeit wird in den Verweilzeit-basierten Modellen allgemein als unabhängige Variable verwendet. Die Haupthypothese dieser Arbeit ist, dass die als Funktion von Zeit und Verweilzeit bestimmte Konzentration chemischer Verbindungen an jedem Punkt des Modellraums eine gute Näherung für die explizit räumliche Konzentration ist - auch dann, wenn nicht-ideale Bedingungen herrschen und das reaktive Verhalten der Verbindungen beeinflussen. Um die Gültigkeit dieser Hypothese zu testen, werden verschiedene repräsentative Fallbeispiele betrachtet. Diese Fallbeispiele basieren auf realen Beobachtungen von Oberflächenwasser-Grundwasser-Interaktionen in der sogenannten hyporheischen Zone, wo gelöster organischer Kohlenstoff, Sauerstoff und Nitrat in das Grundwasser infiltrieren und den aeroben und anaeroben Abbau organischer Substanzen durch aerobe und denitrifizierende Bakterien anregen. In einer ersten Studie werden in sechs Szenarien unterschiedliche Annahmen bezgl. der Varianz der hydraulischen und der Randbedingungen analysiert. Die Ergebnisse zeigen, dass die Konzeptualisierung des nichtlinearen bioreaktiven Transports in komplexen multidimensionalen Modellräumen durch quasi 1-D Verweilzeitmodelle gültig ist bei stationärer Strömung, wenn die reaktiven Verbindungen über einen breiten Querschnitt eingeführt werden, und dispersive Mischungsprozesse angemessen parametrisiert werden. Die Ergebnisse eines zweiten Fallbeispiels für periodisch wechselnde Strömungsverhältnisse zeigen, dass der reaktive Stofftransport mit einem modifizierten Verweilzeit-basierten Modell korrekt beschrieben werden kann, wenn nur die Höhe jedoch nicht die Richtung der Grundwasserströmungs

geschwindigkeit schwankt. In einer dritten Studie wurde zur Simulation des reaktiven Stofftransports in geochemisch und geophysikalisch heterogenen porösen Medien ein Expositionszeit-basiertes Modell eingesetzt. Die Expositionszeit berücksichtigt die für die Reaktion zwischen zwei oder mehreren an der Reaktion beteiligten Stoffen zur Verfügung stehende Zeit und ersetzt die Verweilzeit. Die Ergebnisse dieser dritten Studie zeigen, dass es mit Expositionszeit-basierten Modellen möglich ist, nichtlineare reaktive Transportprobleme in guter Näherung zu beschreiben, solange die transversale Mischung nicht der steuernde Prozess des reaktiven Systems ist.

Contents

1. Introduction

1.1. Motivation

Groundwater resources are increasingly intended for water uses that require excellent quality standard. Such important resource is often endangered by natural and anthropogenic hazards. In natural conditions, groundwater may present high toxicity levels due to water-rock interactions in specific geological formations, microbial activity or mixing of water from different sources. Figures 1 and 2 show the problems due to presence of arsenic (Acharyya and Shah, 2007) and fluoride in groundwater (Wang et al., 1999) at regional dimensions. Although main anthropological contaminant activities are originated in the surface (e.g. wastewater discharge into surface waters, mining or landfills), groundwater is not exempt from being affected by pollutants, which could persists given the difficulty to apply efficient treatment methods. In some cases, soil layers act as shield or buffer of pollution alleviating or suppressing negative effects on the aquifers; in other cases, pollution achieves the water table, or it is induced by poor management of wells. These circumstances justify research efforts to increase the understanding of the natural processes in the subsurface systems; however, coupled physical and biogeochemical processes at different time and spatial scales may be involved, and on occasions those are difficult to identify.

Owing to the lack of complete knowledge of the actual chemical interactions and their consequences on the natural systems, an increasing number of investigations on reactive transport processes have been conducted during the last decades. In this regards, noteworthy is the quantification of interactions between environmental compartments tackling multi-scale coupled processes to be solved numerical simulation. Fleckenstein et. al. (2010) noted about the necessity of new reactive transport methods to solve upscaling heterogeneity problems and their influence on biogeochemical processes in alluvial ecosystems. This thesis is focused on the interactions between surface water and subsurface interface.

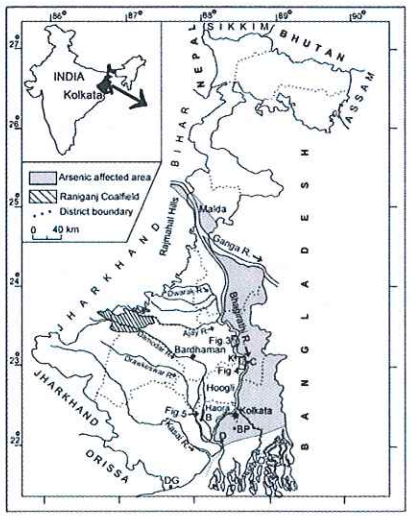

Figure 1. Map showing arsenic-affected area in West Bengal, India (Acharyya and Shah, 2007)

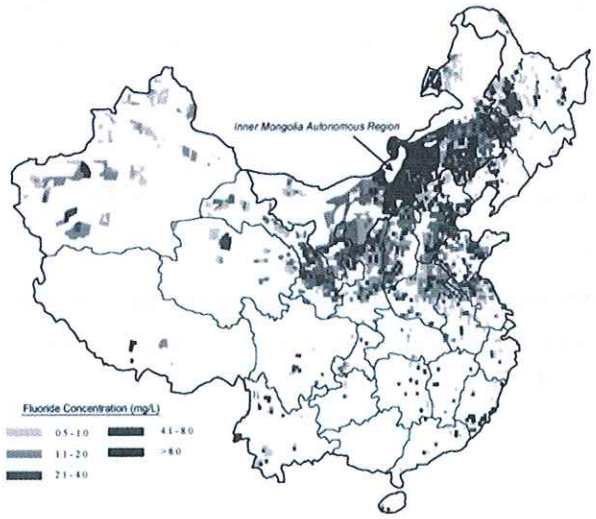

Figure 2. Distribution of fluoride concentration in the groundwater aquifers in China (Wang et al., 2002)

The reactive transport modelling is commonly based on the numerical solution of the governing flow equation and the advective-dispersive transport equation. Among the main challenges of reactive transport modelling are: to capture the scale dependence of the control processes, and the spatial variability of the key model parameters in heterogeneous media (Steefel et. al., 2005). In order to handle such limitations exist two main approaches: deterministic models, in which the reliability of the results depends on the detail of information available to represent spatial and temporal discretization of physical parameters; and stochastic models, in which the physical parameters, source/sink term, or boundary/initial conditions are defined as random variables or functions. In latter cases, the governing equations of flow and transport processes are defined as stochastic differential equations. Hence, the solution is also stochastic process expressed by probability distribution functions or statistics moments (Samper and Carrera, 1990). The stochastic modelling could be suitable in those cases where exhaustive or a priori characterization of the natural system is not possible, or when prompt evaluation of the system is requested.

In the category of stochastic models, several numerical approaches based on travel- and exposure-time as dependent and independent variables of the governing equations have been developed in the past decades (Dagan and Nguyen, 1989; Goode, 1996; Simmons et. al., 1982, 1995a, 1995b; Varni and Carrera, 1998; Ginn et. al., 1999, 2000, 2002; Cornaton et. al., 2006; Seeboonruang et. al., 2006). Such studies provide the basis for representing the spatial distribution of the groundwater age, and for solving conservative and reactive transport problems based on the travel or exposure time models.

1.2. Hypothesis, objectives and structure of this thesis

The fundamental hypothesis to be tested in this thesis is that, under certain conditions, the chemical-compound concentration traditionally estimated by the spatially-explicit advective-dispersive method can be approximated by concentrations expressed as function of the travel time and the simulation time. By posing a quasi 1-D problem, the computation effort and the explicitly-spatial definition of physical-biogeochemical parameters are considerable reduced. The main assumption behind this idea is that the concentration profiles of geochemical systems overlap with the groundwater isochrones, which are defined as lines of equal groundwater age mapped multi-dimensionally. It is truth when reactive systems are linear, or when nonlinear chemical reactions satisfy strictly advective transport mechanism, stationary flow systems, and spatially uniform bioreactive parameters. In contrast, when groundwater and reactive solute mixing processes controls the reactive transport mechanisms, the travel time is not able to capture the evolution of the reactive compounds, no matter those are mobile or immobile.

The current manuscript aims to address the validation of travel-time models to solve nonlinear bioreactive transport problems for those features and conditions that, albeit enhancing the groundwater and reactive solute mixing processes, do not preclude an accurate performance of the travel-time models. The thesis focuses on an aquatic ecosystem that represents surface-groundwater interaction as the hyporheic zone. There, flow and transport boundary conditions of the groundwater domain are sensitive to hydraulic and meteorological events, as well as contaminant discharge on the surface water. The bioreactive system under study represents the redox reactions that take place in a saturated sandy aquifer when dissolved organic matter (electron donor), and dissolved oxygen and nitrate (electron acceptor), are well-mixed and infiltrated from the surface water across the whole inlet boundary of the model domain triggering aerobic degradation of the organic

matter and denitrification. Both chemical reactions are catalysed by two non-competitive bacteria populations, aerobes and denitrifiers.

The following steps provide the insights into the performance of travel time models. Rather than comparing travel time simulation to a real case study or laboratory experiment, a 2-D spatially-explicit model considered as the "virtual truth" provides freedom to design the conceptual model according to the common features that enhance mixing processes into the saturated groundwater systems:

i. Map the travel time (equivalent to the mean groundwater age) in the 2-D domain.
ii. Simulate the 1-D nonlinear bioreactive transport problem.
iii. Map the 1-D concentration with respect to the mapped travel time.
iv. Simulate the 2-D spatially-explicit advective-dispersive model, as "virtual truth".
v. Estimate local residual errors at each position of the domain, along with the root mean standard errors for the whole domain.

The scope of this work covers three main drivers of mixing processes: the hydraulic heterogeneity, expressed by stochastic description of the hydraulic conductivity combined with constant and transient transport boundary conditions; transient flow systems; and coupled physical and geochemical heterogeneity. The content of this manuscript is structured in the following sections:

- Section 2 summarize and compiles the general conclusions detailed in the Appendixes and suggests the outlook of the author for further research topics that may give continuity to the travel-time based bioreactive model applications.

- Appendix A discusses the effects of physical heterogeneity coupled with transient transport boundary conditions on the travel time approach. For that purpose, a total of six case studies are defined by the combination of three degrees of physical heterogeneity, defined by the variance in the hydraulic conductivity field of value 1, 2 and 3; and the continuous and diurnal fluctuation of mobile reactants injected across the whole boundary.

- Appendix B analyses the performance of travel-time models when the flow system undergoes time-periodical fluctuations. In transient flow systems, the mixing processes may break down the application of travel time models. Here, the time-averaged mean travel time, when the inflow rate suffers diurnal and seasonal fluctuations, can be a good estimator of the transient bioreactive system. It is assumed that the flowpaths of the 2-D domain remains constant, whilst the magnitude of the mean seepage velocity fluctuates.

- In Appendix C the concept of geochemical heterogeneity coupled with physical heterogeneity is analysed. To handle the geochemical heterogeneity, travel time is substituted by exposure time, which is defined here as the time that reactive compounds are in contact and able to react. A binary physical-geochemical heterogeneous medium defines reactive lenses of low hydraulic conductivity, and non-reactive matrix of high hydraulic conductivity.

2. Summary and outlook

2.1. Summary and general conclusions

The aim of this thesis is to improve the understanding of the conditions under which travel- and exposure-time bioreactive transport models could be considered as a good approximation to the traditional numerical methods based on spatially-explicit description of the physical-biogeochemical parameters and the resulting dependent variables. Hence, the chemical-compound concentrations commonly expressed as function of time and space in multi-dimensional domains could be simplified as function of time and travel time (exposure time), posing a quasi-one-dimensional simulation in stationary systems. Furthermore, the substantial save in computation resources enables stochastic analysis to assess effective values of key model parameters (e.g. by Monte Carlo simulations), which may manage the uncertainty in their spatial description. The travel-time approach could be exact when strictly advective transport is considered in steady-state flow and reactive properties are uniform in the porous media. Nonetheless, the effects of transverse mixing processes may compromise the application of the travel time models in nonlinear reactive systems. In this work the system of biochemical degradation reactions typically occurring in groundwater is nonlinear and controlled by Monod kinetic parameters. For this reactive system, the role of mixing effects, the error that might be introduced through travel-time based models, and options to account for these mixing effects are quantified and analysed. This is done for different model setting with respect to principal features and boundary conditions of groundwater flow and transport and solute and groundwater mixing processes: spatial variability of physical and geochemical parameters, key variables of the model, as well as transient boundary conditions in flow and transport processes.

The conceptual model of the test case characterizes usual interactions between the well-mixed subsurface water masses, containing dissolved organic carbon (DOC, as electron donor), dissolved oxygen and nitrate (DO, NO_3^-, as electron acceptors) in saturated sandy aquifers. Here, a two-dimensional domain represents the first five meters from the inlet boundary where river water infiltrates, as being prone to great biochemical activity. The (nonlinear) kinetically-controlled reactive system is commonly found beneath the riverbed when it is well connected with a shallow aquifer. Thus, the redox degradation of organic matter by aerobic and anaerobic non-competitive bacteria populations triggers microbial metabolism and redox zonation in the so-called hyporheic zone.

Hereafter, it is presented a brief summary of the work done and the most relevant findings exposed in detail in the corresponding research papers.

The first study (Appendix A) analyses in total six scenarios of the aforementioned test case: the variance of log-hydraulic conductivity defines three two-dimensional stochastic fields from mild to middle physical heterogeneity; for which continuous injection and diurnal fluctuations of the dissolved oxygen inflow concentration are considered. Each scenario is simulated by the following mathematical frameworks:

- Travel time accounting for strictly advective transport mechanism, in which the independent variable is named kinematic age, or advective arrival time and represent a unique value at each location (1-D model).
- Travel time accounting for advective-dispersive transport mechanisms, in which the independent variable is named travel time, or mean groundwater age, and represent the mean value of an inverse Gaussian distribution at each location. Two alternative definitions of dispersion coefficient are evaluated: (i) a constant value for each location; and (ii) an effective coefficient product of the parameterization of mixing processes based on a positive linear correlation with the travel time (2x 1-D model).
- A conservative spatially-explicit transport model provides the necessary information to produce the 2-D mapping of the travel time, later used for the 2-D mapping of the 1-D concentrations with respect to travel time (2-D model).
- An additional simulation of the traditional spatially-explicit reactive advective-dispersive equation is considered throughout this work as the virtual reference or "virtual truth", which is compared with the approximated estimations of the travel-time models (2-D model).

In all the domains the mean travel time, hereinafter named travel time or mean groundwater age, is successfully estimated by the two first temporal moments derived from the local breakthrough curves generated in the conservative transport simulation (Harvey and Gorelick, 1995). The spatial distribution of the mean travel time ratifies its strong dependency with the flow field, by getting older in slow flowpaths and within low hydraulic conductivity lenses. While the injected water penetrates into the domain, the age difference between longitudinal neighbouring streamtubes becomes more evident. The location of the highest values of the variance of travel time observed in the model domain, estimated by the third-order temporal moment of the travel time local breakthrough curves, corresponds with physical features and hot spots where two water parcels with considerable different age signature mix. These transitory zones involve inaccuracies in the estimation of the groundwater age, and consequently denote possible errors in the concentrations of chemicals subjected to nonlinear reactions. Nevertheless, the small variability observed in the 2-D spatially-explicit concentrations expressed as function of travel time suggests an accurate estimation of the independent variable concerning to the test case. Regarding the 2-D mapping of the 1-D concentrations expressed as function of travel time, the mild heterogeneous medium shows excellent fitting between the travel-time concentrations and the "virtual truth", whilst the scenarios with stronger heterogeneity provide moderate deviations between the simplified approach and the results obtained in the spatially-explicit model. Such deviations are more perceptible in the earlier transient periods of the simulation, rather than in the achievement of stationary state.

The consequence of neglecting dispersive coefficients in strictly advective travel time models is the increase of inaccuracies until the reactive system achieves the steady state; such that in long-term stable ecosystems, the kinematic age could capture nonlinearity trends of the reactive components. The results slightly improve when the 1-D model accounts for simple values of local and constant longitudinal dispersivity in the governing equation. An optimized version of the travel-time model considers the parameterization of the dispersive coefficient in the two-dimensional domain described by a linear relationship, such that the mixing coefficient increases with the mean groundwater age. The travel-time based predictions in terms of the magnitude and the patterns of the reactive compound concentrations are excellent, even before steady conditions are achieved. Nonetheless, the finding of the

effective dispersive coefficients is subject to perform feasible conservative tracer tests in real sites, or the setup conservative transport model able to handle with the adequate level of hydraulic parameter´s uncertainty.

The diurnal fluctuation of dissolved oxygen concentration in the inflow is designed as a sinusoidal curve reproducing similar dynamics in the net balance between photosynthesis and respiration processes observed in the surface water (the peak of DO concentration at midday, the valley at midnight, and the wavelength approximately third parts of the inflow concentration in the continuous injection scenario (Diem et. al., 2013). As expected, the diurnal perturbation is almost unnoticed by the microbial population with slow response capacity, due to their small effective growth and decay rates selected in the present test case. Nonetheless, there is an interest to test the potential errors on the estimated mobile reactant concentrations (DO). In comparison with the continuous injected scenario, temporal dynamics in inflow concentration resulted in slightly higher errors maintained over time.

Take away message: travel-time models can provide extremely good agreement with the "virtual truth" for an adequately parameterized dispersive coefficient when mobile reactants are introduced over a wide cross-section, flow is at quasi steady state, and uniform reactive properties; it is expected a good tendency when simple conceptualization of dispersive coefficient are considered (Sanz-Prat et. al, 2015).

The second study (Appendix B) addresses the dynamic hydrological conditions that commonly affect shallow aquifers well-connected with riverbeds. The natural fluctuations of the seepage velocity induce temporal alterations in the local values of the mean groundwater age, therefore also alters the corresponding estimated chemical concentrations. To assess such effects in the travel time model, the study addresses the definition and evaluation of a time-independent characteristic travel time as proxy of bioreactive transport in transient flow systems; in particular when the hydraulic field is affected by time-periodic fluctuations of the inflow boundary conditions and the following assumptions are met: (i) the groundwater storage is neglected in order to keep the magnitude of the seepage velocity uniquely affected by hydraulic dynamics along the inlet boundary; (ii) the spatial orientation of the groundwater flowpath are constant, whereas only the magnitude of the seepage velocity is adjusted by the inflow rate at the boundary; otherwise, intervals of convergence-divergence among flowpaths may cause meaningless counter-clockwise during the groundwater age tracking; (iii) the value of the bioreactive parameters are uniform in the whole domain. Here, the test case is analysed in the following mathematical frameworks of bioreactive transport:

- Conservative transport simulations accounting for (a) strictly advective and (b) advective-dispersive transport mechanisms in: (i) steady flow, and (ii) time-periodic flow conditions. Then, the kinematic age, and the local mean travel time at steady state can be estimated and simultaneously compared with their corresponding mean (or time-averaged) value in transient flow conditions (4x 1-D model; 4x 2-D model).
- Reactive transport travel time simulation accounting for advective and local longitudinal dispersive coefficient in steady flow, for diurnal and seasonal fluctuations (b-i, 2x quasi 1-D model).
- Spatially-explicit reactive advective dispersive simulation, considered the "virtual truth" of the test case reproducing time-periodic flow conditions, for diurnal and seasonal fluctuations (b-ii, 2x 2-D model).

The time-periodic feature of the transient flow one-dimensional and two-dimensional systems clearly induces null variability of the mean travel time value, and the mean kinematic age, in locations which values are integer of periodic fluctuations. Meanwhile, the in-between areas exhibit maximal but acceptable variability values. In spite of differences and uncertainties in the estimation of the independent variable, the four approaches provide similar results of the time-invariant characteristic travel time.

The comparison between the simplified one-dimensional reactive transport model and the two-dimensional "virtual truth" is excellent for mobile compounds. Regarding nonlinearities in the immobile biomass components, small deviations are observed due to the slow response of microbes to diurnal alterations. The resulting aerobic zonation increases or decrease at the same time than seepage velocity, which causes a transition zone with presence of both bacteria populations. However, the seasonality of flow rates provides a better spatial differentiation between the two degradation pathways (location of aerobic and denitrifying bacteria).

Assuming available transient flow information in real sites, by physically-sampled data or statistically approximated, the time-averaged mean seepage velocity still could be estimated and used in a stationary flow simulation expecting similar results to the traditional transient flow simulation. Nonetheless, an important limitation of the proposed simplified model in real applications is to obtain accurate representativeness of non-periodical hydraulic events that define the transient flow system.

Take away message: the one-dimensional steady state simulation of the time-averaged travel-time based model is able to effectively reproduce a multi-dimensional time-periodic simulation of bioreactive transport problem when flow direction does not change (Sanz-Prat et. al, 2016).

The third study (Appendix C) considers the coupled effect of physical and geochemical heterogeneity of the porous medium. Both are defined in the presented work as binary spatial property; such that highly heterogeneous reactive lenses, acting as quasi-infinite sources of dissolved organic matter, which are embedded in an inert matrix with one order of magnitude higher hydraulic conductivity. The principal novelty of this work with respect to the previous ones is that the reactive properties are only spatially uniform in the reactive zones. This assumption implies the use of the exposure time, defined here as the time that an idealized water parcel is exposed to two or more reactive materials, as substitute for the travel time. As expected, the difference between travel time and exposure time is more evident the further it gets form the inlet of the domain. The modified test case is simulated for the following mathematical frameworks:

- Exposure time based reactive transport simulation, for homogeneous and heterogeneous domain (2x 1-D model).
- Conservative advective-dispersive transport simulation, to estimate travel time, mean exposure time (hereinafter exposure time), and time difference at each location (2-D model).
- Reactive transport spatially-explicit based advective-dispersive simulation, as the reference case or virtual truth (2-D model).

Notice that the simplified approach is not able to reproduce concentrations corresponding to non-reactive areas, which may cause overestimation of the chemical-compound

concentrations. Although the uncertainty is significantly higher than in the first and second studies, the exposure-time based model captures the same tendency and magnitude than the "virtual truth" concentrations inside the reactive lenses. With the purpose to simulate more realistic conditions, the test case is designed such that the reactions could take place downstream the reactive lenses due to the excess release of dissolved organic matter not consumed within the reactive lenses.

Take away message: the compound concentrations in the reactive zones estimated by the multi-dimensional and highly heterogeneous spatially-explicit reactive transport model can be successfully replaced by the one-dimensional homogeneous exposure time model, when quasi-steady state is achieved and reactive activity is clearly restricted to certain locations (Sanz-Prat et. al, 2016 submitted).

In general, the travel- and exposure-time bioreactive transport models are good approximations to the traditional numerical methods. The chemical-compound concentrations in 2-D domains simplified as function of time and travel time by posing a quasi 1-D simulation in stationary systems reduces significantly the computation effort a lot. The reduction of computation effort offers an alternative, from small to large scale, to perform numerical models as: uncertainty analysis in multi-dimensional stochastic flow and transport models; calibration or sensitivity analysis of physical and biogeochemical parameters; or the application for inverse models.

2.2 Outlook

The findings presented above prove that the performance of travel- and exposure-time based reactive transport models in non-ideal circumstances deserves more thorough attention. As the presented work was pretty much focused on one specific test case (the redox reactions in the hyporheic zone), more diversified sets of real problems should be considered in future, for instance, different sorts of coupled physical and biogeochemical heterogeneities, e.g. as anisotropic hydraulic fields, different compositions of geochemical facies, and stratigraphic profiles. Besides, the evaluation can be extended to nonlinear chemical reactions, which is not controlled by transverse (and vertical) mixing processes, such as: rock-water interactions; reversible chemical reactions as precipitation/dissolution; to account for retardation factor in attachment/detachment processes (e.g. in active mineral bounds). An interesting research field that increases complexity of exposure time approach is the inclusion of microbial transport processes. The application in the unsaturated zone implies novel findings in the required assumptions to deal with the effects of diffusive processes and multi-phase transport of certain chemical compounds.

The advantage of the comparing idealized travel time models and the spatially-explicit model ("virtual truth") is to avoid disruptions from non-controlled factors that typically appear in real site applications. Nonetheless, testing travel-time models' estimates against observed data in laboratory and field experiments may better proof whether travel time models could infer reactive transport behaviour in real systems.

In three-dimensional domains the effect of vertical and transverse mixing processes get more relevance and may compromise the accuracy of the mean groundwater age value, and its capture of nonlinear behaviour of reactive components, but simultaneously the computational

reduction is more profitable than that in the two-dimensional domains (sixfold faster than in the presented test case). The stochastic groundwater field improves the description of effective flow and transport parameters (Dentz et. al., 2000, 2004, Cirpka, 2002, among others). In this sense, research efforts on the development of parameterization methods according to the effective dispersive coefficients represent a successful strategy to improve the performance of simply one-dimensional advective-dispersive travel-time models.

Another frequent limitation factor is the estimation of travel time in transient flow systems. Here, the proposed case study implies conditions mainly found in confined aquifer where the groundwater storage coefficient could be neglected, and well-connected to recharge areas with the same pattern of inflow rate. However, in the unconfined aquifers with significant specific yield value, or groundwater subsurface undergoing critical changes in flowpath direction are outside the scope of this work. For the author´s knowledge, relevant advances in analytical and numerical solutions have been proposed for other sort transient flow systems by Cornaton (2012) and Soltani et. al. (2013).

Bibliography

Acharyya, S.K, and Shah, B.A., (2007). Arsenic-contaminated groundwater from parts of Damodar fan-delta and west of Bhagirathi River, West Bengal, India: influence of fluvial geomorphology and Quaternary morphostratigraphy. Environ Geol 52:489-501.

Bundschuh, J., Farias, B., Martin R., Storniolo, A., Bhattacharya, P., Cortes, J., Bonorino, G., Albouy, R. (2004). Groundwater arsenic in the Chaco-Pampean Plain, Argentina: case study from Robles county, Santiago del Estero Province. Appl. Geochemistry, 19: 231-243.

Cirpka, O.A., (2002). Choice of dispersion coefficients in reactive transport calculations on smoothed fields. Water Resour. Res. 58 (3–4), 261–282.

Cornaton, F. J., and P. Perrochet (2006a), Groundwater age, life expectancy and transit time distributions in advective-dispersive systems: 1. Generalized reservoir theory, Adv. Water Res., 29, 1267 – 1291.

Cornaton, F.J., (2012). Transient water age distributions in environmental flow systems: the time-marching Laplace transform solution technique. Water Resour. Res. 48,W03524.

Dagan, G., Nguyen, V., (1989). A comparison of travel time and concentration approaches to modelling transport by groundwater. J. Contam. Hydrol. 4, 79–91.

Dentz, M., Kinzelbach, H., Attinger, S., Kinzelbach,W., (2000). Temporal behavior of a solute cloud in a heterogeneous porous medium: 1. Point-like injection Water Resour. Res. 36 (12), 3591–3604.

Dentz, M., Cortis, A., Scher, H., Berkowitz, B., (2004). Time behavior of solute transport in heterogeneous media: transition from anomalous to normal transport. Adv. Water Resour. 27, 155–173.

Diem, S., Cirpka, O.A., Schirmer, M., 2013. Modeling the dynamics of oxygen consumption upon riverbank filtration by a stochastic-convective approach. J. Hydrol. 505, 352–363.

Fleckenstein, J.H., Krause, S., Hannah, D.M., Boano, F., (2010). Groundwater-surface water interactions: New methods and models to improve understanding of processes and dynamics. Advance in Water Resources, 33: 1291-1295.

Ginn, R.T., (1999). On the distribution of multicomponent mixtures over generalized exposure time in subsurface flow and reactive transport: foundations, and formulations for groundwater age, chemical heterogeneity, and biodegradation. Water Resour. Res. 35 (5), 1395–1407.

Ginn, R.T., (2000). On the distribution of multicomponent mixtures over generalized exposure time in subsurface flow and reactive transport: batch and column applications involving residence-time distribution and non-Markovian reaction kinetics. Water Resour. Res. 36 (10), 2895–2903.

Ginn, T.R., (2002). A travel time approach to exclusion on transport in porous media. Water Resour. Res. 38 (4), 1041.

Goode, D.J., (1996). Direct simulation of groundwater age. Water Resources Research, 32: 289-296.

Harvey, F. H., Gorelick, S.M., (1995). Temporal moment-generating equations: Modeling transport and mass transfer in heterogeneous aquifers. Water Resources Research, 31: 1895-1911.

Samper, F.J., Carrera, J. (1990). Geoestadística: aplicaciones a la hidrología subterranean. Ed. CIMNE, 2nd edition.

Sanz-Prat, C. Lu, M. Finkel, O.A. Cirpka, (2015). On the validity of travel-time based nonlinear bioreactive transport models in steady-state flow. J. Contam. Hydrol. 175-176: 26-43.

Sanz-Prat, C. Lu, M. Finkel, O.A. Cirpka, (2016). Using travel times to simulate multi-dimensional bioreactive transport in time-periodic flows. J. Contam. Hydrol. 187: 1-17.

Sanz-Prat, C. Lu, R.T. Amos, M. Finkel, D.W. Blowes, O.A. Cirpka, (2016). Exposure-time based modeling of nonlinear reactive transport in porous media subject to physical and geochemical het-erogeneity. J. Contam. Hydrol. (submitted).

Seeboonruang, U., Ginn, T.R., (2006). Upscaling heterogeneity in aquifer reactivity via exposure-time concept: forward model. J. Contam. Hydrol. 84 (3–4), 127–154.

Steefel, C.I., DePaolo, D.J., Lichtner, P.C., (2005). Reactive transport modelling: An essential tool and a new research approach for the Earth sciences. Earth and Planetary Science Letters 240: 539-558.

Simmons, C.S., (1982). A stochastic-convective transport representation of dispersion in one-dimensional porous-media systems. Water Resour. Res. 18 (4), 1193–1214.

Simmons, C.S., Ginn, T.R., Wood, B.D., (1995a). Stochastic-convective transport with nonlinear reaction: biodegradation with microbial growth. Water Resour. Res. 31 (11), 2689–2700.

Simmons, C.S., Ginn, T.R., Wood, B.D., (1995b). Stochastic-convective transport with nonlinear reaction: mathematical framework. Water Resour. Res. 31 (11), 2675–2688.

Soltani, S.S., Cvetkovic, V., (2013). On the distribution of water age along hydrological pathways with transient flow. Water Resour. Res. 49, 1–8.

Varni, M., Carrera, J. (1998). Simulation of groundwater age distributions. Water Resources Research, 34: 3271-3281.

Wang, X.C., Kawahara, K., Guot, X.J. (1999). Fluoride contamination of groundwater and its impacts on human health in Inner Mongolia area. J Water SRT. 48: 146-153.

Appendix A: First publication

Title

On the validity of travel-time based nonlinear bioreactive transport models in steady-state flow

Authors

Alicia Sanz-Prat, Chuanhe Lu, Michael Finkel, Olaf A. Cirpka

Journal

Journal of Contaminant Hydrology (Volume 175-176, pages 26-43)

Year

2015

Highlights

- We test whether travel time is a good proxy for reactive-species concentrations.
- The agreement is very good for moderate heterogeneity and steady-state flow.
- Effective longitudinal mixing must adequately be addressed.
- Travel-time based simulations thus simplify nonlinear reactive transport.
- The approach is invalid when macroscopically transverse mixing is relevant.

Journal of Contaminant Hydrology 175–176 (2015) 26–43

Contents lists available at ScienceDirect

Journal of Contaminant Hydrology

journal homepage: www.elsevier.com/locate/jconhyd

On the validity of travel-time based nonlinear bioreactive transport models in steady-state flow

Alicia Sanz-Prat, Chuanhe Lu, Michael Finkel, Olaf A. Cirpka *

University of Tübingen, Center for Applied Geosciences, Hölderlinstraße 12, 72074 Tübingen, Germany

ARTICLE INFO

Article history:
Received 26 August 2014
Received in revised form 30 January 2015
Accepted 5 February 2015
Available online 12 February 2015

Keywords:
Travel time
Groundwater age
Reactive transport
Streamtube methods
Biodegradation
Mixing

ABSTRACT

Travel-time based models simplify the description of reactive transport by replacing the spatial coordinates with the groundwater travel time, posing a quasi one-dimensional (1-D) problem and potentially rendering the determination of multidimensional parameter fields unnecessary. While the approach is exact for strictly advective transport in steady-state flow if the reactive properties of the porous medium are uniform, its validity is unclear when local-scale mixing affects the reactive behavior. We compare a two-dimensional (2-D), spatially explicit, bioreactive, advective–dispersive transport model, considered as "virtual truth", with three 1-D travel-time based models which differ in the conceptualization of longitudinal dispersion: (i) neglecting dispersive mixing altogether, (ii) introducing a local-scale longitudinal dispersivity constant in time and space, and (iii) using an effective longitudinal dispersivity that increases linearly with distance. The reactive system considers biodegradation of dissolved organic carbon, which is introduced into a hydraulically heterogeneous domain together with oxygen and nitrate. Aerobic and denitrifying bacteria use the energy of the microbial transformations for growth. We analyze six scenarios differing in the variance of log-hydraulic conductivity and in the inflow boundary conditions (constant versus time-varying concentration). The concentrations of the 1-D models are mapped to the 2-D domain by means of the kinematic (for case i), and mean groundwater age (for cases ii & iii), respectively. The comparison between concentrations of the "virtual truth" and the 1-D approaches indicates extremely good agreement when using an effective, linearly increasing longitudinal dispersivity in the majority of the scenarios, while the other two 1-D approaches reproduce at least the concentration tendencies well. At late times, all 1-D models give valid approximations of two-dimensional transport. We conclude that the conceptualization of nonlinear bioreactive transport in complex multidimensional domains by quasi 1-D travel-time models is valid for steady-state flow fields if the reactants are introduced over a wide cross-section, flow is at quasi steady state, and dispersive mixing is adequately parametrized.

1. Introduction

Travel-time based models of reactive transport rely on substituting the spatial coordinates of a multi-dimensional model domain by the groundwater travel time, posing a quasi 1-D problem (e.g., Feyen et al., 1998; Luo, 2012). They may be regarded as alternatives to traditional spatially explicit models, as they alleviate the characterization of the domain with respect to hydraulic parameters and significantly reduce the computational effort of solving reactive transport (e.g., Atchley et al., 2014; Diem et al., 2013; Engdahl and Maxwell, 2014; Gong et al., 2011; Luo et al., 2007). The underlying assumption is that the spatial positions of propagating concentration contrasts, or reaction fronts, are aligned with isochrones (i.e., lines of equal travel time), which requires that the reactive properties of the porous medium (e.g., sorption capacity, reaction rate constants) are uniform in the domain, that the concentrations in the inflow

* Corresponding author. Tel.: +49 7071 29 789 28; fax: +49 7071 29 5059.
E-mail address: olaf.cirpka@uni-tuebingen.de (O.A. Cirpka).

http://dx.doi.org/10.1016/j.jconhyd.2015.02.003
0169-7722/

are uniform along the corresponding model boundary (i.e., the inlet of the domain), and that flow is at steady state. The effects of solute mixing on the applicability of travel-time based methods deserve further analysis, which is the main purpose of the present study.

The travel time τ [T] is defined as the time that a water (or idealized solute) particle needs to travel from the inlet of the domain to the observation or exit point. At any point in the domain, the travel-time distribution is equivalent to the measured breakthrough curve when a unit pulse input of an inert solute is uniformly injected along the inflow boundary (Danckwerts, 1953; Jury, 1982; Jury and Roth, 1990). It allows constructing expected breakthrough curves of conservative compounds for any input function by convolution, provided that the flow field does not change with time.

The travel-time distribution for Fickian transport, that is, advective–dispersive transport with temporally and spatially uniform velocity and dispersion coefficients, is the inverse Gaussian distribution, which is fully defined by the first and second-central moments of the distribution (Kreft and Zuber, 1978). Non-Fickian transport, e.g. resulting from the upscaling of small-scale heterogeneities (Berkowitz et al., 2006; Gouze et al., 2008; Sanchez-Vila and Carrera, 2004; Willmann et al., 2008; among others), leads to travel-time distributions that require more temporal moments for their characterization. Harvey and Gorelick (1995) presented temporal-moment generating equations (see Appendix A) and suggested reconstructing the full distribution from a few low-order moments by applying the maximum-entropy principle. The mean groundwater age (Goode, 1996) is the ratio of the first over the zeroth temporal moment (see Subsection 4.1).

There are different reasons why observed and analyzed travel times are distributions rather than single values, and the underlying assumptions are important when characterizing nonlinear reactive transport within a travel-time framework. The earliest travel-time models considered physical transport to be strictly advective, leading to the so-called advective travel time, also denoted as kinematic groundwater age, which can best be computed by Lagrangian methods (e.g., Botter et al., 2005; Cketkovic et al., 1996; Dagan and Bresler, 1979). Since advection causes no mixing, a water parcel conceptualized in this model carries its chemical information without exchanging mass with surrounding parcels. If the reactive properties of the medium are uniform, the progress of reaction within the water parcel exclusively depends on the time since release, and a unique mapping from travel time to space is possible by means of the kinematic age.

Within the strictly advective framework, travel times may still be distributions, either because of spatial averaging over a cross-section within a non-uniform domain, or as a result of uncertainty in hydraulic conductivity and flow velocity within a stochastic framework. At an individual point within a single realization, however, the travel-time distribution collapses to a single value in advective transport. The stochastic analysis of advective travel times within heterogeneous domains using Lagrangian methods and the subsequent unique mapping of the probability density function (*pdf*) of travel time to that of reactive-species concentrations is at the core of the stochastic-convective reactive model (SCR) introduced by Dagan and Bresler (1979), and further analyzed in groundwater transport by Cvetkovic et al. (1996), Cvetkovic and Dagan (1994), Dagan and Nguyen (1989), Ginn (2002), Simmons (1982) and Simmons et al. (1995a,b), and in soil sciences by Feyen et al. (1998), Köhne et al. (2009), Leij et al. (2007), Moore and Grayson (1991), and Shuang et al. (2011), among others.

A second, but conceptually quite different reason why travel times are distributions rather than single values is pore-scale dispersion, based ultimately on diffusion. This is a mixing process where water parcels of different ages exchange solutes. The resulting travel-time distributions are neither scale effects nor manifestations of uncertainty. For linear processes, the order of mixing and reaction does not matter, but for nonlinear reactive processes completely different behaviors may be observed (Cirpka and Kitanidis, 2000a; De Simoni et al., 2005, 2007; Luo and Cirpka, 2011; Willmann et al., 2010; Zwietering, 1959).

To handle the problem of mixing-controlled reactions, Cirpka and Kitanidis (2000b) characterized point-like breakthrough curves of conservative compounds undergoing advection and pore-scale dispersion by their first and second-central moments. A key observation was that the spatial variability in the local first moment is transferred to increased local second-central moments by transverse dispersion. For reactive transport, Cirpka and Kitanidis (2000a) developed the advective–dispersive stream-tube (ADS) method, in which advective–dispersive–reactive transport in multidimensional domains was conceptualized as transport within independent stream-tubes in which the effects of local transverse dispersion on macroscopic longitudinal mixing was parametrized by increased within-stream-tube dispersion. Cirpka (2002) applied linear stochastic theory to estimate the corresponding effective mixing coefficients in mildly heterogeneous domains (Dentz et al., 2000).

The stochastic-convective framework and the advective–dispersive stream-tube approach have in common that they conceptualize a multidimensional transport domain as a bundle of 1-D systems that are characterized by travel times. The difference is that the stochastic-convective framework neglects pore-scale dispersion and related mixing altogether, whereas the advective–dispersive stream-tube method allows for longitudinal mixing within the stream tubes. In the stochastic-convective model, the travel time considered is the kinematic age, whereas in the advective–dispersive stream-tube method it is the mean groundwater age (see Appendix A). Distributing the solutes at an individual point among different groundwater ages, as is possible with the approach of Ginn and coworkers (e.g., Ginn, 1999, 2000; Ginn et al., 2009), is neither considered by the advective–dispersive stream-tube approach nor by the stochastic-convective method. The computational burden introduced by the latter approach, however, is quite high because an additional dimension, namely that of groundwater age, is introduced.

The key question to be addressed in the present study is under which conditions travel-time based nonlinear reactive transport models, which are based on a single travel time at an individual point, yield acceptable results despite known inconsistencies when water bodies with different ages and chemical signatures mix, fostering nonlinear chemical reactions (Bethke and Johnson, 2002; Cornaton, 2003; Ginn, 2002; Goode, 1996). We expect that transient flow and transport boundary conditions, as well as hydraulic and chemical heterogeneity, may cause the breakdown of the simple travel-time approaches, but restrict our analysis to hydraulic heterogeneity and transient transport boundary conditions.

The hypothesis to be tested in this paper is that, under certain conditions, describing reactive transport in travel time rather than following a spatially-explicit approach introduces only negligible error. Mathematically, this proposition is expressed as:

$$\mathbf{c}(\mathbf{x},t)\approx\mathbf{c}(\tau(\mathbf{x}),t) \quad (1)$$

in which $\mathbf{c}$ $[ML^{-3}]$ is the vector of reactive-species concentrations, $\mathbf{x}$ $[L]$ is the vector of spatial coordinates, t $[T]$ is time, and $\tau(\mathbf{x})$ $[T]$ is a characteristic groundwater age at location $\mathbf{x}$. In practice, the acceptability of Eq. (1) may be divided into four research questions to be studied hereafter:

1. Is Eq. (1) valid at individual points in the domain? If not (everywhere), is it possible to identify physical features or processes as corresponding causes of the breakdown of the travel-time approach? Conversely, should Eq. (1) hold throughout the domain, any integral quantity, such as the average solute flux leaving the domain via an outflow boundary, can in principle be accurately computed by travel-time based methods.
2. Is the mean groundwater age a sufficient predictor? As discussed before, the groundwater age at any given point is a distribution and characterizing the latter by its mean may introduce bias in predicting concentrations of reactive solutes.
3. Which error is introduced by neglecting local dispersion altogether, as done in the stochastic-convective model?
4. Can we derive a simple approach of obtaining effective longitudinal mixing coefficients within the travel-time framework from conservative transport and apply these mixing coefficients to reactive-transport problems?

To answer these questions, we consider the case of non-linear bioreactive transport in heterogeneous porous media caused by random log-hydraulic conductivity fields under steady-state flow conditions. Spatially explicit 2-D bioreactive transport models are compared with three homologue cases defined by 1-D models. These 1-D cases differ in the treatment of dispersive mixing: (i) neglecting all dispersive mixing effects, which correspond to the stochastic-convective-reactive approach, in which physical transport is characterized by the kinematic age; (ii) applying the local-scale longitudinal dispersivity from the spatially explicit 2-D model also in the 1-D, travel-time based model and considering it uniform throughout the domain; and (iii) improving the latter 1-D model with an empirical longitudinal dispersivity that increases with travel distance to account for enhanced within-stream-tube mixing caused by the unresolved interplay between heterogeneity and transverse pore-scale dispersion (Cirpka and Kitanidis, 2000a,b).

In all cases, we map the purely advective 1-D model results according to the local kinematic age 9, and the two other 1-D models according to the local mean groundwater age 6 onto the 2-D domain. This allows quantifying the errors introduced by the various travel-time based methods that may be used for evaluating the acceptability of the underlying simplifications. As potential pitfalls for the travel-time based approaches we suspect cases of high spatial variability and strongly transient transport behavior. We have thus designed six scenarios by combining three levels of heterogeneity with constant and with time-varying concentration boundary conditions each. Fig. 1 describes the work flow of the simulations performed in this study.

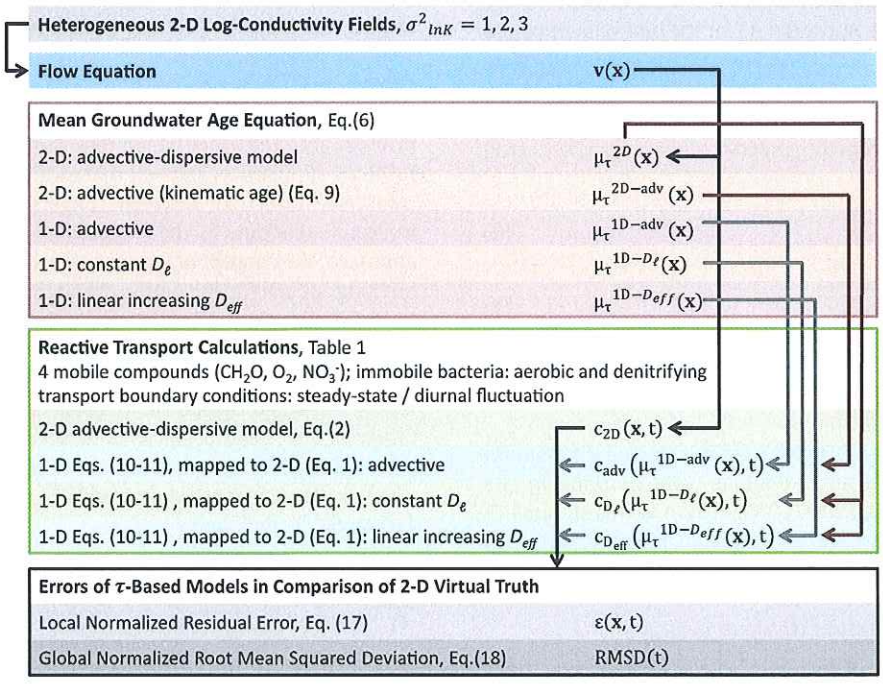

Fig. 1. Work flow of the simulations performed.

2. Mathematical framework

2.1. Multidimensional transport

In this study, the multidimensional reactive transport equations for mobile (m) and immobile (im) compounds are based on the traditional advection–dispersion equation (ADE) with spatially variable seepage velocity $\mathbf{v}$ [LT^{-1}] and a local dispersion tensor $\mathbf{D}$ [L^2T^{-1}] that is oriented in the direction of flow:

$$\frac{\partial c_m^{(i)}}{\partial t} + \mathbf{v}\cdot\nabla c_m^{(i)} - \nabla\cdot\left(\mathbf{D}\nabla c_m^{(i)}\right) = r_m^{(i)}(\mathbf{c}(\mathbf{x},t)) \tag{2}$$

$$\frac{\partial c_{im}^{(i)}}{\partial t} = r_{im}^{(i)}(\mathbf{c}(\mathbf{x},t)) \tag{3}$$

subject to:

$$\mathbf{n}\cdot\left(\mathbf{v}c_m^{(i)} - \mathbf{D}\nabla c_m^{(i)}\right) = \mathbf{v}c_{inflow}^{(i)}(t) \text{ at } \Gamma_{in} \tag{4}$$

$$\mathbf{n}\cdot\left(\mathbf{D}\nabla c_m^{(i)}\right) = 0 \text{ at } \Gamma_{out}\cup\Gamma_0 \tag{5}$$

in which $c_m^{(i)}[ML^{-3}]$ is the concentration of mobile compound i, $r_m^{(i)}[ML^{-3}T^{-1}]$ is the reactive source–sink term for that compound, whereas $c_{im}^{(i)}$ and $r_{im}^{(i)}$ are the corresponding expressions for an immobile compound. $c_{inflow}^{(i)}[ML^{-3}]$ is the concentration of mobile compound i in the inflow. Γ_{in}, Γ_{out}, and Γ_0 denote inflow, outflow, and no-flow boundaries, respectively.

To relate the reactive-species concentrations of the 1-D models, formulated in travel time, to the multidimensional virtual truth, we compute the mean groundwater age μ_τ [T] by the mean groundwater age equation (Goode, 1996), which can be derived from the generating equations of the zeroth and first temporal moments (see Appendix A) for the case of a unit pulse injection at the inflow boundary. Formally, it is a steady-state advection–dispersion equation with a uniformly distributed zero-order source term of unit strength. The inflowing water has an age of zero, whereas the dispersive flux of age is zero at all other boundaries:

$$\mathbf{v}\cdot\nabla\mu_\tau - \nabla\cdot(\mathbf{D}\nabla\mu_\tau) = 1 \tag{6}$$

$$\mathbf{n}\cdot(\mathbf{v}\mu_\tau - \mathbf{D}\nabla\mu_\tau) = 0 \text{ at } \Gamma_{in} \tag{7}$$

$$\mathbf{n}\cdot(\mathbf{D}\nabla\mu_\tau) = 0 \text{ at } \Gamma_{out}\cup\Gamma_0. \tag{8}$$

Note that Eqs. (6)–(8) cannot consider the full distribution of groundwater age at an individual point as done in the approach of Ginn et al. (2009). When two water streams of different ages mix by transverse dispersion, the resulting mean groundwater age is the (volume-weighted) arithmetic average.

2.2. Travel-time based reactive transport models

In the case that advection is the dominant transport mechanism, Eqs. (6)–(8) may be simplified to pure advective transport. Under such conditions, the advective travel time, or kinematic groundwater age, is obtained by integration of the inverse velocity along a particle trajectory:

$$\tau_{adv}(\mathbf{x}) = \int_{\mathbf{x}_0}^{\mathbf{x}} \frac{d\mathbf{x}_p}{\left\|\mathbf{v}\left(\mathbf{x}_p\right)\right\|} = \int_{\mathbf{x}_0}^{\mathbf{x}} \frac{\theta}{q\left(\mathbf{x}_p\right)} d\mathbf{x}_p \tag{9}$$

in which $\mathbf{x}_p$ [L] is the position vector of a particle along its trajectory from starting point $\mathbf{x}_0$ [L] to the observation point $\mathbf{x}$ [L], θ [$-$] is the porosity, and q [LT^{-1}] is the absolute value of the specific discharge vector.

The stochastic-convective-reactive approach (e.g., Simmons et al., 1995b) conceptualizes reactive solute transport along independent streamlines. All concentration-independent reaction coefficients are assumed uniform within the whole domain, and the seepage velocity is at steady state:

$$\frac{\partial c_m^{(i)}}{\partial t} + \frac{\partial c_m^{(i)}}{\partial \tau_{adv}} = r_m^{(i)}(\mathbf{c}(\tau_{adv},t)) \tag{10}$$

$$\frac{\partial c_{im}^{(i)}}{\partial t} = r_{im}^{(i)}(\mathbf{c}(\tau_{adv},t)) \tag{11}$$

subject to:

$$c_m^{(i)}(0,t) = c_{inflow}^{(i)}(t). \tag{12}$$

The stochastic-convective-reactive approach accounts for macrodispersion as statistical distribution of advective arrival times within an observation or control plane. Correspondingly, the breakthrough curve of a conservative tracer injected as Dirac pulse over the entire inflow boundary is equivalent to the *pdf* of advective arrival times $p(\tau_{adv})$ in independent stream tubes.

Local-scale dispersion is the main cause of solute mixing, but it is completely neglected in the stochastic-convective approach. Cirpka and Kitanidis (2000a) considered scenarios in which a solution containing a reacting compound was injected into a domain containing the reaction partner, denoted replacement scenario. On a macroscopic scale, mixing in this scenario is oriented into the longitudinal direction, even though the fully resolved simulations showed that local mixing occurred in the transverse direction between "fingers" of the invading and receding solutions. In their advective–dispersive stream-tube approach, the concept of independent 1-D stream tubes is kept, but longitudinal mixing within the stream tubes is accounted for by an appropriate effective dispersion coefficient $D_\tau(\mu_\tau)$ [T] making the second-central temporal moments of the stream-tube approach match the average second-central moments of locally measured breakthrough curves in an observation plane. Cirpka (2002) used coefficients derived from linear stochastic theory that grow with distance in a nonlinear way (Dentz et al., 2000). In the present study, we will use simpler approaches. The 1-D model formulation reads as:

$$\frac{\partial c_m^{(i)}}{\partial t} + \frac{\partial c_m^{(i)}}{\partial \mu_\tau} - \frac{\partial}{\partial \mu_\tau}\left(D_\tau \frac{\partial c_m^{(i)}}{\partial \mu_\tau}\right) = r_m^{(i)}(\mathbf{c}(\mu_\tau,t)) \tag{13}$$

$$\frac{\partial c_{im}^{(i)}}{\partial t} = r_{im}^{(i)}(\mathbf{c}(\mu_\tau,t)) \tag{14}$$

subject to:

$$c_m^{(i)} - D_\tau \frac{\partial c_m^{(i)}}{\partial \mu_\tau} = c_{inlet}^{(i)} \text{ at } \Gamma_{in} \tag{15}$$

$$D_\tau \frac{\partial c_m^{(i)}}{\partial \mu_\tau} = 0 \text{ at } \Gamma_{out}. \tag{16}$$

The model is formulated for macroscopically 1-D problems, as an alternative scenario of the 2-D models. If the reaction is controlled by macroscopically transverse mixing, e.g. in the case of a plume originating from a continuously emitting source that reacts with the ambient water, both the stochastic-convective approach and the advective–dispersive stream-tube method fail as they do not consider transverse mixing.

The two approaches have been derived to predict breakthrough curves of reactive compounds averaged over the flux crossing a control plane. Within this control plane, the local mean groundwater age μ_τ and the kinematic age τ_{adv} vary, and the expected mean concentration $\bar{c}_{out}^{(i)}(t)$ in the outflow is a flux-weighted average of $c_m^{(i)}(\tau, t)$ over the travel-time τ. In the present study, we do not analyze averaged breakthrough curves $\bar{c}_{out}^{(i)}(t)$, as in practice the associated uncertainty is largely related to the parametrization of travel-time distribution across the outflow boundary. Instead, we ask whether the underlying basic proposition of Eq. (1) holds locally within the domain. We do this by mapping the travel-time based reactive species concentrations to the two-dimensional domain using the correct local values of the mean groundwater age μ_τ and the advective travel time τ_{adv}, respectively, and comparing the projected concentrations to the concentrations obtained by solving the spatially explicit reactive transport equation, Eqs. (2)–(5).

We denote the "virtually true" concentration of reactive compound i, represented by the 2-D model, as $c_{2D}^{(i)}(\mathbf{x}, t)$, and the corresponding projection from the travel-time based models as $c_{1D}^{(i)}(\mu_\tau(\mathbf{x}), t)$. We normalize the residual error by the inflow concentration in the case of mobile compounds, and by the maximum concentration in the case of immobile compounds:

$$\varepsilon_i(\mathbf{x}, t) = \frac{c_{2D}^{(i)}(\mathbf{x}, t) - c_{1D}^{(i)}(\mu_\tau(\mathbf{x}), t)}{c_{inflow/max}^{(i)}}. \tag{17}$$

As global metric for the agreement between the spatially explicit model and the travel-time based models within the entire domain Ω, we compute the normalized root mean squared deviation (NRMSD) by squaring the normalized residual error $\varepsilon_i(\mathbf{x}, t)$, averaging it over the domain, and taking the square-root of the resulting expression:

$$NRMSD_i(t) = \sqrt{\frac{\int_\Omega \varepsilon_i^2(\mathbf{x}, t) d\mathbf{x}}{\int_\Omega d\mathbf{x}}} \tag{18}$$

which is computed for each compound and each time point of the simulation.

3. Test case

3.1. Conceptual model

To test the applicability of travel-time based multi-component reactive-transport models, we consider a case that mimics river-bank filtration originated by fluvial erosion in sedimentary basins, such media are defined by isotropic and heterogeneous log-hydraulic conductivity fields commonly used to represent sandy aquifer with clay and gravel lenses (e.g., Marzadri et al., 2011): Dissolved organic carbon (DOC), denoted CH_2O, dissolved oxygen, denoted O_2, and nitrate, denoted NO_3^-, are jointly introduced into a hydraulically heterogeneous aquifer with the infiltrating water. The synchronous injection of an idealized conservative tracer provides information about the groundwater behavior without the influence of bioreactive processes. Aerobic and denitrifying bacteria, denoted CH_2O^{aer} and CH_2O^{den}, transform DOC to CO_2 and biomass. The presence of dissolved oxygen inhibits denitrification in a non-competitive way, whereas aerobic degradation is not affected by nitrate. The two microbial populations grow upon the transformation of DOC but cannot exceed a maximum biomass concentration. The latter accounts for real limitation factors commonly found in nature, such as restricted nutrient availability or predator–prey balance. The two types of biomass are considered immobile and undergo first-order decay, which may reflect biomass maintenance, grazing, or any other process reducing the biomass in non-growth periods. Table 1 lists the reactions considered.

The mathematical expressions substituted as reactive source–sink terms into the 2-D and 1-D transport equations to account for the microbial reactions are listed in Appendix B. The associated parameters are listed in Table B.1.

3.2. Setup of the model

The virtual truth consists of 2-D heterogeneous aquifers with spatially correlated random log-hydraulic conductivity fields $\ln K(\mathbf{x})$ shown in the top row of Fig. 2. These fields are multi-Gaussian random space variables with an isotropic exponential covariance function. The integral scale of the covariance function is $l_x = l_y = 0.1$ m. In the base case, the variance of log-hydraulic conductivity is $\sigma_{lnK}^2 = 1$ and the uniform

Table 1
Microbial reactions considered.

Growth of aerobic bacteria:
$$CH_2O + (1 - Y_{eff}^{aer})O_2 \rightarrow (1 - Y_{eff}^{aer})CO_2 + (1 - Y_{eff}^{aer})H_2O + Y_{eff}^{aer}CH_2O^{aer}$$
Mineralization of aerobic bacteria:
$$Y_{eff}^{aer}CH_2O^{aer} + Y_{eff}^{aer}O_2 \rightarrow Y_{eff}^{aer}CO_2 + Y_{eff}^{aer}H_2O$$
Net aerobic degradation at steady state ($\Delta G^0 = -501$ kJ/mol at pH 7):
$$CH_2O + O_2 \rightarrow CO_2 + H_2O$$
Growth of denitrifying bacteria:
$$CH_2O + \tfrac{4}{5}\left(1 - Y_{eff}^{den}\right)NO_3^- + \tfrac{4}{5}\left(1 - Y_{eff}^{den}\right)H^+ \rightarrow \rightarrow \tfrac{4}{10}\left(1 - Y_{eff}^{den}\right)N_2 + \left(1 - Y_{eff}^{den}\right)CO_2 + \tfrac{7}{5}\left(1 - Y_{eff}^{den}\right)H_2O + Y_{eff}^{den}CH_2O^{den}$$
Mineralization of denitrifying bacteria:
$$Y_{eff}^{den}CH_2O^{den} + \tfrac{4}{5}Y_{eff}^{den}NO_3^- + \tfrac{4}{5}Y_{eff}^{den}H^+ \rightarrow \tfrac{4}{10}Y_{eff}^{den}N_2 + Y_{eff}^{den}CO_2 + \tfrac{7}{5}Y_{eff}^{den}H_2O$$
Net denitrification at steady state ($\Delta G^0 = -476$ kJ/mol at pH 7):
$$CH_2O + \tfrac{4}{5}NO_3^- + \tfrac{4}{5}H^+ \rightarrow \tfrac{4}{10}N_2 + CO_2 + \tfrac{7}{5}H_2O$$

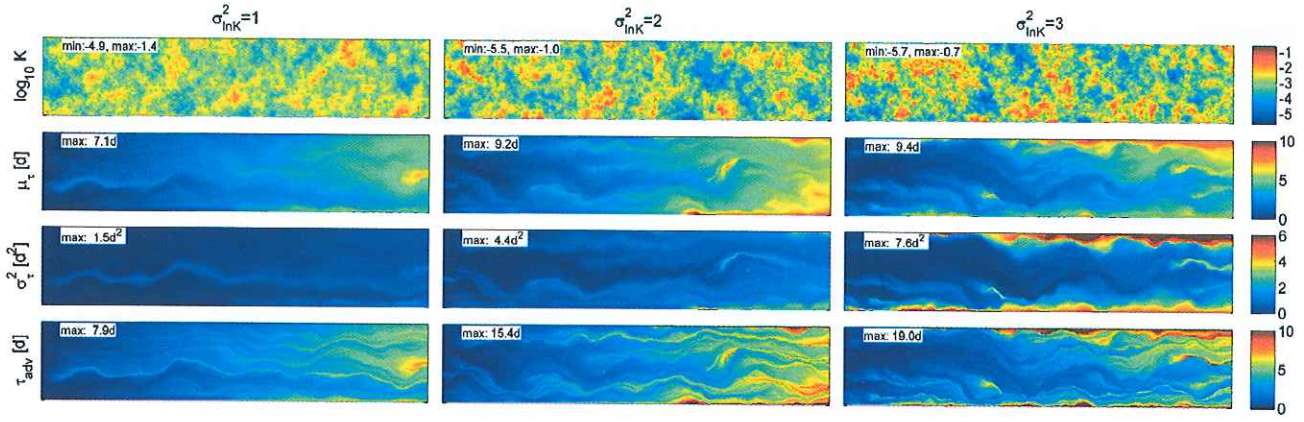

Fig. 2. Spatial distribution of the log-hydraulic conductivity for three levels of heterogeneity (top row); corresponding local mean groundwater age μ_τ (second row), local variance σ^2_τ of groundwater age (third row), and advective arrival time τ_{adv} (bottom row). Left column: variance of log-conductivity $\sigma^2_{\ln K} = 1$, center column: $\sigma^2_{\ln K} = 2$, right column: $\sigma^2_{\ln K} = 3$.

geometric mean K_g of hydraulic conductivity is $1 \cdot 10^{-3}$ m/s. The domain size is length × width = 5 m × 1 m. At the left and right boundaries of the domain, the hydraulic head is fixed, whereas the top and bottom boundaries are closed for flow. The head difference between the left and right boundaries is adjusted in such a way that the mean seepage velocity is 1 m/day, 0.02315 m for the 2-D domain, and 0.2315 m for the 1-D domain, which is ten times longer. Table 2 contains values of geometrical, flow, and transport parameters.

For solute transport, the domain is discretized by a streamline-oriented grid with $n_{str} = 500$ stream tubes and $n_{sec} = 200$ sections in flow direction (Cirpka et al., 1999b,c). Table 3 lists the initial and boundary conditions for reactive transport. The simulated time period is 30 days, which is 6 times the overall mean travel time at the outflow boundary. It is assumed that reactive transport achieves quasi-steady state conditions at the end of the simulation.

The travel-time based transport models consist of a single stream-tube each. They differ in the definition of the dispersion coefficient: (i) Zero dispersion is considered in the stochastic-convective model. Here the concentration only depends on the advective arrival time, τ_{adv}. (ii) In the simple advective–dispersive stream-tube model, we assume the same local longitudinal dispersion coefficient as that applied in the 2-D model, but rescaled to be applicable in travel-time rather than spatial coordinates: $D_\tau = D_\ell/\bar{v}^2$. (iii) In the improved advective–dispersive stream-tube model, we estimate an effective dispersion coefficient in travel-time coordinates, D_τ, which increases linearly with distance/mean groundwater age: $D_\tau = D_{\tau,0} + s\mu_\tau$, in which $D_{\tau,0}$ is the dispersion coefficient at the inflow boundary and s [−] is the derivative $\partial D_\tau/\partial\mu_\tau$. These coefficients are evaluated by performing a 2-D conservative transport simulation with the spatially explicit model, mapping the concentrations onto the mean groundwater age μ_τ at each point $\mathbf{x}$ in the domain, and fitting a 1-D model in travel-time coordinates to meet the breakthrough curves.

The 2-D model and the three travel-time based 1-D models are computed for six scenarios constructed by combination of the selected two key parameters: the variance of log-hydraulic conductivity $\sigma^2_{lnK} = 1, 2, 3$, and the transport boundary conditions, where we compare a Heaviside injection of solutes and transient inflow concentrations of dissolved oxygen and

Table 2
Geometrical and hydraulic parameters.

Symbol	Meaning	Value
Geometrical parameters of the 2-D domain		
L	Length of the 2-D domain	5 m
w	Width of the 2-D domain	1 m
n_x	Number of cells in x-direction for flow calculation	250
n_y	Number of cells in y-direction for flow calculation	200
Δx	Cell size in x-direction for flow calculation	0.02 m
Δy	Cell size in y-direction flow calculation	0.005 m
n_{str}	Number of stream tubes for transport	500
n_{sec}	Number of stream-tube-sections for transport	200
Discretization of travel-time models		
τ_{max}	Length of the travel-time domain	50 days
$\Delta\tau$	Travel-time increment	0.02 days
Geostatistical parameter of K-field		
$l_x = l_y$	Correlation length	0.1 m
σ^2_{lnK}	Variance of log-hydraulic conductivity	1,2,3
K_g	Geometric mean of hydraulic conductivity	$1 \cdot 10^{-3}$ m/s
Flow characteristics (for $\sigma^2_{lnK} = 1$)		
K_{eff}	Effective hydraulic conductivity	$1.1 \cdot 10^{-3}$ m/s
$\bar{q}_x$	Mean specific discharge ($\forall\ \sigma^2_{\ln K}$)	0.4 m/day
$\bar{v}_x$	Mean seepage velocity ($\forall\ \sigma^2_{\ln K}$)	1 m/day
J	Mean hydraulic gradient	$4.63 \cdot 10^{-3}$
Transport parameters		
θ	Porosity	0.4
α_ℓ	Longitudinal dispersivity (2-D)	0.01 m
α_t	Transverse dispersivity (2-D)	0.001 m
D_p	Pore diffusion coefficient	10^{-9} m²/s

Table 3
Initial and boundary conditions for reactive transport.

Symbol	Meaning	Initial conc.	Inflow conc.
$c_m^{CH_2O}$	Dissolved organic carbon	0 μM	500 μM
$c_m^{O_2}$	Dissolved oxygen	0 μM	250 μM
$c_m^{NO_3^-}$	Nitrate	0 μM	100 μM
c_m^{tracer}	Tracer	0 μM	100 μM
c_{im}^{aer}	Aerobic bacteria	1 μM	n.a.
c_{im}^{den}	Denitrifying bacteria	1 μM	n.a.

the inert tracer. The latter case aims at simulating diurnal fluctuations of dissolved oxygen in surface water due to radiation-dependent photosynthesis. The oxygen concentration ranges between $c^{O_2}_{min} = 200$ μmol/L and $c^{O_2}_{max} = 400$ μmol/L. The time-periodic inflow concentration of oxygen is defined by:

$$c^{(i)}_{daily} = \frac{c^{(i)}_{min} + c^{(i)}_{max}}{2} + \left(\frac{c^{(i)}_{max} - c^{(i)}_{min}}{2.313}\right) \cdot \sum_{j=1}^{\infty} \exp(1-j) \cdot \cos(2\pi j f t + 1.5\pi - 0.6 j\pi) \quad (19)$$

in which f [T^{-1}] is the base frequency of 1/day, and index j is the order of the harmonics. The diurnal signal rises more quickly than it drops.

3.3. Numerical methods

The auto-correlated hydraulic-conductivity fields are generated by the spectral approach of Dietrich and Newsam (1993) on a rectangular grid, on which the groundwater flow equation is solved by the cell-centered Finite Volume Method (FVM). For the 2-D spatially explicit transport model, we generate streamline-oriented grids and apply the cell-centered FVM to solve advective–dispersive transport on these grids using upwind differentiation of the advective term (Cirpka et al., 1999b,c) and the implicit Euler method for temporal discretization. The streamline-oriented grids suppress artificial transverse dispersion commonly encountered when solving solute transport in heterogeneous domains. We thus can study effects of solute mixing on reactive transport without interference by numerical discretization errors. The bioreactive transport forms a nonlinear system of equations which is numerically solved by a fully implicit scheme based on the Newton–Raphson method. An adaptive time-step approach reduces the computational effort when the system is approaching steady state. The code is written in MATLAB®, and the UMFPACK solver is used to solve for the resulting systems of linear equations (Davis and Duff, 1997). The travel-time based 1-D models use the same methods (fully implicit coupling, cell-centered FVM, upwind differentiation, Newton–Raphson method) for bioreactive transport.

4. Results

4.1. Spatial distribution of groundwater age

Fig. 2 shows the spatial distributions of the log-hydraulic conductivity $\log_{10}K$ (top row), the mean (second row) and variance (third row) of groundwater age, μ_τ and σ^2_τ, and the advective arrival time τ_{adv} (bottom row) for the cases of $\sigma^2_{lnK} = 1$ (left column), $\sigma^2_{lnK} = 2$ (center column), and $\sigma^2_{lnK} = 3$ (right column). Flow is from left to right, and thus travel times increase in this direction, too. The advective arrival time τ_{adv} increases monotonically with travel distance. In low-velocity regions, which coincide with low-conductivity regions, the gradient of τ_{adv} in the local flow direction is the highest (see bottom row of Fig. 2). The higher the variance of log-conductivity σ^2_{lnK}, the larger is the range of log-conductivity and thus velocity values. This leads to a stronger variability of τ_{adv}, with narrow stripes of advectively old water adjacent to stripes of young water. In principle, the mean groundwater age μ_τ (see Appendix A) follows the same patterns (see second row of Fig. 2), but local-scale transverse dispersion makes adjacent stream tubes exchange water parcels of different ages. As a consequence, the variability of the mean groundwater age μ_τ within a cross-section for a given longitudinal coordinate x is considerably smaller than that of advective arrival time τ_{adv}. Locations at which strong contrasts in mean groundwater age μ_τ are smoothed are those where the variance σ^2_τ of groundwater age (see Appendix A) increases (see third row of Fig. 2). Places with a large value of σ^2_τ are those locations where we expect that a travel-time based non-linear reactive transport model relying on a single characteristic travel time at each location may fail. This holds particularly true for "hot spots" of large σ^2_τ-values, where most likely the full distribution of τ does not resemble the inverse Gaussian distribution expected by Fickian-like dispersion.

4.2. Reactive system behavior in 1-D transport

Fig. 3 shows the concentrations of the mobile compounds (inert tracer, DOC, oxygen, and nitrate) and the immobile microbial biomasses (aerobic and denitrifying bacteria) as a function of travel time and real time for the case of a continuous injection of the mobile compounds into the 1-D travel-time domain with constant dispersion coefficient D_τ. Note that with the given seepage velocity of $v = 1$ m/day, the advective travel time τ_{adv} in days is identical to the travel distance x in meters. The concentrations of mobile compounds are normalized by the corresponding inflow concentrations, whereas the bacteria concentrations are normalized by the corresponding maximum biomass concentrations. We may characterize the reactive system by means of characteristic times, τ_{aer} and τ_{den}, for aerobic degradation and denitrification, respectively, scaling the inflow concentration of the corresponding electron acceptor with the product of the maximum specific turnover rate of that electron acceptor and the maximum biomass concentration:

$$\tau_{aer} = \frac{c^{O_2}_{in}}{k^{max}_{aer,growth} \cdot F_{O_2/DOC} \cdot c^{aer}_{max}} \Rightarrow L_{aer} = v\tau_{aer} \quad (20)$$

$$\tau_{den} = \frac{c^{NO_3^-}_{in}}{k^{max}_{den,growth} \cdot F_{NO_3^-/DOC} \cdot c^{den}_{max}} \Rightarrow L_{den} = v\tau_{den} \quad (21)$$

in which we have also computed characteristic length scales, L_{aer} and L_{den}, for aerobic degradation and denitrification. Eqs. (20) & (21) pose lower limits of reaction times and distances because neither the maximum biomass concentration nor the maximum specific reaction rate will be achieved throughout the domain. With the reactive parameter values listed in Table B.1, we obtain $\tau_{aer} = 0.66$ days and $\tau_{den} = 1$ day. As the mean groundwater age at the outlet of the 2-D domain is five days, complete consumption of both oxygen and nitrate within the domain appears possible if the delivery of the organic substrate is sufficient.

The space–time behavior of the reactive system may be described as follows: Initially, the domain does not contain dissolved oxygen, nitrate, and DOC; and the initial biomass

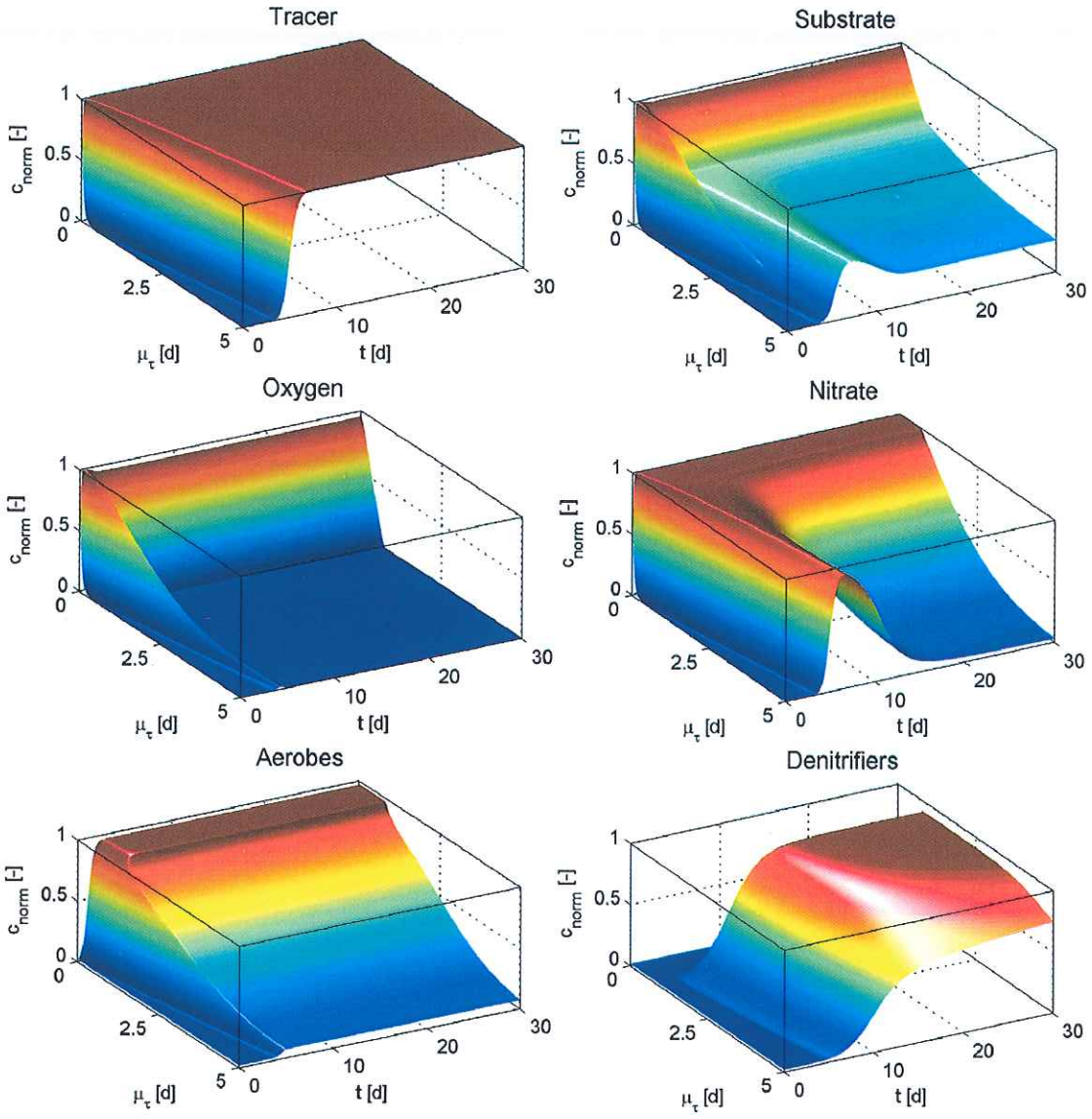

Fig. 3. Normalized concentrations of tracer and reactive compounds as function of mean groundwater age μ_τ and real time t in the 1-D model with constant local dispersion coefficient. Heaviside injection of the dissolved compounds.

concentrations of aerobic and denitrifying bacteria are small. The dissolved compounds are jointly introduced into the system. Because the biomass concentrations are so small, the dissolved compounds can penetrate the system at early times, fostering the growth of aerobic bacteria whereas the denitrifying bacteria are inhibited by the presence of oxygen. Near the inlet, the aerobic bacteria nearly reach the maximum biomass concentration. As a consequence, the oxygen concentration starts dropping, finally reaching an almost linear steady-state spatial profile over the characteristic travel time τ_{aer} given above. At locations depleted of oxygen, the aerobic bacteria slowly become extinct due to aerobic-biomass decay. Once the oxygen concentrations are below the inhibition concentration for the denitrifying bacteria, the latter start growing. The inhibition of denitrification by oxygen leads to a clear zonation of a denitrifying zone downstream of the aerobic zone (Kinzelbach et al., 1991). In the aerobic zone, the biomass concentration of the denitrifying bacteria remains low and may even further decrease, whereas at the upstream end of the denitrifying zone the biomass concentration of the denitrifying bacteria approaches almost the prescribed maximum value.

At steady state, the profiles of concentration in travel time exhibit a clear bend at the transition between the aerobic and denitrifying zones. Here, the oxygen profile turns from a linear trend to an approximately constant value of zero; the nitrate profile turns from the constant value of the inflow concentration to an approximately linear trend; the DOC profile turns from an approximately steep linear trend to another almost linear trend with smaller slope; the biomass of aerobic bacteria starts dropping; and a rapid increase of denitrifying bacteria can be observed. This nonlinear behavior is of particular relevance when assessing effects of transverse mixing in the 2-D simulations.

Fig. 4 shows the same plot for the diurnal fluctuations of the tracer- and oxygen-concentration in the inflow. Here, the zone penetrated by oxygen moves back and forth. This also affects

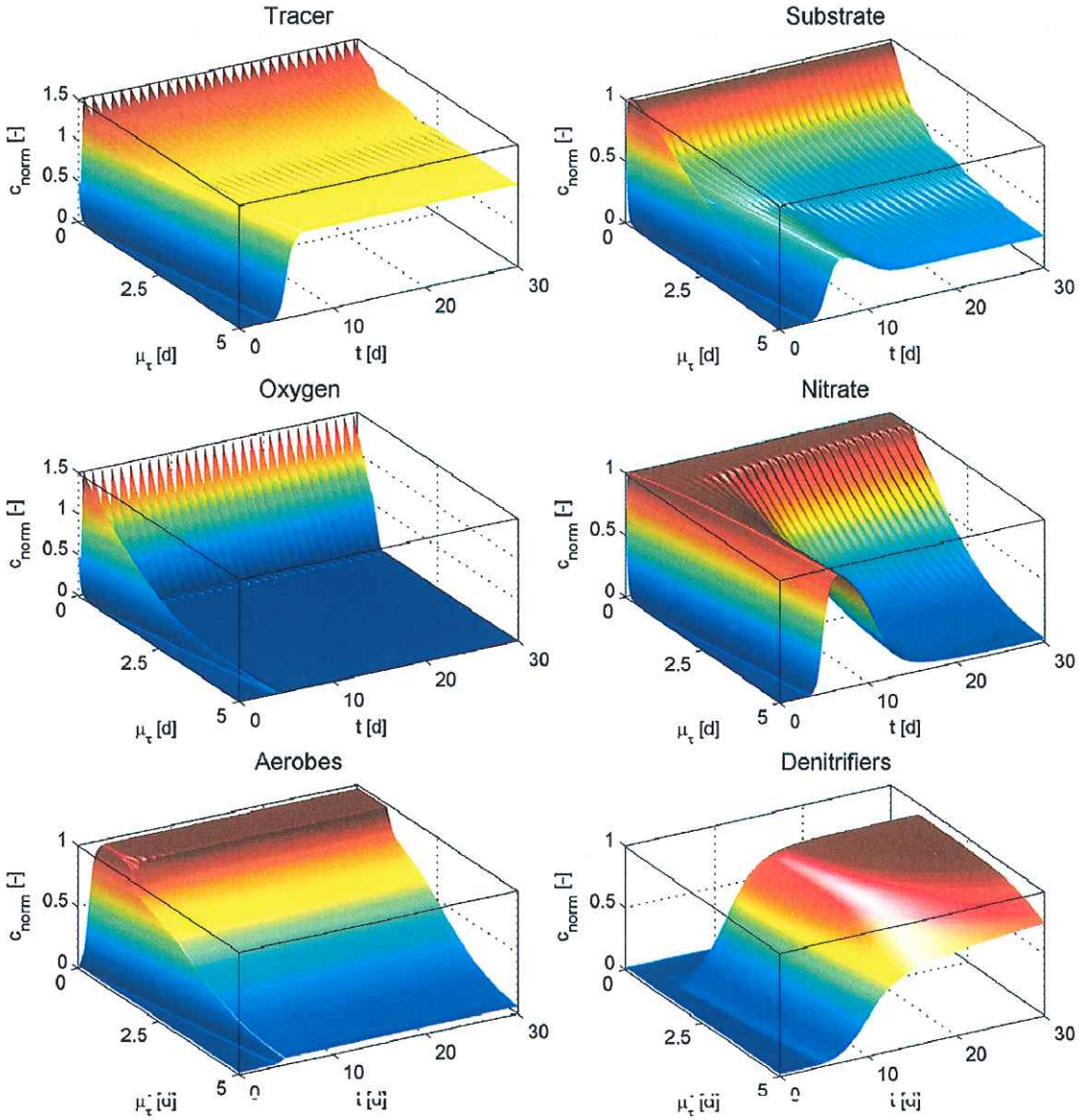

Fig. 4. Normalized concentrations of tracer and reactive compounds as function of mean groundwater age μ_τ and real time t in the 1-D model with constant local dispersion coefficient. Diurnal fluctuation of the tracer and oxygen concentration in the inflow.

the inhibition of denitrification so that the nitrate profiles exhibit oscillations. The fluctuating input of electron acceptors also causes time-periodic variations of the substrate concentration. In the zone where oxygen at a significant concentration is present only over a fraction of time, aerobic and denitrifying bacteria coexist at high concentrations, but they are active at different times. The maximum decay rate coefficients of the bacteria $k^{max}_{aer,dec} = k^{max}_{den,dec} = 0.1$/day are so small that diurnal fluctuations are strongly smoothed.

4.3. Comparison between spatially explicit and travel-time based models

In the following, we denote the concentrations of the spatially explicit, 2-D "virtual truth" $c^{(i)}_{2D}$, whereas the three travel-time based models are denoted $c^{(i)}_{adv}$ for the model with zero dispersion, $c^{(i)}_{D_\ell}$ for the case with a uniform dispersion coefficient $D_\tau = D_\ell/\overline{v}^2$ in travel-time coordinates, and $c^{(i)}_{D_{eff}}$ for the case with a linearly increasing dispersion coefficient $D_\tau = D_{\tau,0} + s\mu_\tau$, respectively.

4.3.1. Base case with mild heterogeneity and continuous substrate injection

Fig. 5 shows a comparison of concentrations for constant inflow concentrations and mild heterogeneity ($\sigma^2_{lnK} = 1$) at times $t = 3$ days (left two columns) and $t = 30$ days (right two columns). The first time point is when the solution of dissolved compounds has not yet penetrated the entire domain. This example highlights the effects of heterogeneity and mixing on the validity of travel-time based models at an invading front. The second time point is when steady state of the mobile compounds has almost been reached. All concentrations are expressed as a function of travel times. That is, the virtually true concentrations $c^{(i)}_{2D}(\mathbf{x})$ are plotted as a function of the travel

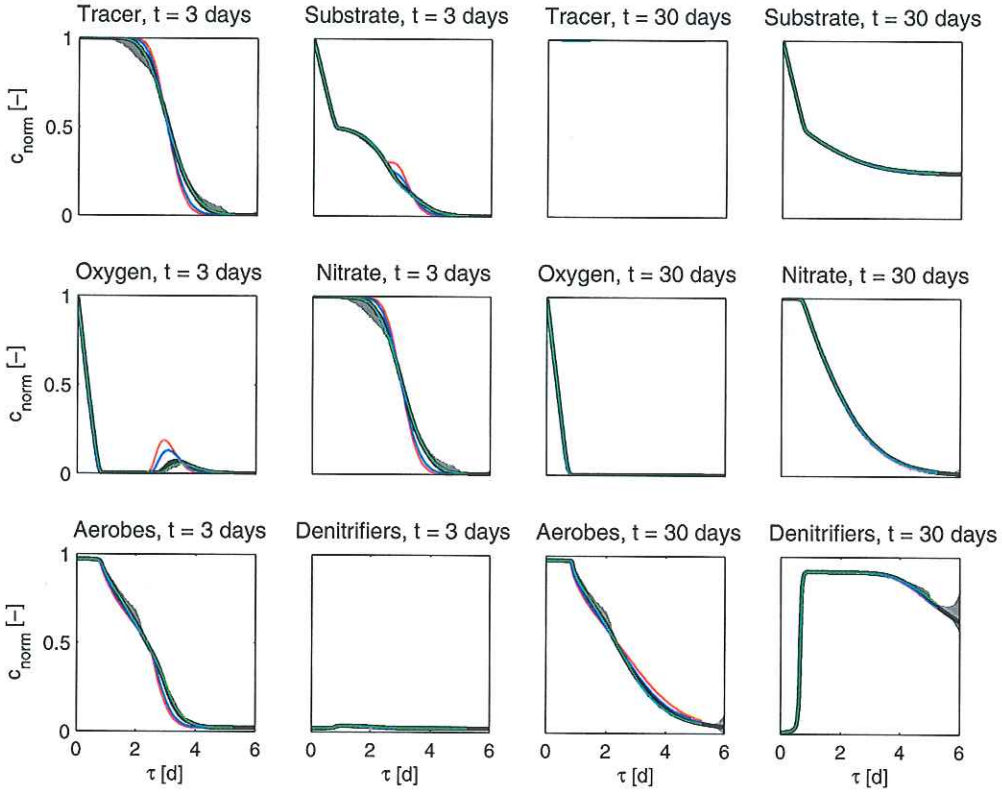

Fig. 5. Comparison of normalized concentrations between the "virtually true" 2-D model and the various travel-time based models at times $t = 3$ days and $t = 30$ days for continuous injection and $\sigma^2_{\ln K} = 1$. The 2-D concentrations are also plotted as function of travel time. Gray area: 5% to 95% quantiles of $c^{(i)}_{2D}$; bold black line: median of $c^{(i)}_{2D}$; red line: results of the stochastic-convective model ($c^{(i)}_{adv}$); blue line: advective–dispersive stream-tube model with constant local-scale dispersion coefficient $\left(c^{(i)}_{D_\ell}\right)$; green line: advective–dispersive stream-tube model with linearly increasing dispersion coefficient $\left(c^{(i)}_{D_{eff}}\right)$. (For interpretation of the references to color in this figure legend, the reader is referred to the web version of this article.)

time $\mu_\tau(\mathbf{x})$, resulting in a distribution of values for any given mean groundwater age.

At the invading front (see the two left columns of Fig. 5), we see that the tracer shows some variation of concentration when plotted in terms of travel time, which indicates that the proposition of Eq. (1) cannot be fully true. However, the 5%-to-95% range of $c^{tracer}_{2D}(\mu_\tau)$, expressed as gray band, is comparably narrow even at the invading front. As we will see in the following, the spatial variability is quite considerable, and it appears that a large fraction of the variability can be explained by the variability of groundwater age. Among the 1-D travel-time based models, the one with the fitted linear trend of $D_\tau(\mu_\tau)$ shows the best reproduction of the tracer front, which is not surprising as it was fitted to meet the tracer breakthrough curves. The purely advective model shows the least spread of the profile; the numerically correct solution would actually show a perfect step-like front, which is not achievable by using a Finite Volume Method for advection with upstream differentiation and implicit time integration. The model with the constant value of D_τ shows more spreading than the presumably advective model, but not as much as observed in the virtual truth $c^{tracer}_{2D}(\mu_\tau)$.

The mixing at the invading front affects the concentrations of the tracer and nitrate in a similar way. This is so because denitrification is inhibited by the presence of oxygen, and oxygen is introduced into the domain together with nitrate, DOC, and the tracer. The oxygen profile shows a peak running ahead, which is approximated at the wrong location and with a wrong peak height in the case of the 1-D models underestimating effective mixing. This first peak coincides with the head of the tracer front. At the invading front, the biomass density of the aerobes is too small to cause significant biodegradation. At locations closer to the inlet, the aerobic biomass has already grown to concentrations that allow practically complete oxygen degradation within a small distance.

At the late time point of $t = 30$ days the agreement between all travel-time based models and the virtual truth is very good. The narrow 5%-to-95% range of $c^{(i)}_{2D}(\mu_\tau)$, shown as gray band, implies that the basic proposition of Eq. (1), namely that local concentrations of reactive species can be explained by the travel time at that location, holds for the given scenario at late times, when the initial front has passed through and biomass has grown up almost to steady-state densities. The 5%-to-95% range of $c^{(i)}_{2D}(\mu_\tau)$ gets wider for mean groundwater ages larger than 5 days, which we attribute to outflow boundary effects, because the overall mean travel time through the entire domain is 5 days, and the sample size of concentration gets smaller and non-representative for any local mean groundwater age larger than that value. A second case of deviations in the given scenario at the given time can be observed for the concentration of the aerobic bacteria in the part of the domain where oxygen has already been completely consumed. The

deviations are remnants of bigger differences between the spatially explicit and travel-time based models at earlier times.

For the sake of clarity, Fig. 6 shows the spatial distribution of normalized c_{2D} of nitrate during the initial invasion ($t = 3$ days, left column) and at quasi steady state ($t = 30$ days, right column) together with the associated normalized residual errors of the three travel-time approaches according to Eq. (17) for the base case with continuous injection and $\sigma^2_{\ln K} = 1$. The plot at $t = 3$ days illustrates how irregularly the compounds invade the domain. The interplay between variability of advection and local transverse dispersion causes enhanced dilution at the front, which is not sufficiently captured by the 1-D travel-time based models with zero or constant local longitudinal dispersion coefficients. This is clearly reflected by a band of positive residual errors at the head and negative residual errors at the tail of the front. A specific low-conductivity feature at the lower half of the domain close to the inlet poses a problem to all three travel-time based models. This feature causes a "shadow" of low concentration values further downstream where old water and young water mix.

The late-time results, shown in the right column of Fig. 6, exhibit a continuous band of small negative residual errors along the transition zone where nitrate starts to decrease in concentration. Here, mixing of younger and older water deteriorates the performance of travel-time based models because the dependence of nitrate (and oxygen) concentrations on travel time is strongly nonlinear. However, the error along this band is smaller than two distinct features of positive residual errors that coincide with areas of large variance σ^2_τ of groundwater age (see Fig. 2, third row, first column). The first feature at the left half of the domain can be attributed to a low-K lens and has been discussed above, the feature causes low velocity and large values of mean groundwater age μ_τ (see Fig. 2, second row, first column). Also the second such feature originates at a low-K inclusion at the bottom of the right half of the domain. The residual errors are the biggest for the stochastic-convective model neglecting dispersive mixing altogether, and the smallest for the model with the fitted linear increase of D_τ that captures part of the mixing effects, but the differences among the travel-time based models are subtle at quasi steady state.

The magnitude of residual errors is smaller for the other mobile compounds (not shown), whereas they are somewhat bigger for the two types of biomass concentration. Fig. 7 shows the spatial profiles of concentrations of aerobic biomass at $t = 3$ days (left column) and $t = 30$ days (right column) together with the residual errors of the projected 1-D concentrations. The general patterns are comparable to those shown for nitrate (Fig. 6). However, at the invading front we see two bands of positive residuals along the front position, whereas the residuals of nitrate exhibit a positive band and a negative band. The first front of residual errors may be caused by the underestimation of oxygen at the same location, whereas the second front may reflect the mixing zone in aerobes growth.

4.3.2. Normalized root mean square deviation as function of time

This section discusses the transient behavior of the residual errors in the whole domain for all hydraulic conductivity fields, $\sigma^2_{lnK} = 1$, 2 and 3. Fig. 8 represents the evolution of the NRMSD according to Eq. (18) as a function of time, here expressed as pore volumes $PV = t \cdot \bar{v}/L$, for the scenarios of constant inflow concentrations. As discussed above, the travel-time based models with zero and constant small D_τ underestimate solute mixing at the invading front, which is seen by comparably large NRMSD-values for the tracer and nitrate in about the first two pore volumes until the first front has fully broken through. Increasing the strength of heterogeneity (see the dashed lines for $\sigma^2_{lnK} = 2$ and the dotted lines for $\sigma^2_{lnK} = 3$) increases the effects; also the stronger spreading of the solute front leads to a large temporal extent of the error. The concentrations for the linearly increasing D_τ, i.e. $c^{tracer}_{D_{eff}}$ and $c^{NO_3}_{D_{eff}}$, show approximately the same small NRMSD for $\sigma^2_{lnK} = 1$ and $\sigma^2_{lnK} = 2$, whereas the error is larger even though less than 5% for $\sigma^2_{lnK} = 3$. The latter indicates that the assumption that effective solute mixing can be parametrized by a dispersion law with scale dependent dispersion coefficient becomes invalid if heterogeneity is too big. Whether in these cases non-Fickian formulations for effective transport behavior in travel-time coordinates would lead to better results, is beyond the scope of the present study.

The NRMSD for oxygen decreases more quickly than that of the tracer and of nitrate. This is so because the aerobic bacteria

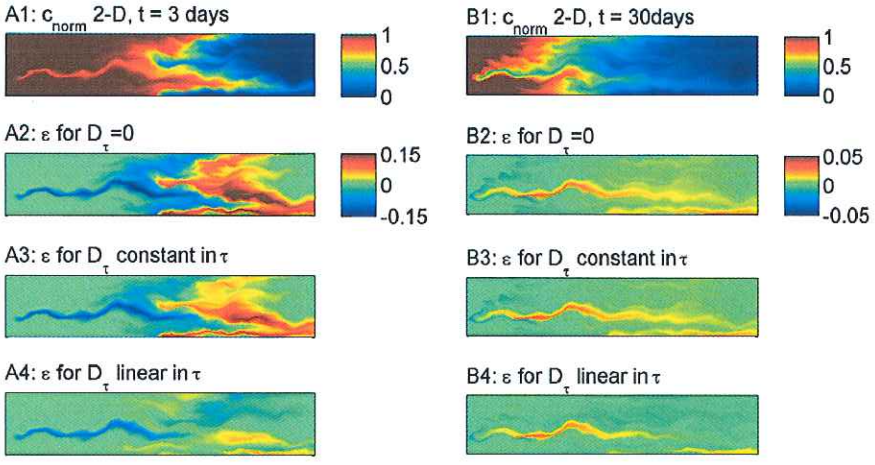

Fig. 6. Spatial distribution of the normalized nitrate concentration, $c^{NO_3^-}_{norm}$, (top row) and normalized residual errors obtained by comparison of the "virtual truth" with the concentration of the travel-time based models. Second row: stochastic-convective model; third row: advective–dispersive stream-tube model with constant D_τ; bottom row: advective–dispersive stream-tube model with linearly increasing D_τ. Left column: $t = 3$ days; right column: $t = 30$ days. Continuous injection of compounds, $\sigma^2_{\ln K} = 1$.

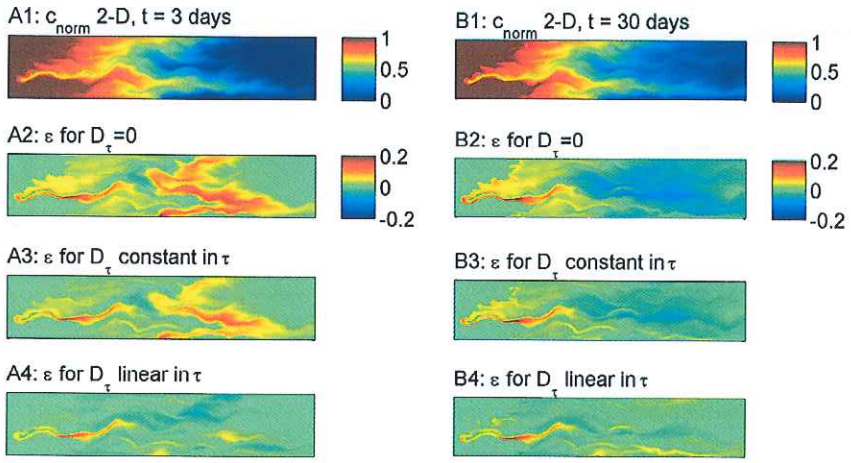

Fig. 7. Spatial distribution of the normalized concentration of aerobic bacteria (top row) and normalized residual errors obtained by comparison of the "virtual truth" with the concentration of the travel-time based models. Second row: stochastic-convective model; third row: advective–dispersive stream-tube model with constant D_τ; bottom row: advective–dispersive stream-tube model with linearly increasing D_τ. Left column: $t = 3$ days; right column: $t = 30$ days. Continuous injection of compounds, $\sigma^2_{\ln K} = 1$.

grow quickly and oxygen does not penetrate the domain very far, with the exception of the small peak unaffected by aerobic degradation discussed above. The approximation of aerobic bacteria evolves together with that of oxygen. The biggest errors occur when the oxygen and DOC fronts move into the system. In contrast to oxygen, however, the NRMSD-values of the aerobic bacteria remain at a higher value at late times. We interpret this as a slightly wrong spatial distribution of these bacteria in quasi steady state when using the travel-time based models, but they hardly influence the concentrations of the dissolved compounds. Note again, that the model with the fitted effective dispersion coefficient D_τ scores best.

As long as oxygen is present where nitrate can be found, denitrification is suppressed. This explains why the NRMSD-values for the denitrifiers are initially zero: No matter which model is applied, at early times there is no denitrification and

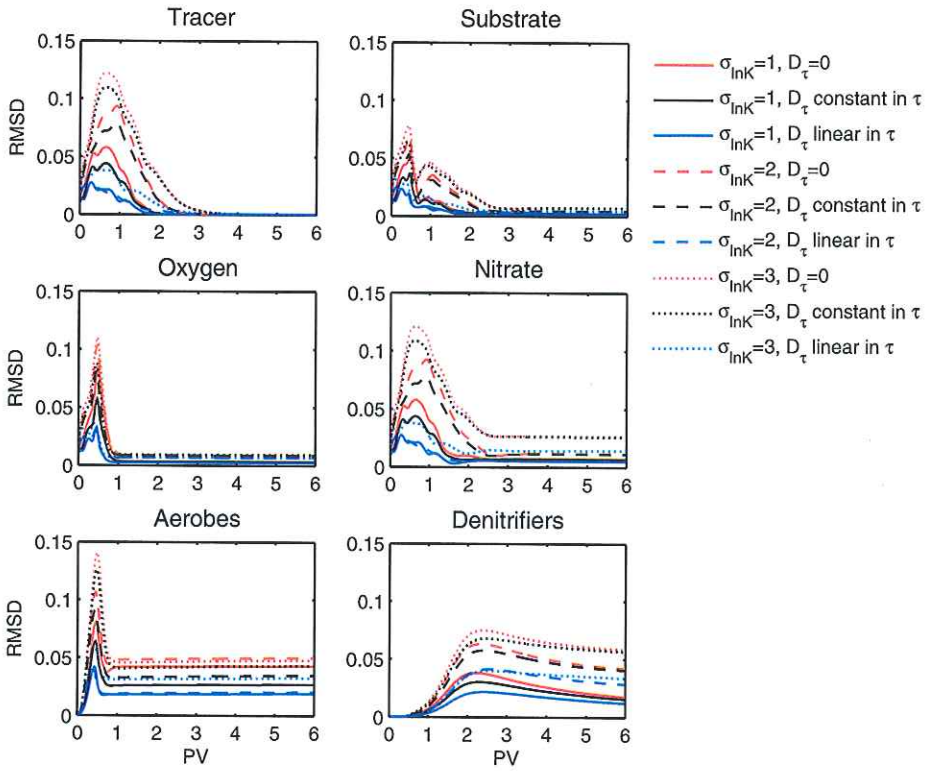

Fig. 8. Normalized root mean squared deviation (NRMSD) of all compounds over the entire domain as function of dimensionless time (*PV*) for the case of continuous injection. The three 1-D transport models are represented as follow: strictly advective transport (red), constant local-scale dispersion coefficient (black), and linearly increasing dispersion coefficient (blue). The variance of the log-hydraulic conductivity field is represented by solid lines for $\sigma^2_{lnK} = 1$, dashed lines for $\sigma^2_{lnK} = 2$, and dotted lines for $\sigma^2_{lnK} = 3$. (For interpretation of the references to color in this figure legend, the reader is referred to the web version of this article.)

thus no growth of denitrifiers. Already within the first pore volume denitrification starts to develop. The associated errors of mixing in the models with zero or constant D_τ lead to errors in substrate consumption (see the secondary peak of NRMSD for DOC at about 1 pore volume), nitrate (for which NRMSD does not decrease to zero at late times) and denitrifiers (exhibiting a smooth increase and slow decrease to a non-zero asymptotic value comparable to that of the aerobes). For all compounds, the error increases with σ^2_{lnK}, is the smallest for $c^{(i)}_{D_{eff}}$ and is the biggest for $c^{(i)}_{adv}$.

Fig. 9 shows the same plot of NRMSD as a function of dimensionless time as Fig. 8, but now for the fluctuating inflow concentration of the tracer and oxygen. The fluctuating boundary conditions make the travel-time based approximations much more sensitive with respect to effective longitudinal mixing. In essence, fronts are permanently propagating through the domain. As a consequence, the 1-D models with zero and constant D_τ exhibit non-zero NRMSD values for the tracer, oxygen, and DOC at late times. The error increases with increasing variance σ^2_{lnK} of log-hydraulic conductivity.

Fig. 10 summarizes the normalized root mean square deviations (NRMSD) of all compounds in all scenarios, averaged over the last day of simulation, when quasi-steady state has been reached. In all cases NRMSD remains below 8%. As stated above, increasing the variance σ^2_{lnK} of log-hydraulic conductivity and switching from constant to fluctuating inflow concentrations cause stronger deviations, particularly for the 1-D models with zero and small uniform dispersion coefficient D_τ in travel-time coordinates. In general, the biomass concentrations are less accurately approximated by the travel-time based models than the concentrations of mobile compounds, at least after the first invading front has moved through the entire domain.

5. Discussion and conclusions

Based on the analyses presented above we may try to answer the four main research questions listed in the Introduction section:

1 Is the proposition of Eq. (1) valid at individual points in the domain?
Eq. (1) proposes that the spatial variability of the "virtually true" concentrations $c^{(i)}_{2D}(\mathbf{x}, t)$ in the 2-D domain collapses to a clear dependence of concentration on time and travel-time, $c^{(i)}_{1D}(\tau(\mathbf{x}), t)$, thus reducing the dimensionality of the problem and also simplifying the calculation of reactive-species concentrations. We have explicitly addressed this question for the case of a small variance of log-hydraulic conductivity, $\sigma^2_{lnK} = 1$, and constant inflow concentrations of the tracer and oxygen in Fig. 5. The gray band in this plot indicates the 5%-to-95% quantiles of the spatially explicit reactive species concentrations as a function of local mean groundwater age μ_τ. These bands are quite narrow, even at early times when the initial front still propagates through the domain. For larger values of σ^2_{lnK}, these bands increase in

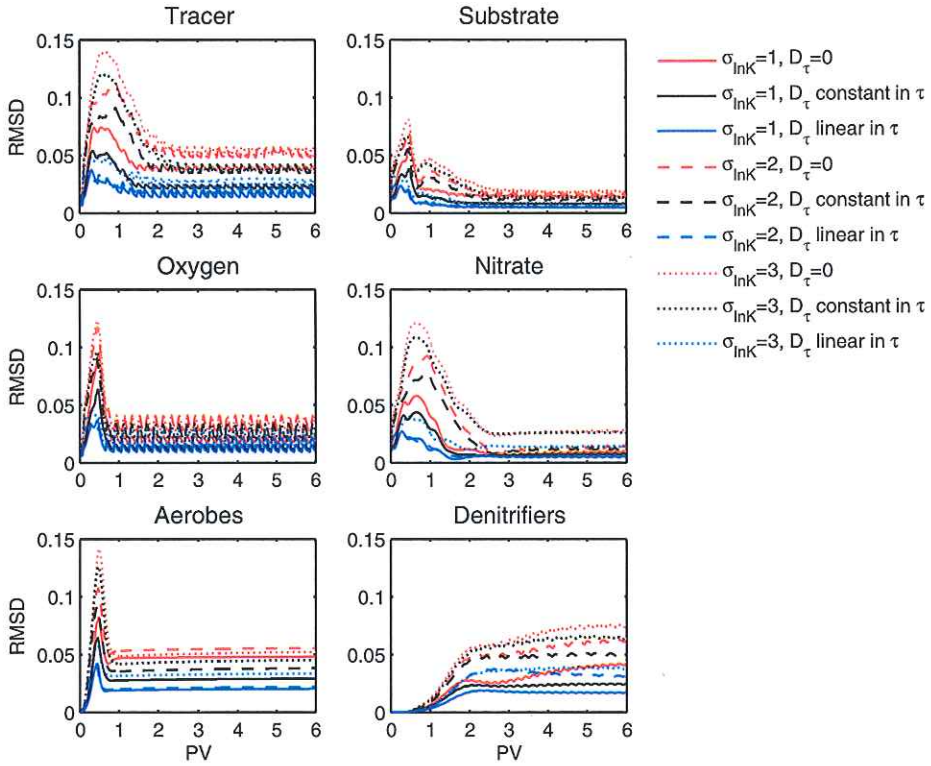

Fig. 9. Normalized root mean squared deviation (NRMSD) of all compounds over the entire domain as function of dimensionless time (*PV*) for the case of diurnal fluctuations in the tracer and oxygen inflow concentrations. The three 1-D transport models are represented as follow: strictly advective transport (red), constant local-scale dispersion coefficient (black), and linearly increasing dispersion coefficient (blue). The variance of the log-hydraulic conductivity field is represented by solid lines for $\sigma^2_{lnK} = 1$, dashed lines for $\sigma^2_{lnK} = 2$, and dotted lines for $\sigma^2_{lnK} = 3$. (For interpretation of the references to color in this figure legend, the reader is referred to the web version of this article.)

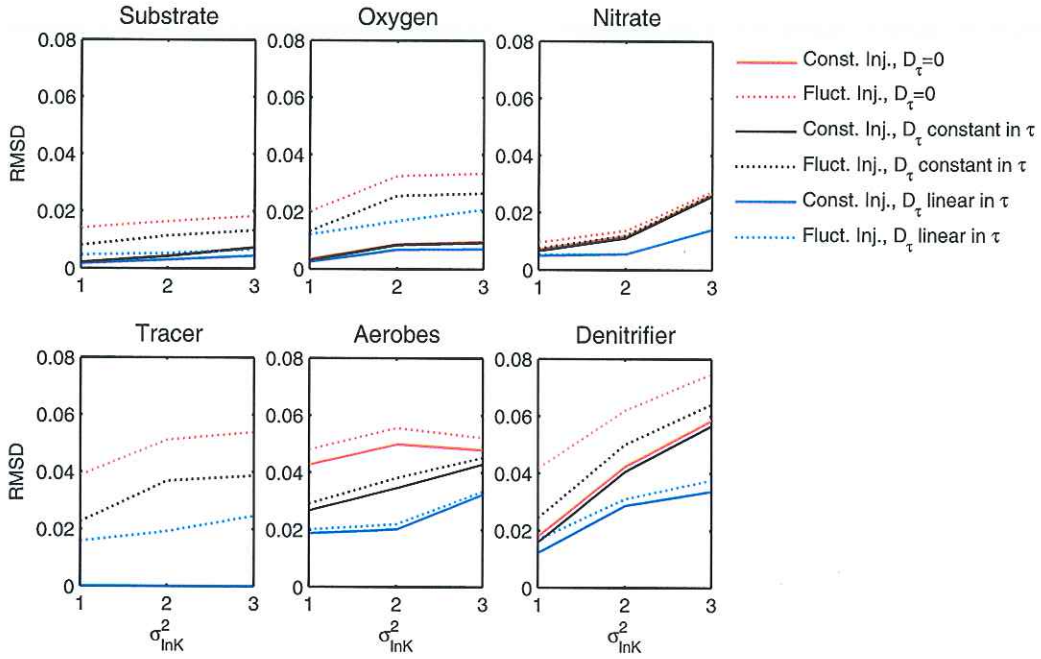

Fig. 10. Normalized root mean square deviations (NRMSD) of all compounds integrated over the whole domain and averaged over the entire day 30. The three 1-D transport models are represented as follow: strictly advective transport (red), constant local-scale dispersion coefficient (black), and linearly increasing dispersion coefficient (blue). Solid lines: constant inflow concentrations of the tracer and oxygen; dotted line: fluctuating inflow concentrations of the tracer and oxygen. Abscissa: variance σ^2_{lnK} of log-hydraulic conductivity. (For interpretation of the references to color in this figure legend, the reader is referred to the web version of this article.)

width but remain acceptable for most practical applications, given the usual uncertainty in the description of reactive processes. A small variation of $c^{(i)}_{1D}(\tau(\mathbf{x}), t)$ implies that a parametrization of reactive transport in travel-time coordinates may be possible, without indicating which parametrization would be most suitable.

The plots of normalized residuals in Figs. 6 & 7 point to locations in space and time where the validity of Eq. (1) is jeopardized. They are characterized by (i) mixing of young and old water in a travel-time range where (ii) the dependence of reactive-species concentrations on groundwater age is nonlinear. Hydraulic heterogeneity causes irregular propagation of solutes and thus facilitates mixing of water with different ages. In the discussion of Figs. 6 & 7, we have highlighted individual features of low-conductivity zones creating high variability of mean travel time and large variance of the local travel-time distribution. The relevance of this variability for approximating multidimensional transport by travel-time based models, however, is included in the 1-D plots of reactive-species concentrations in Figs. 3 & 4: Wherever these plots show nonlinear dependencies of $c^{(i)}_{1D}(\tau, t)$ on τ, the mixing of solute concentrations leads to results differing from evaluating reactive-species concentrations at the mixed groundwater age. This is more prevalent at the invading front than at quasi steady state, explaining the larger NRMSD-values at earlier times.

2 Is the mean groundwater age a sufficient predictor?
This question has already positively been answered by the comparably narrow distribution of reactive-species concentrations for a given mean groundwater age μ_τ discussed above. The narrow distribution of reactive-species concentration does not necessarily point to a narrow distribution of groundwater age at any given point, but the distribution must either be similar at points with identical mean groundwater age μ_τ, or the dependence of the reactive-species concentration on age must be almost linear. In the advective–dispersive stream-tube approach, it is implicitly assumed that the distribution of groundwater age follows an inverse Gaussian distribution, and that the variance σ^2_τ of travel time increases in a well defined manner with μ_τ. Strong deviations from this behavior are more likely in highly heterogeneous media than in mildly heterogeneous ones, which explains why the performance of the travel-time based model with linearly increasing D_τ deteriorates with increasing variance σ^2_{lnK} of log-hydraulic conductivity.

3. Which error is introduced by neglecting local dispersion altogether, as done in the stochastic-convective model?
In all scenarios considered, the stochastic-convective model gave the least accurate predictions of local concentrations in the 2-D domain, even though the normalized root mean square deviations may be considered moderate even in the worst case ($\sigma^2_{lnK} = 3$, fluctuating inflow concentration). There are two interrelated reasons for this behavior. First, the advective travel time τ_{adv} exhibits strong small-scale variations and is a poorer predictor of reactive-species concentrations than the smoother mean groundwater age μ_τ, because the variability of reactive-species concentrations is overestimated. Second, the implicit assumption of the stochastic-convective model is that the travel time at a given point is a unique value, whereas the other two models assume an inverse Gaussian distribution. It is interesting to see that neglecting mixing altogether has an effect on the performance of travel-time based models even for the given test case in which all reacting compounds are jointly introduced into the domain. While mixing is not a prerequisite for the reaction to take place, it affects reactive-species

concentrations and should be accounted for in an appropriate way. At quasi steady state in a mildly heterogeneous domain, the effects of mixing are the weakest and neglecting it altogether introduces only minor errors.

4. Can we derive a simple approach of obtaining effective longitudinal mixing coefficients within the travel-time framework from conservative transport and apply these mixing coefficients to reactive-transport problems?
   In the present study, we have successfully fitted a simple linear expression $D_\tau = D_{\tau,0} + s\tau$ for the effective dispersion coefficient in travel-time coordinates to the locally observed conservative-tracer breakthrough curves. We obtained an excellent performance of the travel-time based reactive transport simulations when using this parametrization in all the studied scenarios for mobile and immobile compounds at all times. This approach may be seen as a simple alternative to applying more complicated closed-form expressions, such as those of Dentz et al. (2000), as suggested by Cirpka (2002). A disadvantage of the approach is that local conservative-tracer data must be available to perform the fit. However, we see the proposed method mainly as a means to reduce computational costs of multidimensional reactive transport simulations. In this context, performing conservative-tracer simulations may be seen as an acceptable computational burden. Also, fitting empirical relationships to numerical tracer breakthrough curves has the advantage that typical restrictions of closed-form expressions, such as spatially uniform mean hydraulic gradient and a sufficiently large domain to achieve ergodicity do not apply.

In conclusion, travel-time models to solve nonlinear reactive transport problems in heterogeneous media pose an attractive alternative to spatially explicit multidimensional simulations because the computationally expensive reactive transport problem becomes one-dimensional in travel time (CPU sixfold lower in the present test case). We have designed our application such that the travel-time based approaches have a good chance in approximating two-dimensional reactive transport. Please recall that we considered a case in which the reaction is not controlled by macroscopic transverse mixing, as it is the case when compounds react with each other that enter the domain side by side. Furthermore we assumed that the reactive properties of the porous medium and the bacteria (e.g., maximum growth rate, Monod coefficients, specific yields) are uniform in space. Finally, we did not consider transient flow. This does not imply that the modeling approach taken here is limited to problems of this kind but consideration of either point will complicate the task of using travel-time based models when simulating contaminant transport in multiple dimensions. We believe that the additional use of exposure times, that is, the time that a solute parcel has been exposed to particular conditions rather than the mere time it has spent within the domain (Ginn, 1999), may help in overcoming problems of chemical heterogeneity. Macroscopic transverse mixing has already been taken into account in Cirpka et al. (1999a); Cirpka and Valocchi (2007); and Cirpka et al. (2012), among others. The consideration of transient flow is the subject of our current research.

A key result of our analysis is that solute mixing should be parametrized adequately in travel-time based models, even in applications where reacting compounds are jointly introduced. The computationally and conceptually simplest approach, in which dispersive mixing is neglected altogether, may lead to moderate errors. Mapping from 1-D travel-time based models to three-dimensional space is possible with the same procedures described herein. Compared to 2-D, solute mixing may have in 3-D a larger impact on reactive solute transport (e.g., Cirpka et al., 2015; Ye et al., 2015). We therefore assume that in 3-D applications the consideration of mixing in the travel-time based model is even more important. As an example, Marzadri et al. (2011) presented an advective–reactive model of dissolved oxygen and inorganic nitrogen in the hyporheic zone relying on an analytical flow field for gravel bars in the hyporheic zone characterized by a strong pool and ripple morphology of the river beds. This is a scenario comparable to our test case. Because oxygen concentrations in rivers are dynamic, the sensitivity of reactive transport with respect to solute mixing is relevant, so that we would argue that a parametrization of within-stream-tube mixing is advisable for the case studied by Marzadri et al. (2011), whereas we believe that a full-blown three-dimensional simulation of reactive transport is not necessary. This, however, needs to be confirmed in future research.

In the present study, we have restricted the parametrization of solute mixing to within-stream-tube dispersion. In the case of strong heterogeneity, this approach may not be sufficient and non-Fickian parametrizations such as multi-rate mass transfer (e.g., Willmann et al., 2010) or continuous-time random walk (e.g., Dentz et al., 2004; Edery et al., 2010) may become necessary. Most of these approaches are derived for a statistical ensemble of many aquifer realizations sharing the same geostatistical characterization. The typical target quantity is the concentration (or travel-time distribution crossing an observation plane) averaged over all members of the ensemble, whereas the reality consists only of a single realization. This implies potential confusion between mixing and spreading (Luo and Cirpka, 2008, 2011). That is, while describing solute transport along streamlines by non-Fickian transport equations may be necessary for strongly heterogeneous domains, currently no simple expressions are available that allow predicting the parameters of these models from available aquifer characteristics.

Acknowledgments

This research was funded by Deutsche Forschungsgemeinschaft (DFG) in the framework of the International Research Training Group GRK1829 "Integrated Hydrosystem Modelling" of the Universities of Tübingen, Hohenheim, and Waterloo.

Appendix A. Temporal moment generating equations

The k-th raw temporal moment of concentration at location $\mathbf{x}$ is defined as:

$$m_c^k(\mathbf{x}) = \int_0^\infty t^k c(\mathbf{x}, t)\, dt. \tag{A.1}$$

Under steady-state flow conditions, temporal-moment generating equations can be derived from the advection–dispersion equation (Eq. (2)) and its boundary conditions, Eqs. (4)&(5), for non-reactive constituents, by multiplying the

equations with t^k, integrating over time from zero to infinity, and applying rules of integration by parts, leading to:

$$\mathbf{v}\cdot\nabla m_c^k - \nabla\cdot\left(\mathbf{D}\nabla m_c^k\right) = k m_c^{k-1} \tag{A.2}$$

$$\mathbf{n}\cdot\left(\mathbf{v}m_c^k - \mathbf{D}\nabla m_c^k\right) = \mathbf{n}\cdot\mathbf{v}m_{inflow}^k \text{ at } \Gamma_{inlet} \tag{A.3}$$

$$\mathbf{n}\cdot\left(\mathbf{D}\nabla m_c^k\right) = 0 \text{ at } \Gamma_{outlet}\cup\Gamma_0 \tag{A.4}$$

where m_{inflow}^k is the k-th temporal moment of the inflow concentration c_{inflow}. The same equations can be derived by Laplace transformation of Eqs. (2)–(5) for the conservative case at steady-state flow, and considering the derivatives of the Laplace transform with respect to the Laplace coordinate at the origin Harvey and Gorelick, 1995.

Wherever the compound passes by, the zeroth temporal moment $m_c^0(\mathbf{x})$ differs from zero, and the second-central moment $m_c^{2c}(\mathbf{x})$, which is a measure of spread in the local breakthrough curve, can be computed:

$$m_c^{2c}(\mathbf{x}) = \int_0^\infty \left(t - \frac{m_c^1(\mathbf{x})}{m_c^0(\mathbf{x})}\right)^2 c(\mathbf{x},t)dt = m_c^2(\mathbf{x}) - \frac{\left(m_c^1(\mathbf{x})\right)^2}{m_c^0(\mathbf{x})}. \tag{A.5}$$

For non-zero $m_c^0(\mathbf{x})$ throughout the domain, a generating equation for the second-central moment can be derived by combining Eqs. (A.2)–(A.4) for $k = 1, 2$, considering Eq. (A.5), and performing some algebraic transformations (e.g., Cirpka and Kitanidis, 2000b):

$$\mathbf{v}\cdot\nabla m_c^{2c} - \nabla\cdot\left(\mathbf{D}\nabla m_c^{2c}\right) = \frac{2}{m_c^0}\nabla m_c^1\cdot\left(\mathbf{D}\nabla m_c^1\right) \tag{A.6}$$

$$\mathbf{n}\cdot\left(\mathbf{v}m_c^{2c} - \mathbf{D}\nabla m_c^{2c}\right) = \mathbf{n}\cdot\mathbf{v}m_{inflow}^{2c} \text{ at } \Gamma_{in} \tag{A.7}$$

$$\mathbf{n}\cdot\left(\mathbf{D}\nabla m_c^{2c}\right) = 0 \text{ at } \Gamma_{out}\cup\Gamma_0. \tag{A.8}$$

As discussed by Cirpka and Kitanidis (2000b), among others, the source term of Eq. (A.6) is an efficient indicator of dispersive mixing. In this regard, the three one-dimensional models designed in the present paper are distinguished by their source term such that: (i) in the case of strictly advective transport, it equals zero throughout the domain; (ii) in the case of a constant local-scale dispersion coefficient, it becomes a constant; and (iii) in the case of the linearly increasing effective dispersion coefficient, the source term also increases with travel distance.

To obtain the moments of local travel-time distribution at a point, we consider a uniform Dirac-pulse inflow concentration on the entire inflow boundary Γ_{inlet}:

$$c_{inflow}(\mathbf{x}) = \delta(t) \text{ at } \Gamma_{in} \tag{A.9}$$

$$\Rightarrow m_{inflow}^0 = 1 \tag{A.10}$$

$$m_{inflow}^k = 0 \forall k > 0. \tag{A.11}$$

Then, the mean local groundwater age $\mu_\tau(\mathbf{x})$ and the variance $\sigma_\tau^2(\mathbf{x})$ of the local travel-time distributions are:

$$\mu_\tau(\mathbf{x}) = \frac{m_c^1}{m_c^0};\ \sigma_\tau^2(\mathbf{x}) = \frac{m_c^{2c}}{m_c^0} \text{ for } c_{inflow}(\mathbf{x}) = \delta(t) \text{ at } \Gamma_{in}$$

leading to the mean groundwater-age equations (Eqs. (6)–(8)) and an equivalent transport equation for $\sigma_\tau^2(\mathbf{x})$ (not shown).

Appendix B. Bioreactive source/sink terms

In this study, the concentrations of the aerobic and denitrifying bacteria are given in moles of carbon within the biomass per volume of water, even though the biomasses are considered immobile. With the simplified elemental composition of CH_2O for dissolved organic carbon and the two types of biomass, the stoichiometries of the reactions listed in Table 1 hold. For aerobic degradation, we consider standard dual-Monod kinetics growth, and a single Michaelis–Menten term for oxygen in the otherwise linear aerobic biomass decay rate law. The effective yield Y_{eff}^{aer} of the aerobic bacteria depends on the aerobic biomass concentration c_{im}^{aer} to account for a maximum biomass concentration c_{max}^{aer}. The corresponding mathematical expressions read as follows:

$$r_{growth}^{aer} = k_{aer,growth}^{max}\cdot\frac{c_m^{O_2}}{c_m^{O_2}+K_{O_2}}\cdot\frac{c_m^{DOC}}{c_m^{DOC}+K_{DOC}^{aer}}\cdot c_{im}^{aer} \tag{B.1}$$

$$r_{dec}^{aer} = k_{aer,dec}^{max}\cdot\frac{c_m^{O_2}}{c_m^{O_2}+K_{O_2}}\cdot c_{im}^{aer} \tag{B.2}$$

$$Y_{eff}^{aer} = Y_{max}^{aer}\cdot\left(1-\frac{c_{im}^{aer}}{c_{max}^{aer}}\right) \tag{B.3}$$

leading to the reactive source–sink terms in Eqs. (2) & (3) for the aerobic biomass (r_{im}^{aer}) and dissolved oxygen ($r_m^{O_2}$):

$$r_{im}^{aer} = Y_{eff}^{aer}\cdot r_{growth}^{aer} - r_{dec}^{aer} \tag{B.4}$$

$$r_m^{O_2} = -F_{O_2/CH_2O}\cdot\left(1-Y_{eff}^{aer}\right)\cdot r_{growth}^{aer} - F_{O_2/CH_2O}\cdot r_{dec}^{aer} \tag{B.5}$$

in which F_{O_2/CH_2O} is the stoichiometric ratio of dissolved oxygen to organic carbon for the net reaction at steady state.

The rate laws for denitrification are quite similar, but denitrification is inhibited by the presence of dissolved oxygen, which is accounted for by a non-competitive inhibition term including the inhibition constant $K_{O_2,inh}^{aer}$:

$$r_{growth}^{den} = k_{den,growth}^{max}\cdot\frac{c_m^{NO_3^-}}{c_m^{NO_3^-}+K_{NO_3^-}}\cdot\frac{c_{DOC}}{c_{DOC}+K_{DOC}^{den}}\cdot\frac{K_{O_2,inh}^{aer}}{K_{O_2,inh}^{aer}+c_m^{O_2}}\cdot c_{im}^{den} \tag{B.6}$$

$$r_{dec}^{den} = k_{den,dec}^{max}\cdot\frac{c_m^{NO_3^-}}{c_m^{NO_3^-}+K_{NO_3^-}}\cdot\frac{K_{O_2,inh}^{aer}}{K_{O_2,inh}^{aer}+c_m^{O_2}}\cdot c_{im}^{den} \tag{B.7}$$

$$Y_{eff}^{den} = Y_{max}^{den}\cdot\left(1-\frac{c_{im}^{den}}{c_{max}^{den}}\right) \tag{B.8}$$

leading to the reactive source–sink terms in Eqs. (2) & (3) for the denitrifying biomass (r_{im}^{den}) and nitrate ($r_m^{NO_3^-}$):

$$r_{im}^{den} = Y_{eff}^{den} \cdot r_{growth}^{den} - r_{dec}^{den} \tag{B.9}$$

$$r_m^{NO_3^-} = -F_{NO_3^-/CH_2O} \cdot \left(1 - Y_{eff}^{den}\right) r_{growth}^{den} - F_{NO_3^-/CH_2O} \cdot r_{dec}^{den} \tag{B.10}$$

Finally, the reactive source/sink-term of dissolved organic carbon compiles the growth-specific reaction rate of aerobic respiration and denitrification:

$$r_m^{DOC} = -r_{growth}^{aer} - r_{growth}^{den} \tag{B.11}$$

Table B.1
Biokinetic parameters.

Symbol	Meaning	Value
$k_{aer,growth}^{max}$	Maximum specific DOC-reaction rate of aerobic bacteria under growth conditions	7.5/day
$k_{den,growth}^{max}$	Maximum specific DOC-reaction rate of denitrifying bacteria under growth conditions	2.5/day
$k_{aer,dec}^{max}$	Maximum decay rate coefficient of aerobic bacteria	0.1/day
$k_{den,dec}^{max}$	Maximum decay rate coefficient of denitrifying bacteria	0.1/day
K_{DOC}^{aer}	Monod coefficient of *DOC* in aerobic degradation	10 μM
K_{DOC}^{den}	Monod coefficient of *DOC* in denitrification	11.4 μM
K_{O_2}	Monod coefficient of dissolved oxygen in aerobic degradation	3 μM
$K_{NO_3^-}$	Monod coefficient of nitrate in denitrification	70 μM
$K_{O_2}^{inh}$	Biomass inhibition coefficient of oxygen in denitrification	10 μM
Y_{max}^{aer}	Maximum specific yield of aerobic bacteria	0.5
Y_{max}^{den}	Maximum specific yield of denitrifying bacteria	0.5
F_{O_2/CH_2O}	Stoichiometric ratio O_2/CH_2O in net aerobic degradation at steady state	1
$F_{NO_3^-/CH_2O}$	Stoichiometric ratio NO_3^-/CH_2O in net denitrification at steady state	0.8
c_{max}^{aer}	Maximum concentration of aerobic bacteria	50 μM
c_{max}^{den}	Maximum concentration of denitrifying bacteria	50 μM

References

Atchley, A.L., Navarre-Sitchler, K.A., Maxwell, R.M., 2014. The effects of physical and geochemical heterogeneities on hydro-geochemical transport and effective reaction rates. J. Contam. Hydrol. 165, 53–64.

Berkowitz, B., Cortis, A., Dentz, M., Scher, H., 2006. Modeling non-Fickian transport in geological formations as a continuous time random walk. Rev. Geophys. 44 (2), RG2003.

Bethke, C., Johnson, T.M., 2002. Ground water age. Ground Water 40 (4), 337–339.

Botter, G., Bertuzzo, E., Bellin, A., Rinaldo, A., 2005. On the Lagrangian formulations of reactive solute transport in the hydrologic response. Water Resour. Res. 41 (4), W04008.

Cirpka, O.A., 2002. Choice of dispersion coefficients in reactive transport calculations on smoothed fields. Water Resour. Res. 58 (3–4), 261–282.

Cirpka, O.A., Kitanidis, P.K., 2000a. An advective–dispersive stream tube approach for the transfer of conservative-tracer data to reactive transport. Water Resour. Res. 36 (5), 1209–1220.

Cirpka, O.A., Kitanidis, P.K., 2000b. Characterization of mixing and dilution in heterogeneous aquifers by means of local temporal moments. Water Resour. Res. 36 (5), 1221–1236.

Cirpka, O.A., Valocchi, A.J., 2007. Two-dimensional concentration distribution for mixing-controlled bioreactive transport in steady state. Adv. Water Resour. 30 (6–7), 1668–1679.

Cirpka, O.A., Frind, E.O., Helmig, R., 1999a. Numerical simulation of biodegradation controlled by transverse mixing. J. Contam. Hydrol. 40 (2), 159–182.

Cirpka, O.A., Frind, E.O., Helmig, R., 1999b. Streamline-oriented grid-generation for transport modelling in two-dimensional domains including wells. Adv. Water Resour. 22 (7), 697–710.

Cirpka, O.A., Helmig, R., Frind, E.O., 1999c. Numerical methods for reactive transport on rectangular and streamline-oriented grids. Adv. Water Resour. 22 (7), 711–728.

Cirpka, O.A., Rolle, M., Chiogna, G., de Barros, F.P.J., Nowak, W., 2012. Stochastic evaluation of mixing-controlled steady-state plume lengths in two-dimensional heterogeneous domains. J. Contam. Hydrol. 138–139, 22–39.

Cirpka, O.A., Chiogna, G., Rolle, M., Bellin, A., 2015. Transverse mixing in three-dimensional nonstationary anisotropic heterogeneous porous media. Water Resour. Res. 51.

Cornaton, F., 2003. Deterministic Models of Groundwater Age, Life Expectancy and Transit Time Distributions in Advective–Dispersive Systems. (Phd thesis). Centre of Hydrogeology. University of Neuchâtel.

Cvetkovic, V., Dagan, G., 1994. Transport of kinetically sorbing solute by steady random velocity in heterogeneous porous formations. J. Fluid Mech. 265, 189–215.

Cvetkovic, V., Cheng, H., Wen, X.-H., 1996. Analysis of nonlinear effects on tracer migration in heterogeneous aquifers using Lagrangian travel time statistics. Water Resour. Res. 32 (6), 1671–1680.

Dagan, G., Bresler, E., 1979. Solute dispersion in unsaturated heterogeneous soil at field scale: I. Theory. Soil Sci. Soc. Am. J. 43, 461–467.

Dagan, G., Nguyen, V., 1989. A comparison of travel time and concentration approaches to modelling transport by groundwater. J. Contam. Hydrol. 4, 79–91.

Danckwerts, P.V., 1953. Continuous flow system: distribution of residence time. Chem. Eng. Sci. 2, 1–13.

Davis, T.A., Duff, I.S., 1997. An unsymmetric-pattern multifrontal method for sparse LU factorization. SIAM J. Matrix Anal. Appl. 18 (1), 140–158.

De Simoni, M., Carrera, J., Sanchez-Vila, X., Guadagnini, A., 2005. A procedure for the solution of multicomponent reactive transport problems. Water Resour. Res. 41 (11), W11410.

De Simoni, M., Sanchez-Vila, X., Carrera, J., Saaltink, M.W., 2007. A mixing ratios-based formulation for multicomponent reactive transport. Water Resour. Res. 43 (7), W07419.

Dentz, M., Kinzelbach, H., Attinger, S., Kinzelbach, W., 2000. Temporal behavior of a solute cloud in a heterogeneous porous medium: 1. Point-like injection. Water Resour. Res. 36 (12), 3591–3604.

Dentz, M., Cortis, A., Scher, H., Berkowitz, B., 2004. Time behavior of solute transport in heterogeneous media: transition from anomalous to normal transport. Adv. Water Resour. 27, 155–173.

Diem, S., Cirpka, O.A., Schirmer, M., 2013. Modeling the dynamics of oxygen consumption upon riverbank filtration by a stochastic-convective approach. J. Hydrol. 505, 352–363.

Dietrich, C., Newsam, G., 1993. A fast and exact method for multidimensional Gaussian stochastic simulations. Water Resour. Res. 29 (8), 2861–2869.

Edery, Y., Scher, H., Berkowitz, B., 2010. Particle tracking model of bimolecular reactive transport in porous media. Water Resour. Res. 46 (7), W07524.

Engdahl, N.B., Maxwell, R.M., 2014. Approximating groundwater age distributions using simple streamtube models and multiple tracers. Adv. Water Resour. 66, 19–31.

Feyen, J., Jacques, D., Timmerman, A., Vanderborght, J., 1998. Modelling water flow and solute transport in heterogeneous soils: a review of recent approaches. J. Agric. Eng. Res. 70 (3), 231–256.

Ginn, R.T., 1999. On the distribution of multicomponent mixtures over generalized exposure time in subsurface flow and reactive transport: foundations, and formulations for groundwater age, chemical heterogeneity, and biodegradation. Water Resour. Res. 35 (5), 1395–1407.

Ginn, R.T., 2000. On the distribution of multicomponent mixtures over generalized exposure time in subsurface flow and reactive transport: batch and column applications involving residence-time distribution and non-Markovian reaction kinetics. Water Resour. Res. 36 (10), 2895–2903.

Ginn, T.R., 2002. A travel time approach to exclusion on transport in porous media. Water Resour. Res. 38 (4), 1041.

Ginn, T.R., Hanieh, H., Massoudieh, A., Foglia, L., 2009. Notes on groundwater age in forward and inverse modelling. Transp. Porous Media 79, 117–134.

Gong, R., Lu, C., Wu, W.M., Cheng, H., Gu, B., Watson, D., Jardine, P.M., Brooks, S.C., Criddle, C.S., Kitanidis, P.K., Luo, J., 2011. Estimating reaction rate coefficients within a travel-time modeling framework. Ground Water 49 (2), 209–218.

Goode, D.J., 1996. Direct simulation of groundwater age. Water Resour. Res. 32 (2), 289–296.

Gouze, P., Melean, Z., Borgne, T.L., Dentz, M., Carrera, J., 2008. Non-Fickian dispersion in porous media explained by heterogeneous microscale matrix diffusion. Water Resour. Res. 44, W11416.

Harvey, C.F., Gorelick, S.M., 1995. Temporal moment-generating equations: modeling transport and mass-transfer in heterogeneous aquifers. Water Resour. Res. 31 (8), 1895–1911.

Jury, W.A., 1982. Simulation of solute transport using a transfer function model. Water Resour. Res. 18 (2), 363–368.
Jury, W.A., Roth, K., 1990. Transfer Functions and Solute Movement Through Soil: Theory and Applications. Birkhauser Boston, Cambridge, Mass.
Kinzelbach, W., Schäfer, W., Herzer, J., 1991. Numerical modeling of natural and enhanced denitrification processes in aquifers. Water Resour. Res. 27 (6), 1123–1135.
Köhne, J., Köhne, S., Šimunek, J., 2009. A review of model applications for structured soils: a) water flow and tracer transport. J. Contam. Hydrol. 104, 4–35.
Kreft, A., Zuber, A., 1978. On the physical meaning of the dispersion equation and its solutions for different initial and boundary conditions. Chem. Eng. Sci. 33 (11), 1471–1480.
Leij, F., Sciortino, A., Dane, J., 2007. Analytical solutions to evaluate the stream tube approach for field-scale modeling of evaporation. Soil Phys. 71 (2), 289–297.
Luo, J., 2012. Travel-time based reactive transport modeling for in situ subsurface reactor. In: Kitanidis, P.K., McCarty, P.L. (Eds.), Delivery and Mixing in the Subsurface: Processes and Design Principles for In Situ Remediation. Vol. 4 of SERDP ESTCP Remediation Technology. Springer, New York, pp. 117–138 (Ch. 5).
Luo, J., Cirpka, O.A., 2008. Travel-time based descriptions of transport and mixing in heterogeneous domains. Water Resour. Res. 44 (9), W09407.
Luo, J., Cirpka, O.A., 2011. How well do mean breakthrough curves predict mixing-controlled reactive transport. Water Resour. Res. 47 (2), W02520.
Luo, J., Weber, F.-A., Cirpka, O.A., Wu, W.-M., Carley, J., Nyman, J., Jardine, P., Criddle, C.S., Kitanidis, P.K., 2007. Modeling in-situ U(VI) bioreduction by sulfate-reducing bacteria in the presence of nitrate. J. Contam. Hydrol. 92 (1–2), 129–148.
Marzadri, A., Tonina, D., Bellin, A., 2011. A semianalytical three-dimensional process-based model for hyporheic nitrogen dynamics in gravel bed rivers. Water Resour. Res. 47 (11), W11518.
Moore, I., Grayson, R., 1991. Terrain-based catchment partitioning and runoff prediction using vector elevation data. Water Resour. Res. 27 (6), 1177–1191.
Sanchez-Vila, X., Carrera, J., 2004. On the striking similarity between the moments of breakthrough curves for a heterogeneous medium and a homogeneous medium with a matrix diffusion term. J. Hydrol. 294 (1–3), 164–175.
Shuang, C., Li, S., Yin-huan, Z., 2011. Research on the distributing law of the gas in the gob area based on flow-tube model. Procedia Eng. 26, 1043–1050.
Simmons, C.S., 1982. A stochastic-convective transport representation of dispersion in one-dimensional porous-media systems. Water Resour. Res. 18 (4), 1193–1214.
Simmons, C.S., Ginn, T.R., Wood, B.D., 1995a. Stochastic-convective transport with nonlinear reaction: biodegradation with microbial growth. Water Resour. Res. 31 (11), 2689–2700.
Simmons, C.S., Ginn, T.R., Wood, B.D., 1995b. Stochastic-convective transport with nonlinear reaction: mathematical framework. Water Resour. Res. 31 (11), 2675–2688.
Willmann, M., Carrera, J., Sanchez-Vila, X., 2008. Transport upscaling in heterogeneous aquifers: what physical parameters control memory functions? Water Resour. Res. 44, W12437.
Willmann, M., Carrera, J., Sanchez-Vila, X., Silva, O., Dentz, M., 2010. Coupling of mass transfer and reactive transport for nonlinear reactions in heterogeneous media. Water Resour. Res. 46 (7), W07512.
Ye, Y., Chiogna, G., Cirpka, O., Grathwohl, P., Rolle, M., 2015. Experimental investigation of compound-specific dilution of solute plumes in saturated porous media: 2-D vs. 3-D flow-through systems. J. Contam. Hydrol. 172, 33–47.
Zwietering, T., 1959. The degree of mixing in continuous flow systems. Chem. Eng. Sci. 11 (1), 1–15.

Appendix B: Second publication

Title

Using travel times to simulate multi-dimensional bioreactive transport in time-periodic flows

Authors

Alicia Sanz-Prat, Chuanhe Lu, Michael Finkel, Olaf A. Cirpka

Journal

Journal of Contaminant Hydrology (Volume 187, pages 1-17)

Year

2016

Highlights

- Velocity fields with periodically fluctuating magnitude and constant direction.
- Perform nonlinear bioreactive transport in 1-D domain.
- Transfer 1-D results to 2-D domains by mean groundwater age at steady state.
- Application to oxygen-inhibited denitrification.
- Excellent agreement between mapped and spatially explicit results.

Journal of Contaminant Hydrology 187 (2016) 1–17

Contents lists available at ScienceDirect

Journal of Contaminant Hydrology

journal homepage: www.elsevier.com/locate/jconhyd

Using travel times to simulate multi-dimensional bioreactive transport in time-periodic flows

Alicia Sanz-Prat, Chuanhe Lu, Michael Finkel, Olaf A. Cirpka *

University of Tübingen, Center for Applied Geoscience, Hölderlinstraße 12, 72074 Tübingen, Germany

ARTICLE INFO

Article history:
Received 14 August 2015
Received in revised form 13 January 2016
Accepted 21 January 2016
Available online 26 January 2016

Keywords:
Bioreactive transport
Travel-time model
Denitrification
Transient flow

ABSTRACT

In travel-time models, the spatially explicit description of reactive transport is replaced by associating reactive-species concentrations with the travel time or groundwater age at all locations. These models have been shown adequate for reactive transport in river-bank filtration under steady-state flow conditions. Dynamic hydrological conditions, however, can lead to fluctuations of infiltration velocities, putting the validity of travel-time models into question. In transient flow, the local travel-time distributions change with time. We show that a modified version of travel-time based reactive transport models is valid if only the magnitude of the velocity fluctuates, whereas its spatial orientation remains constant. We simulate nonlinear, one-dimensional, bioreactive transport involving oxygen, nitrate, dissolved organic carbon, aerobic and denitrifying bacteria, considering periodic fluctuations of velocity. These fluctuations make the bioreactive system pulsate: The aerobic zone decreases at times of low velocity and increases at those of high velocity. For the case of diurnal fluctuations, the biomass concentrations cannot follow the hydrological fluctuations and a transition zone containing both aerobic and obligatory denitrifying bacteria is established, whereas a clear separation of the two types of bacteria prevails in the case of seasonal velocity fluctuations. We map the 1-D results to a heterogeneous, two-dimensional domain by means of the mean groundwater age for steady-state flow in both domains. The mapped results are compared to simulation results of spatially explicit, two-dimensional, advective-dispersive-bioreactive transport subject to the same relative fluctuations of velocity as in the one-dimensional model. The agreement between the mapped 1-D and the explicit 2-D results is excellent. We conclude that travel-time models of nonlinear bioreactive transport are adequate in systems of time-periodic flow if the flow direction does not change.

1. Introduction

Numerical simulation is indispensable for the quantitative understanding of compounds undergoing transport and chemical transformations in the subsurface (e.g., Barry et al., 2002; MacQuarrie and Mayer, 2005; Steefel et al., 2005). The most typical approach taken is to solve the coupled, multi-dimensional advection-dispersion-reaction equations of all reactants, either as a single system of nonlinear partial differential equations, or as decoupled equations in sequential or iterative operator-split approaches. The resulting computational effort is high, and the spatially explicit description requires hydraulic and reactive parameters as spatial fields throughout the domain. In order to reduce the computational effort and avoid the spatially explicit description of the required multi-dimensional parameter fields, travel-time based reactive transport models (hereafter denoted simply as travel-time models) may be preferred over spatially explicit Eulerian methods (e.g., Cirpka and Kitanidis, 2000; Cvetkovic et al., 1996; Cvetkovic and Dagan, 1996; Dagan and Cvetkovic, 1996; Ginn et al., 1995; Janssen et al., 2006; Kaluarachchi et al., 2000; Malmström et al., 2004; Sanz-Prat et al., 2015; Simmons et al., 1995; Yabusaki et al., 1998). While in spatially explicit models the spatial

* Corresponding author.
E-mail address: olaf.cirpka@uni-tuebingen.de (O.A. Cirpka).

http://dx.doi.org/10.1016/j.jconhyd.2016.01.005
0169-7722/

coordinates (together with time) are considered as independent variables, travel-time models replace space by travel time. This leads to quasi one-dimensional transport under the assumption that reaction fronts coincide with groundwater isochrones (i.e., lines of equal travel time).

The travel time, $\tau(\mathbf{x})[T]$, is defined as the time that a water particle resides in the domain of interest, from the entry point at the domain inlet to the point of observation $\mathbf{x}[L]$. There are at least four reasons why the travel time is not a unique value: (1) Pore-scale dispersion leads to a local distribution of travel time, $p(\tau(\mathbf{x}))[T^{-1}]$ at any point within the domain even for deterministic flow fields, (2) dynamic boundary conditions or time-varying fluid and aquifer properties cause velocity variations in time, making the local travel-time distributions dependent on time, (3) sampling over a larger control plane (or considering breakthrough curves in pumping wells) in a non-uniform flow field leads to a distribution of arrival times within the observation plane, and (4) considering the uncertainty of aquifer properties using stochastic methods leads to a statistical distribution of travel time over an ensemble of aquifer realizations (e.g., Cvetkovic et al., 1992; Dagan et al., 1992; Dagan and Nguyen, 1989; Shapiro and Cvetkovic, 1988, among others). In this study, we restrict ourselves to point observations in single aquifer realizations so that only the first two causes of non-unique travel times are considered.

Travel-time models of reactive transport conceptualize a multi-dimensional transport domain as an ensemble of independent 1-D systems, i.e., stream tubes, in which the longitudinal coordinate is the associated travel time along the stream tube (e.g., Luo, 2012). As the stream tubes along different groundwater flow paths are treated as independent systems, transverse dispersion and related mixing processes cannot explicitly be considered. In stochastic-convective transport, pore-scale dispersion is neglected altogether, and typically breakthrough curves averaged over an extended control plane or an ensemble of many aquifer realizations are considered (e.g., Dagan et al., 1992; Dagan and Nguyen, 1989; Shapiro and Cvetkovic, 1988; Simmons, 1982). Stochastic-convective transport models also have a long tradition in soil science, where they are used to describe solute transport in percolating soil water (see the reviews of Feyen et al., 1998; Köhne et al., 2009). First extensions towards advective-reactive transport included linear kinetic sorption and first-order decay (Cvetkovic and Dagan, 1994; Cvetkovic and Shapiro, 1990; Selroos and Cvetkovic, 1992; Severino et al., 2012).

The extension to nonlinear reactions (stochastic convective reactive transport – SCR), including reactions between mobile and immobile phases, is straightforward in steady-state flow fields (e.g., Cvetkovic et al., 1996; Cvetkovic and Dagan, 1996; Dagan and Cvetkovic, 1996; Simmons et al., 1995): The spatial coordinates of the standard advection-reaction equation are replaced by the advective travel time (or kinematic age), $\tau_{adv}[T]$, and the velocity becomes unity; nonlinear multi-component reactive transport is solved in these coordinates; and the reactive-species concentrations at a point $\mathbf{x}$ within the domain are obtained by looking up the reactive-species concentrations in the travel-time domain at the specific kinematic age $\tau_{adv}(\mathbf{x})$ of the observation point. While closed-form expressions can be derived for comparably simple reaction laws (e.g., Ginn et al., 1995), numerical simulation of 1-D reactive transport is computationally so inexpensive that the approach is feasible also for more complex reaction systems (e.g., Kaluarachchi et al., 2000; Malmström et al., 2004; Yabusaki et al., 1998).

A major concern with convective-reactive models is their conceptual inadequacy in describing mixing-controlled reactions (Luo and Cirpka, 2008, 2011). In the stochastic-convective framework a distribution of travel times, observed over a larger control plane, is interpreted as the result of many non-interacting stream tubes being mixed upon the observation rather than within the domain. To predict reactive-species concentrations, the advection-reaction equation is solved in the travel-time domain, the resulting concentrations are weighted by the probability density of a certain kinematic age to occur within the control plane and integrated over all advective travel times. By construction, this approach cannot handle reactions that are controlled by dispersive solute mixing within the domain. In reactive-transport applications that don't require dispersive mixing, the SCR models perform much better than models in which "macrodispersive" spreading is introduced into macroscale advective-dispersive-reactive transport (Molz and Widdowson, 1988). In order to handle mixing-controlled reactions in travel-time models, Cirpka and Kitanidis (2000) developed the advective-dispersive stream-tube model (ADS), which parametrizes the effects of local transverse dispersion on macroscopic longitudinal mixing by an increasing within-stream-tube dispersion coefficient and handles the variability of the mean groundwater age within a control plane by a stochastic description. Intra-streamtube mixing was also accounted for in other stream-tube models (e.g., Ginn, 2001; Ginn et al., 2001).

In a preceding study, we analyzed which error is introduced by the mapping of reactive-species concentrations from the travel-time domain to the spatial domain using the mean groundwater age assuming advective-dispersive transport in a heterogeneous domain (Sanz-Prat et al., 2015). The application involved oxygen, nitrate, dissolved organic carbon as dissolved species as well as aerobic and denitrifying bacteria as immobile species. All dissolved compounds were introduced jointly into the domain; the concentration in the inflow were spatially uniform; reactive parameters did not vary within the domain; and flow was at steady state. We found that the spatial concentration distributions of all compounds organized themselves in zones that are essentially aligned with isochrones: A water parcel carrying a certain chemical signature kinetically interacts with the immobile phases, which in turn are modified by the reactions. We could predict local reactive-species concentrations quite accurately from the mean groundwater age at that location combined with one-dimensional simulations of the same reactive-transport problem by mapping the 1-D results to the 2-D domain according to the mean travel time. The mapping performed best with an advective-dispersive-reactive 1-D model in which the longitudinal mixing coefficient increased with distance, which was calibrated by the relationship between second-central and first temporal moments in the 2-D simulations. However, mapping by the kinematic age, which is conceptually much simpler, did not introduce a large error.

The assumption of steady-state flow, made in the preceding study, is crucial and not very realistic in many situations. An exemplary zone with intensive natural biogeochemical cycling is the surface-water/groundwater interface, where infiltrating river water gets in contact with microbial biomass in the river sediments. These transition zones are known to be dynamic with

respect to flow (e.g., Hatch et al., 2006; Keery et al., 2007; Silliman et al., 1995), which also influences the biotransformations therein. River-stage fluctuations can occur on many time scales, reflecting individual short-term events, diurnal cycles, mesoscale weather, and seasonality of climate. Hydrological dynamics at the river-groundwater interface can of course also be driven from the groundwater side, e.g., by cyclic withdrawal of groundwater, or seasonality of groundwater recharge. While in principle hydrological dynamics can change both the magnitude and direction of flow, the situation in which the direction remains more or less constant is fairly common. As outlined in this paper, we see good chances that fluctuating velocity magnitudes can still be handled in travel-time based bioreactive transport codes, whereas changes in the flow direction may cause more severe problems. Thus, the present study aims to test the reliability, and required adaptation, of travel-time models to perform nonlinear reactive transport when the groundwater-flow magnitude is subject to periodic transient fluctuations.

Under transient flow conditions, both travel times at individual points and the residence-time distribution of the entire domain vary with time. Several studies have analyzed how dynamic travel times can be analytically estimated (e.g., Cornaton, 2012; Soltani and Cvetkovic, 2013; van der Velde et al., 2015), which is not in the focus of the present study. Instead, we want to address how dynamic travel times put the entire concept of travel-time based reactive transport into question. In the strictly Lagrangian world, in which individual water parcels are followed through the domain, it appears at first irrelevant whether the parcels move with constant or time-varying speed: With increasing age, the chemical composition of the water parcel alters. This concept is applied in dynamic watershed-scale models of solute transport (e.g., Lindgren et al., 2004; Botter et al., 2010). These models consider the distribution of residence times throughout the catchment as the interplay between the time-varying input of water into the system and the way how the catchment outlet samples the residence-time distribution. The concentration in the outlet is then calculated from the concentration in the input at the time when the water entered the watershed (exit time minus travel time) and the modification of concentrations due to aging. As the outlet samples a distribution of travel times, the resulting outlet concentration is a weighted average of travel-time dependent concentrations. Reactions are typically represented in these approaches in simplified manners, such as first-order decay. In this framework, the travel-time of a water parcel can also be subdivided into the time spent in different compartments, each of which exhibiting a different first-order decay coefficient (Destouni et al., 2010). These models, however, do not account for immobile reactive constituents, such as microbial biomass, as dynamic state variables.

Selroos et al. (2013) considered the transport of radionuclides in crystalline rock at geological time scales over which the entire flow system may change. Since all processes considered (advective transport, longitudinal dispersion, diffusion into the rock matrix, equilibrium sorption, and radioactive decay) were linear, they could formulate the mobile–immobile reactive-transport problem in a strictly Lagrangian framework of non-interacting particles even in transient flow (Painter et al., 2008). They compared model runs, in which the direction of flow was kept constant whereas the magnitude changed over time (denoted "flow-factor approach"), with those accounting for time-varying trajectories. In their application, the resulting breakthrough curves differed, but the flow-factor estimates were considered acceptable.

In the present study, we analyze nonlinear, mixing-affected transport of multiple compounds reacting with an immobile phase that changes upon the reaction. Under such conditions, a Lagrangian framework of non-interacting particles is questionable. Currently, we don't see how such a system can be conceptually simplified when the direction of flow changes. However, we would argue that domain-wide fluctuations of the velocity magnitude, with spatial orientation of travel paths remaining constant, would not change the overall alignment of reaction zones with some kind of isochrones because all water parcels with identical age will have seen very similar reaction zones, which in turn are influenced by a similar history of water parcels passing by. In this regard, the questions to be addressed in this study are: (1) How do transients in flow magnitude influence local travel-time distributions, (2) how does transient flow alter biogeochemical zonation, (3) which travel time or travel-time metric should be used to map travel-time based results of nonlinear (bio)reactive-transport simulations to multi-dimensional domains, and (4) how large is the error introduced by the mapping approach? As pointed out, we restrict the analysis to the case that the direction of flow does not change with time. We consider periodic fluctuations of hydraulic boundary conditions (water level, infiltration rates, etc), whose periodicity mimics natural dynamics but, unlike Selroos et al. (2013), we do not analyze under which conditions the flow-factor approach is valid. In a nutshell, we hypothesize that the spatial dimensions could be replaced by a characteristic travel time at each position of the domain in order to capture the reactive-species concentrations of nonlinear reactive transport in transient flow systems:

$$\mathbf{c}(\mathbf{x},t) \approx \mathbf{c}_{\mathbf{1D}}(\tau_{ch}(\mathbf{x}),t) \tag{1}$$

in which $\mathbf{c}[ML^{-3}]$ is the vector of all reactive-species concentrations in the multi-dimensional domain, $\mathbf{x}[L]$ denotes the vector of spatial coordinates, $t[T]$ is the simulation time, $\mathbf{c}_{\mathbf{1D}}[ML^{-3}]$ is the vector of reactive-species concentration in the equivalent, one-dimensional travel-time model, $\tau_{ch}(\mathbf{x})[T]$ is a characteristic travel time at the location $\mathbf{x}$ in the multi-dimensional domain that does not depend on time t. In this study, we assume that the concentrations in the inflow don't vary along the boundary. If this was the case, we would also need to track the origin of the water at the observation point $\mathbf{x}$. The equivalent one-dimensional model must undergo the same relative fluctuations of flow velocity as the multi-dimensional model for Eq. (1) to be valid. In this regard, our approach differs from classical Lagrangian models of reactive transport. Explicitly considering the time-fluctuations of velocity in the 1-D model enables us to make water parcels of identical age interacting with immobile reactants at different positions along the pathline at different times.

As characteristic travel time $\tau_{ch}(\mathbf{x})$, we test the mean groundwater age $\mu_{\tau_{ss}}(\mathbf{x})[T]$ computed for steady-state flow. We compare this characteristic travel time with the time-averaged kinematic age $\overline{\tau}_{adv}(\mathbf{x})[T]$ at the same location and the time-averaged mean groundwater age $\overline{\mu}_{\tau}(\mathbf{x})[T]$ for advective-

dispersive transport, in which overbars denote time averages. Because we assume time-periodic fluctuations of velocity, the arithmetic time average is performed over one period of the cycle.

As discussed above, we consider a flow system where the flow rates fluctuate, but the trajectories of water particles remain constant (flow-factor approach according to Selroos et al., 2013). The proposed test case represents an idealized scenario of a mildly heterogeneous hydraulic-conductivity field and constant values of the local dispersivities; the reactive system describes aerobic respiration and denitrification of dissolved organic carbon, catalyzed by aerobic and obligatory denitrifying bacteria (Sanz-Prat et al., 2015; similar to Kaluarachchi et al., 2000). We assume stepwise diurnal fluctuations of the velocity compared to smooth periodic fluctuations on seasonal time scales. Both input signals can be attributed to relevant anthropogenic and natural processes (e.g., hydropower operation causing daily hydropeaking in rivers and natural seasonality of groundwater recharge).

The approach of this work is summarized in three main tasks: (i) to perform conservative transport simulations in 1-D and 2-D models to estimate the spatio-temporal distribution of travel time and its time-related statistics; (ii) to simulate the bioreactive transport problem of the 1-D travel time model and map results to 2-D with respect to $\tau_{ch}(\mathbf{x})$; (iii) to simulate the 2-D advective-dispersive-reactive transport, here named our "virtual truth"; (iv) to estimate residual errors in concentrations derived with the 1-D model, which are mapped to 2-D, compared to the results of the 2-D virtual truth.

2. Theory

The reliability of a time-independent characteristic travel time as indicator of reactive transport in transient flow depends on the following assumptions:

1. Groundwater storage is neglected, that is, changes in hydraulic boundary conditions are assumed to cause immediate changes of the velocity field without transition. This is known as quasi steady-state flow. This assumption is needed to keep spatial velocity *patterns* constant under transient conditions, whereas the magnitude of velocity fluctuates. In unconfined aquifers the assumption of quasi steady-state flow may be unrealistic because the specific yield is fairly large so that water-table fluctuations are strongly dampened. Conversely, in confined aquifers alterations of hydraulic head could be considered as instantaneous due to the small storage coefficient and hence rather negligible storage effects.
2. The dynamic changes of boundary conditions must not cause fluctuations in the spatial orientation of velocity, which implies some uniformity of the fluctuations along the boundaries. By this, trajectories of water parcels do not change with time, only the speed by which the water parcels are transported along the trajectories changes.
3. The reactive parameters are assumed to be spatially and temporally uniform, that is, the rules of the reactions are the same in the entire domain of interest. Otherwise, the travel time and the time of reaction do not match, and a specific groundwater age does not reflect a unique evolution of chemical-compound concentrations. As an alternative, one may replace the travel time by the exposure time, i.e., the time that a water parcel is exposed to conditions facilitating the reactions in the corresponding models (Ginn, 1999; Seeboonruang and Ginn, 2006), but this analysis is beyond the scope of the current work. Note that uniform reactive parameters don't imply a uniform biomass distribution, as the biomass concentrations are dynamic state variables in our model.

These conditions may be met in confined aquifers or hyporheic zones when fluctuations of the hydraulic head at one boundary trigger velocity fluctuations in the entire domain of interest.

2.1. Quasi steady-state groundwater flow

We assume that transient groundwater flow can be computed by multiplying steady-state flow with a spatially uniform time flow-factor $f(t)[-]$ (Selroos et al., 2013):

$$\mathbf{q}(\mathbf{x},t) = \mathbf{q}_{SS}(\mathbf{x}) f(t) \quad \text{with} \frac{1}{T}\int_0^T f(t)dt = 1 \tag{2}$$

in which $\mathbf{q}(\mathbf{x},t)[LT^{-1}]$ is the transient specific-discharge field, $\mathbf{q}_{SS}(\mathbf{x})[LT^{-1}]$ is the so-called equivalent steady-state flow field, and $T[T]$ is the period over which $f(t)$ fluctuates. The equivalent steady-state groundwater-flow equation reads as:

$$\nabla \cdot (\mathbf{K}(\mathbf{x})\nabla h_{SS}) = R_{SS}(\mathbf{x}) \tag{3}$$

subject to:

$$h_{SS} = h_{SS,fix} \ \ at \ \ \Gamma_{1,out} \tag{4}$$

$$h_{SS} = h_{SS,fix} + \Delta h_{SS,fix} \ \ at \ \ \Gamma_{1,in} \tag{5}$$

$$-\mathbf{n} \cdot (\mathbf{K}(\mathbf{x})\nabla h_{SS}) = q_{SS,fix} \ \text{at} \ \Gamma_2 \tag{6}$$

in which $\mathbf{K}(\mathbf{x})[LT^{-1}]$ is the hydraulic conductivity tensor, $h_{SS}[L]$ is the steady-state hydraulic head, $R_{SS}[T^{-1}]$ is a steady-state volumetric source/sink-term, $\mathbf{n}[-]$ denotes the outward pointing unit vector normal to the boundary, $\Gamma_{1,in}$ and $\Gamma_{1,out}$ are fixed-head inlet and outlet boundaries, Γ_2 is a fixed-flux boundary, $h_{SS,fix}$ $[L]$ and $\Delta h_{SS,fix}$ $[L]$ are the steady-state fixed head at $\Gamma_{1,out}$ and the head-difference between $\Gamma_{1,in}$ and $\Gamma_{1,out}$, whereas $q_{SS,fix}$ $[LT^{-1}]$ is a fixed normal flux across Γ_2.

In order to meet Eq. (2), the following conditions must be met in transient flow:

$$\nabla \cdot (\mathbf{K}(\mathbf{x})\nabla h) = R_{SS}(\mathbf{x}) f(t) \tag{7}$$

$$h = h_{SS,fix} \ \ at \ \ \Gamma_{1,out} \tag{8}$$

$$h = h_{SS,fix} + \Delta h_{SS,fix} f(t) \ \ at \ \ \Gamma_{1,in} \tag{9}$$

$$-\mathbf{n}\cdot(\mathbf{K}(\mathbf{x})\nabla h) = q_{SS,fix} f(t) \text{ at } \Gamma_2 \tag{10}$$

so that the resulting hydraulic gradients ∇h under transient conditions are identical to $\nabla h_{SS} f(t)$ at all locations and times. The seepage velocity $\mathbf{v}[LT^{-1}]$, needed in solute transport, is computed by dividing the specific discharge by the flow-effective porosity θ:

$$\mathbf{v}_{SS}(\mathbf{x}) = \frac{1}{\theta}\mathbf{K}(\mathbf{x})\nabla h_{SS} \tag{11}$$

$$\mathbf{v}(\mathbf{x},t) = \mathbf{v}_{SS}(\mathbf{x}) f(t) \tag{12}$$

We choose two different periodic time functions $f(t)$ to express the fluctuations. For diurnal fluctuations, we assume a stepwise change of a river stage, keeping the fixed hydraulic head at the outflow boundary constant:

$$f(t) = \begin{cases} f_1 & \text{if } \mathrm{mod}(t, T_1+T_2) \le T_1 \\ f_2 = \dfrac{(1-f_1)T_1 + T_2}{T_2} & \text{if } \mathrm{mod}(t, T_1+T_2) > T_1 \end{cases} \tag{13}$$

in which $\mathrm{mod}(t, T_1+T_2)$ denotes the remainder of the floored division of t by (T_1+T_2), $T_1[T]$ and $T_2[T]$ are the durations over which $f(t)$ assumes the values f_1 and f_2, and $T = T_1 + T_2$ is the entire period. In our application, $T_1 + T_2 = 12\ h$, and f_1 is set to 0.2, leading to a factor of nine between the high and low velocities.

For seasonal fluctuations, we consider a smoothly varying time function $f(t)$:

$$f(t) = \frac{f_{min}+f_{max}}{2} + \left(\frac{f_{max}-f_{min}}{2.313}\right)\sum_{j=1}^{\infty}\exp(1-j)\cos\left(2\pi j\frac{t}{T} + 1.5\pi - 0.6j\pi\right) \tag{14}$$

in which $f_{\min}[-]$ and $f_{\max}[-]$ are the minimum and maximum values assumed by $f(t)$, and $T[T]$ is the period of one year.

2.2. Calculation and characterization of travel-time distributions in transient flow

In order to evaluate the local mean travel time $\mu_\tau(\mathbf{x})$ and the variance of local travel time $\sigma_\tau^2(\mathbf{x})$, both in steady-state and transient flow fields, we solve conservative advective-dispersive transport problems in the one- and two-dimensional domains. Here, we simulate the continuous injection of an idealized tracer over the inlet boundary with a constant inlet concentration of unity. The resulting breakthrough curves $c(\mathbf{x}, t)$ can be interpreted as cumulative distribution function of solute arrival time. Then, the mean and variance of the local travel-time distribution can be computed via truncated temporal moments by (e.g., Jose and Cirpka, 2004):

$$\mu_\tau(\mathbf{x}) = T_{tr} - \int_0^{T_{tr}} c(\mathbf{x},t)dt \tag{15}$$

$$\sigma_\tau^2(\mathbf{x}) = T_{tr}^2 - 2\int_0^{T_{tr}} tc(\mathbf{x},t)dt - \mu_\tau^2(\mathbf{x}) \tag{16}$$

in which $T_{tr}[T]$ is a truncation time, which must be chosen such that $c(\mathbf{x}, T_{tr})$ has already approached the asymptotic value of unity. In steady-state flow, $\mu_\tau(\mathbf{x})$ and $\sigma_\tau^2(\mathbf{x})$ are time-invariant quantities. In transient flow, these values change with the time point at which the tracer injection starts. In order to assess the variability of $\mu_\tau(\mathbf{x})$ and $\sigma_\tau^2(\mathbf{x})$ in transient flows with time, we repeated the conservative-tracer injections, shifting the evaluation of the time function $f(t)$ to $f(t+j\Delta t)$, in which Δt $[T]$ is an integer fraction of the period of fluctuations (one hour for the diurnal case, one day for the seasonal one). This is done for all time increments filling the period, now leading to sets of N values of $\mu_\tau^{(j)}(\mathbf{x})$ and $\sigma_\tau^{2\,(j)}(\mathbf{x})$ each, in which the index j refers to the j-th increment, and N denotes the number of increments ($N = 24$ for the diurnal case, $N = 365$ for the seasonal one). From these sets, we compute the time-averaged mean travel time $\overline{\mu}_\tau(\mathbf{x})$ and the corresponding time-standard deviation $\sigma_{\mu_\tau}(\mathbf{x})$ of mean travel time by:

$$\overline{\mu}_\tau(\mathbf{x}) = \frac{1}{N}\sum_{j=1}^{N}\mu_\tau^{(j)}(\mathbf{x}) \tag{17}$$

$$\sigma_{\mu_\tau}(\mathbf{x}) = \sqrt{\frac{1}{N-1}\sum_{j=1}^{N}\left(\mu_\tau^{(j)}(\mathbf{x}) - \overline{\mu}_\tau(\mathbf{x})\right)^2} \tag{18}$$

The time-standard deviation $\sigma_{\mu_\tau}(\mathbf{x})$ of the local mean travel time may be compared to the root time-averaged variance of travel time:

$$\mu_{\sigma_\tau^2}^{0.5}(\mathbf{x}) = \sqrt{\frac{1}{N}\sum_{j=1}^{N}\sigma_\tau^{2\,(j)}(\mathbf{x})} \tag{19}$$

If $\sigma_{\mu_\tau}(\mathbf{x})$ is larger than $\mu_{\sigma_\tau^2}^{0.5}(\mathbf{x})$, the local travel-time distributions at location $\mathbf{x}$ differ significantly between different time points, whereas a large spread of the individual local travel-time distributions could make the variation in time insignificant, which is the case for $\mu_{\sigma_\tau^2}^{0.5}(\mathbf{x}) \gg \sigma_{\mu_\tau}(\mathbf{x})$.

2.3. Multi-dimensional advective-dispersive-Reactive transport

As virtual truth, we consider the traditional, multi-dimensional advection-dispersion-reaction equation (ADRE) under transient flow conditions for each reactive component i:

$$\frac{\partial c_m^{(i)}}{\partial t} + \mathbf{v}\cdot\nabla c_m^{(i)} - \nabla\cdot\left(\mathbf{D}\nabla c_m^{(i)}\right) = r_m^{(i)}(\mathbf{c}) \tag{20}$$

$$\frac{dc_{im}^{(i)}}{dt} = r_{im}^{(i)}(\mathbf{c}) \tag{21}$$

subject to:

$$\mathbf{n}\cdot\left(\mathbf{v}c_m^{(i)} - \mathbf{D}\nabla c_m^{(i)}\right) = \mathbf{n}\cdot\mathbf{v}c_{inlet}^{(i)} \text{ at } \Gamma_{in} \tag{22}$$

$$\mathbf{n}\cdot\left(\mathbf{D}\nabla c_m^{(i)}\right)=0 \text{ at } \Gamma_{out}\cup\Gamma_{no\ flow} \tag{23}$$

$$\mathbf{c}(\mathbf{x},t=0)=\mathbf{c}_0\forall\mathbf{x} \tag{24}$$

in which $c_m^{(i)}(\mathbf{x},t)$ $[ML^{-3}]$ is the concentration of mobile component i, $r_m^{(i)}(\mathbf{x},t)$ $[ML^{-3}T^{-1}]$ is the reactive source-sink term for that compound, whereas $c_{im}^{(i)}(\mathbf{x},t)$ and $r_{im}^{(i)}(\mathbf{x},t)$ correspond to immobile components; $\mathbf{c}(\mathbf{x},t)[ML^{-3}]$ is the vector of all concentrations, both of mobile and immobile species, with the corresponding initial value $\mathbf{c}_0(\mathbf{x})[ML^{-3}]$, assumed uniform; $c_{inlet}^{(i)}[ML^{-3}]$ is the concentration of compound i in the inflow; $\mathbf{v}(\mathbf{x},t)=\mathbf{v}_{SS}(\mathbf{x})f(t)[LT^{-1}]$ is the time-dependent seepage velocity vector, and $\mathbf{D}(\mathbf{x},t)[L^2T^{-1}]$ is the local dispersion tensor, depending on $\mathbf{v}(\mathbf{x},\ t)$ via the classical Scheidegger (1961) parametrization:

$$\mathbf{D}=\frac{\mathbf{v}\otimes\mathbf{v}}{\|\mathbf{v}\|}\left(\alpha_\ell-\alpha_t\right)+\mathbf{I}\left(\|\mathbf{v}\|\alpha_t+D_p\right) \tag{25}$$

where $\mathbf{v}\otimes\mathbf{v}$ is the matrix product of $\mathbf{v}$ with itself, $\|\mathbf{v}\|$ is the absolute value of $\mathbf{v}$, α_ℓ $[L]$ and α_t $[L]$ are the longitudinal and transverse dispersivities, $\mathbf{I}$ $[-]$ is the identity matrix, and D_p $[L^2T^{-1}]$ is the pore-diffusion coefficient. Γ_{in}, Γ_{out}, and $\Gamma_{no\ flow}$ denote inflow, outflow, and no-flow boundaries, respectively. Γ_{in} and Γ_{out} may contain both fractions of constant-head and constant-flux boundaries of the flow problem, whereas $\Gamma_{no\ flow}$ is the fraction of the constant-flux boundary with a prescribed normal volumetric flux of zero.

In our application, the vector $\mathbf{c}(\mathbf{x},\ t)$ comprises the concentrations of an ideal tracer, oxygen, nitrate, and dissolved organic carbon as mobile species, and of aerobic and denitrifying bacteria as immobile species. The reactions include aerobic respiration and denitrification with corresponding growth of the biomass, as well as biomass decay. The equations and parameters are listed in Appendix A.

2.4. One-dimensional reactive transport in travel-time coordinates

The one-dimensional reactive transport equation in spatial coordinates and its boundary and initial conditions read as Eqs. (20)–(24), replacing the vector $\mathbf{x}$ of spatial coordinates by the scalar distance x and the nabla-operator by the partial derivative $\partial/\partial x$. In travel-time coordinates, the latter derivative is replaced by $(\partial\tau_{ch}/\partial x)\partial/\partial\tau_{ch}$. In one-dimensional transport with constant and uniform coefficients (implying steady-state flow), the mean travel time $\mu_{\tau_{ss}}(x)$ for steady-state flow and the corresponding kinematic age $\tau_{adv_{ss}}(x)$ are identical, and $\partial x/\partial\mu_{\tau_{ss}}=\partial x/\partial\tau_{adv_{ss}}=v_{SS}$. Thus, taking the mean travel time $\mu_{\tau_{ss}}(x)$ for steady-state flow as the characteristic time-independent travel time τ_{ch} is a natural choice. Considering now that the velocity scales in time with $f(t)$, the one-dimensional advection-dispersion-reaction equation for transient flow reads in travel-time coordinates as:

$$\frac{\partial c_{1D,m}^{(i)}}{\partial t}+f(t)\frac{\partial c_{1D,m}^{(i)}}{\partial\mu_{\tau_{ss}}}-D_\tau(t)\frac{\partial^2 c_{1D,m}^{(i)}}{\partial\mu_{\tau_{ss}}^2}=r_{1D,m}^{(i)}(\mathbf{c}_{1D}(x,t)) \tag{26}$$

$$\frac{dc_{1D,im}^{(i)}}{dt}=r_{1D,im}^{(i)}(\mathbf{c}_{1D}(x,t)) \tag{27}$$

subject to:

$$f(t)c_{1D,m}^{(i)}-D_\tau(t)\frac{\partial c_{1D,m}^{(i)}}{\partial\mu_{\tau_{ss}}}=f(t)c_{inlet}^{(i)} \text{ at } \Gamma_{in} \tag{28}$$

$$D_\tau(t)\frac{\partial c_{1D,m}^{(i)}}{\partial\mu_{\tau_{ss}}}=0 \text{ at } \Gamma_{out} \tag{29}$$

$$\mathbf{c}(x,t=0)=\mathbf{c}_0\forall x \tag{30}$$

where the index "1D" denotes calculations performed in one dimension, and D_τ $[T]$ is a longitudinal dispersion coefficient expressed in travel-time coordinates. The latter relates to the spatial longitudinal dispersion coefficient $D_\ell[L^2T^{-1}]$ by $D_\tau=D_\ell/v_{SS}^2$.

In the following, we apply a modified version of the advective-dispersive stream-tube approach (Cirpka and Kitanidis, 2000) to map 1-D results to the multi-dimensional domain. Here, the characteristic travel-time coordinate is the mean advective-dispersive travel time $\mu_{\tau_{ss}}$ for steady-state flow, and $D_\tau(t)=f(t)\alpha_\ell/v_{SS}+D_p/v_{SS}^2$. In contrast to Sanz-Prat et al. (2015), we don't attempt finding better parametrizations of local dispersion in the travel-time domain and simply apply the local values of α_ℓ and D_p from the 2-D simulations. The 1-D results are correspondingly mapped to the two-dimensional by Eq. (1). We could also apply a modification of the stochastic-convective approach, by taking the kinematic age $\tau_{adv_{ss}}(\mathbf{x})$ for steady-state flow as mapping variable and neglecting dispersion in the 1-D model altogether, which we don't test in the present study.

We compare the reactive-component concentrations obtained by the 1-D travel-time models and mapped to the two-dimensional domain with the concentrations of the multi-dimensional virtual truth at each location of the 2-D domain. We normalize the residual error by the respective inflow concentration for the mobile compounds, and by the maximum biomass concentration for the immobile compounds:

$$\varepsilon^{(i)}(\mathbf{x},t)=\frac{c_{2D}^{(i)}(\mathbf{x},t)-c_{1D}^{(i)}(\tau_{ch}(\mathbf{x}),t)}{c_{inflow/\ max}^{(i)}} \tag{31}$$

in which the index i refers to an individual component.

3. Test case

As test case we consider biogeochemical transformations upon river-bank filtration. The infiltrating surface water is enriched in dissolved organic carbon with a chemical composition of CH_2O, denoted DOC, dissolved oxygen (O_2), and nitrate (NO_3^-), that is, the dissolved electron donor and two competing electron acceptors are concurrently introduced into the water-saturated porous medium. We consider immobile biomass of aerobic and obligatory denitrifying bacteria, catalyzing the oxidation of DOC to CO_2 by dissolved oxygen and nitrate.

Table 1
Biogeochemical reactions considered.

Net aerobic degradation at steady state ($\Delta G^0 = -501\,kJ/mol$ at pH7):
$CH_2O + O_2 \rightarrow CO_2 + H_2O$
Net denitrification at steady state ($\Delta G^0 = -476\,kJ/mol$ at pH7):
$CH_2O + \frac{4}{5}NO_3^- + \frac{4}{5}H^+ \rightarrow \frac{4}{10}N_2 + CO_2 + \frac{7}{5}H_2O$

These transformations are coupled to growth of the respective microorganisms. The elemental composition of both types of bacteria is assumed to be CH_2O. Elevated dissolved-oxygen concentrations non-competitively inhibit denitrification. In the initial state, the biomass concentrations are uniform throughout the domain and low. To limit biomass growth close to the inlet, we introduce maximum biomass concentrations, representing the carrying capacity of the porous medium. Both microorganisms undergo decay requiring nitrate or oxygen as oxidants. Table 1 contains the net chemical reactions, whereas the mathematical description of the reactive sink/source terms and the associated parameters are discussed in Appendix A and listed in Table A.4, respectively.

We consider a two-dimensional, confined, sandy aquifer with mild physical heterogeneity. The hydraulic conductivity field, $K(\mathbf{x})$, has a uniform geometric mean of $K_g = 10^{-3} m/s$, and the variance of $\ln K$ is $\sigma^2_{\ln K} = 1$. The log-hydraulic conductivity field is a single realization of a multi-Gaussian random spatial variable with an anisotropic exponential covariance function with integral scales of $\ell_x = 0.05m, \ell_y = 0.1m$. The domain is 2.5 m long and 1 m wide. The mean seepage velocity at steady state is set at 1.25 m/d. Constant-head boundary conditions at the left and right boundaries are chosen to meet the requested mean velocity; there is no flow across the top and bottom boundaries (see Table 2 for all geometric and hydraulic parameters).

Table 2
Geometric and hydraulic parameters.

Symbol	Meaning	Value
Geometric parameters of the 2-D domain		
L	Length of the 2-D domain	2.5 m
W	Width of the 2-D domain	1 m
n_x	Number of cells in x-direction for flow calculation	250
n_y	Number of cells in y-direction for flow calculation	200
Δx	Cell size in x-direction for flow calculation	0.01 m
Δy	Cell size in y-direction for flow calculation	0.005 m
n_{str}	Number of stream tubes for transport	500
n_{sec}	Number of stream-tube-sections for transport	200
Discretization of travel-time models		
τ_{max}	Length of the travel-time domain	25 d
$\Delta\tau$	Travel-time increment	0.01 d
Geostatistical parameter of K-field		
ℓ_x	Correlation length in x-direction	0.05 m
ℓ_y	Correlation length in y-direction	0.10 m
$\sigma^2_{\ln K}$	Variance of log-hydraulic conductivity	1
K_g	Geometric mean of hydraulic conductivity	1×10^{-3} m/s
Flow characteristics (for $\sigma^2_{\ln K} = 1$)		
K_{eff}	Effective hydraulic conductivity	$1.1 \cdot 10^{-3}$ m/s
$\overline{q}_x$	Mean specific discharge ($\forall \sigma^2_{\ln K}$)	0.4 m/d
$\overline{v}_x$	Mean seepage velocity ($\forall \sigma^2_{\ln K}$) (2-D)	1.25 m/d
$\overline{v}_x$	Mean seepage velocity ($\forall \sigma^2_{\ln K}$) (1-D)	1 m/d
J	Mean hydraulic gradient	$4.63 \cdot 10^{-3}$
Transport parameters		
θ	Porosity	0.4
α_ℓ	Longitudinal dispersivity (2-D)	0.001 m
α_t	Transverse dispersivity (2-D)	0.0001 m
D_p	Pore diffusion coefficient	10^{-9} m^2/s

The spatial discretization of the transport problem is represented by a stream-line oriented grid with 500 stream tubes and 200 sections in the flow direction (Cirpka et al., 1999a, 1999b). The one-dimensional model is conceptualized as a single stream tube of the two-dimensional model, whose dispersion coefficient is taken as the longitudinal dispersion coefficient used in the 2-D model but modified to the travel-time approach by the expression: $D_\tau = D_\ell / v^2_{SS}$. Fig. 1A shows the log-hydraulic conductivity distribution and Fig. 1B the resulting flow net of the two-dimensional domain. Fig. 1C shows the two time functions $f(t)$ considered in this paper in the transport simulations with transient flow, according to Eq. (13) (marked blue) for the diurnal velocity-fluctuations and Eq. (14) for the seasonal one. All mobile compounds (DOC, O_2, NO_3^-, and an idealized conservative tracer) have an initial value of zero and are continuously introduced into the domain via the inflow boundary. Table 3 lists the values of the initial and boundary conditions for flow and reactive transport.

We simulate conservative and reactive transport in the 1-D and 2-D models using the Finite Volume Method with upstream differentiation of the advective term on a streamline-oriented grid (Cirpka et al., 1999a, 1999b). To minimize artificial dispersion, advection is solved by explicit time integration, whereas dispersion and reactions are solved by implicit integration as fully coupled system, using the Newton–Raphson method to handle the non-linearity.

To obtain metrics of the local travel-time distributions, we perform conservative-transport simulations with a step-input function as boundary condition. This is done for steady-state and transient flow. As discussed in Section 2.2, we compute the metrics of the local travel-time distributions in the 2-D domain and in an equivalent 1-D system. We simulate bioreactive transport in the 1-D model considering diurnal velocity fluctuations and map the concentrations to the 2-D domain according to Eq. (1) as outlined above. We compare the mapped results to spatially explicit 2-D simulations of advective-dispersive-bioreactive transport, denoted the "virtual truth", and the error is quantified by the normalized residuals according to Eq. (31). Finally, we analyze the system behavior for seasonal, smooth fluctuations of velocity in the 1-D model only, essentially demonstrating that the system approaches quasi steady state in reactive transport if the time scale of fluctuations is considerably larger than the time needed for the reactive system to adapt to new hydraulic conditions.

4. Results

4.1. Spatial distribution of Travel time metrics

Fig. 2 shows metrics of the local travel time as function of distance in the one-dimensional model with diurnal fluctuations. Fig. 2A shows the range of the local mean travel time $\mu_\tau(x)$, obtained for advective-dispersive transport, as gray band, the

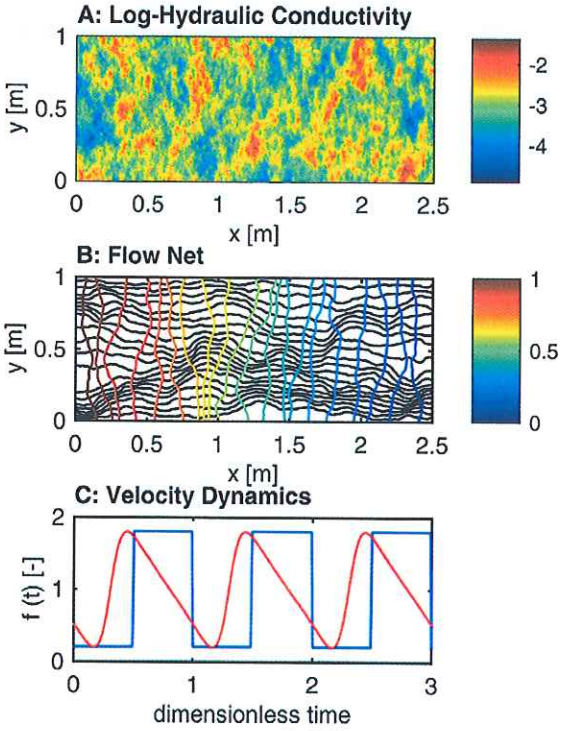

Fig. 1. A: log-hydraulic conductivity field $\ln(K(\mathbf{x}))$ (K in m/s) in the 2-D domain; B: Resulting flow net, the color axis denotes the normalized head (zero at the outlet, unity at the inlet); C: time function $f(t)$ used for the transient calculations, blue: diurnal fluctuations, red: seasonal fluctuations. (For interpretation of the references to color in this figure legend, the reader is referred to the web version of this article.)

arithmetic time average $\overline{\mu}_\tau(x)$ as red line, and the time-median of $\mu_\tau(x)$ as blue line. Fig. 2B shows the same metrics for the kinematic age $\tau_{adv}(x)$ (using the approach of van der Velde et al. (2015)) rather than the mean of the advective-dispersive travel time. For the rather small dispersivity of $\alpha_\ell = 10^{-3}m$ at a mean velocity of 1 m/d, the two types of groundwater ages hardly differ. To be consistent with the description of travel-time transport, the longitudinal coordinate is replaced by the mean travel time for steady-state flow.

The most striking result is that the range of the kinematic age collapses to a single value at points with a mean travel time of 1, 2, 3, ... days. One day is exactly the period of the velocity fluctuations. After one day, a solute particle has exactly experienced the time-averaged velocity, no matter at which time point within the cycle the particle started. At distances with steady-state mean travel times falling between integer multiples of the period of fluctuations, the observed mean groundwater age depends on time: A solute particle may first run ahead and then slow down, or vice versa. Adding dispersion leads to some smearing of these results.

Table 3
Initial and boundary conditions for all components.

Component	Initial concentration	Inflow concentration
Dissolved organic carbon	0 μM	500 μM
Dissolved oxygen	0 μM	250 μM
Nitrate	0 μM	100 μM
Tracer	0 μM	100 μM
Aerobic bacteria	1 μM	n.a.
Denitrifying bacteria	1 μM	n.a.

Fig. 2C compares the time-standard deviations of the mean groundwater age for the ADE ($\sigma_{\mu_\tau}(x)$, blue line) and the kinematic age ($\sigma_{\tau_{adv}}(x)$, red line) with the root time-averaged variance of local travel time for the ADE ($\mu_{\sigma_\tau^2}^{0.5}$, yellow line). As already discussed, at locations with steady-state mean travel times being integer multiples of the period of velocity fluctuations, there is no time-related uncertainty of the kinematic age and the corresponding uncertainty of the mean advective-dispersive groundwater age has a distinct minimum. Interestingly, at these locations the spread of the local breakthrough curves exhibits a local maximum. As the variance of local travel time in steady-state flow increases with distance, the standard deviation is expected to increase with the square-root of distance, a general trend that can be seen in the yellow line of Fig. 2C.

Two conclusions can be drawn from Fig. 2: (1) In time-periodic transient flow, there are locations at which the mean travel time assumes a time-invariant value, namely if this value is an integer multiple of the period of velocity fluctuations. At all other locations, analyzing the groundwater age from an artificial or natural tracer test leads to results that depend on the exact time when the signal was introduced into the porous medium; (2) The time-averaged mean groundwater age $\overline{\mu}_\tau(x)$ and the mean groundwater age for steady-state flow $\mu_{\tau_{ss}}(x)$ are not exactly identical. The latter increases linearly with distance if the velocity is spatially uniform, whereas the former shows slight variations from the linear trend. We conjecture that the mean groundwater age for steady-state flow $\mu_{\tau_{ss}}(x)$ is also the better (and easier to apply) quantity for mapping 1-D results of reactive transport to multi-dimensional domains.

Fig. 3 contains the spatial distributions of the main local travel-time metrics in the two-dimensional domain for four

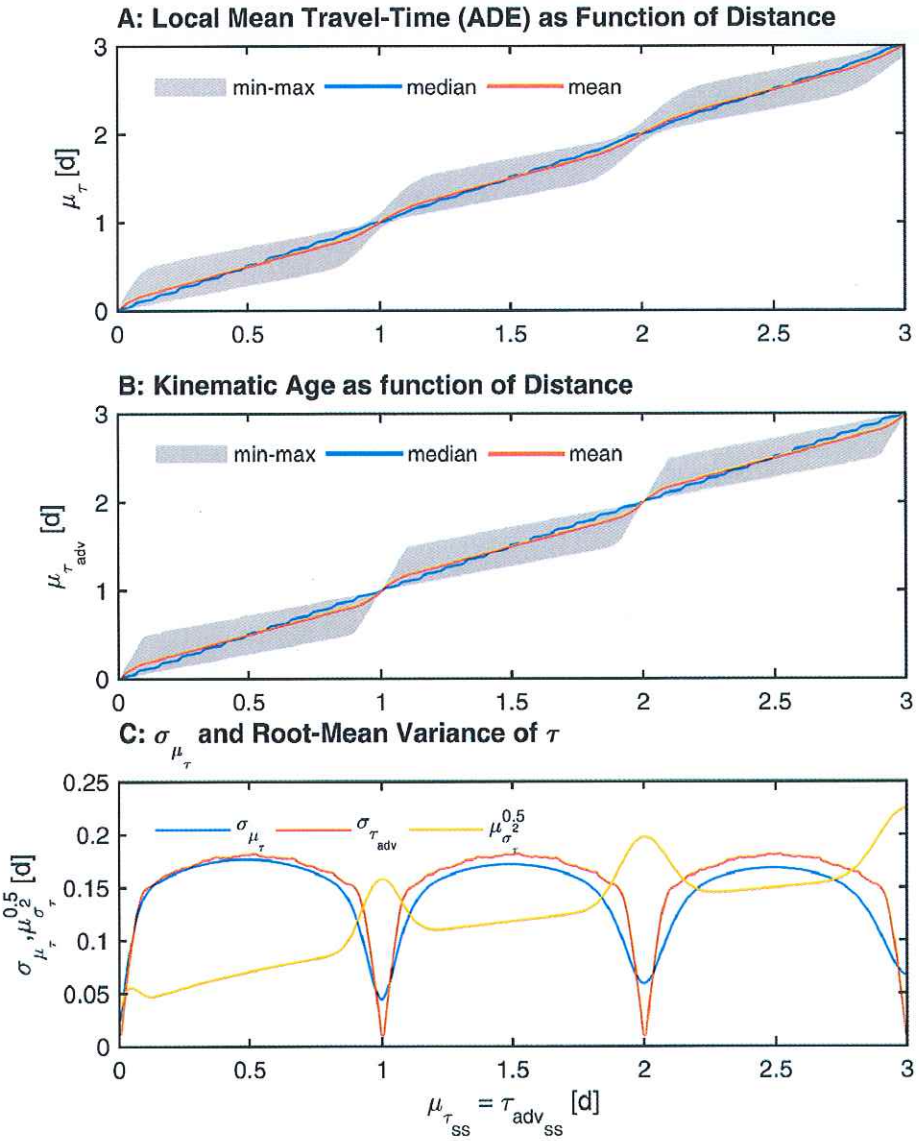

Fig. 2. Metrics of local travel-time distributions in the 1-D model. A: Spatial distributions for advective-dispersive transport; gray area: range of $\mu_\tau^{(i)}(x)$-values for the different time-offsets in $f(t)$; blue line: time-median of the mean travel time; red line: time-averaged mean travel time, $\overline{\mu}_\tau(x)$. B: Identical metrics as in A, but for the kinematic age. C: Blue line: time-standard deviation of the mean travel time in the ADE model, $\sigma_{\mu_\tau}(x)$; red line: time-standard deviation of the kinematic age, $\sigma_{\tau_{adv}}(x)$; yellow line: root time-average of the variance of travel time in the ADE model, $\mu_{\sigma_\tau^2}^{0.5}$. The distances x is replaced by the mean groundwater age for steady-state flow $\mu_{\tau_{ss}}$. (For interpretation of the references to color in this figure legend, the reader is referred to the web version of this article.)

different types of travel times: The kinematic age for steady-state flow ($\tau_{adv_{ss}}(\mathbf{x})$, subplot A1), the kinematic age for transient flow ($\tau_{adv}(\mathbf{x})$, subplots B1 & B2), the advective-dispersive groundwater age for steady-state flow ($\tau_{SS}(\mathbf{x})$, subplots C1& C3), and the advective-dispersive groundwater age for transient flow (subplots D1–D3). The first column contains kinematic ages and local mean groundwater ages either at steady state or averaged over time. The white lines represent daily isochrones of the corresponding (time-averaged) age variable in each case study; the similarities among all cases are obvious, even though dispersion slightly smooths the mean groundwater age distribution and thus straightens isochrones (see C1 and D1) in comparison to the kinematic age (see A1 and B1). Differences between the time-averaged ages and the ages for steady-state flow are hardly detectable. The overall pattern reflects the heterogeneity of the underlying hydraulic-conductivity field (see also the discussion by Sanz-Prat et al. (2015) who used the same conductivity field).

The second column of Fig. 3 shows the time-related uncertainty in kinematic age and local mean groundwater age in transient flow, reproducing the result of the 1-D simulations that the kinematic age and the local mean groundwater age shows zero-to-minimal uncertainty when the value is an integer multiple of the period of velocity fluctuations: The blue zones in B2 and D2 follow the daily isochrones of B1 and D1.

Finally, the third column of Fig. 3 illustrates the spread of local breakthrough curves in the advective-dispersive case. The overall pattern is dominated by effects of heterogeneity: The low-K zone at the bottom quarter of the inflow boundary causes an extended, shadow-like zone of old water that mixes laterally with younger water, causing an increase in the local variance of travel time, which has already been discussed by

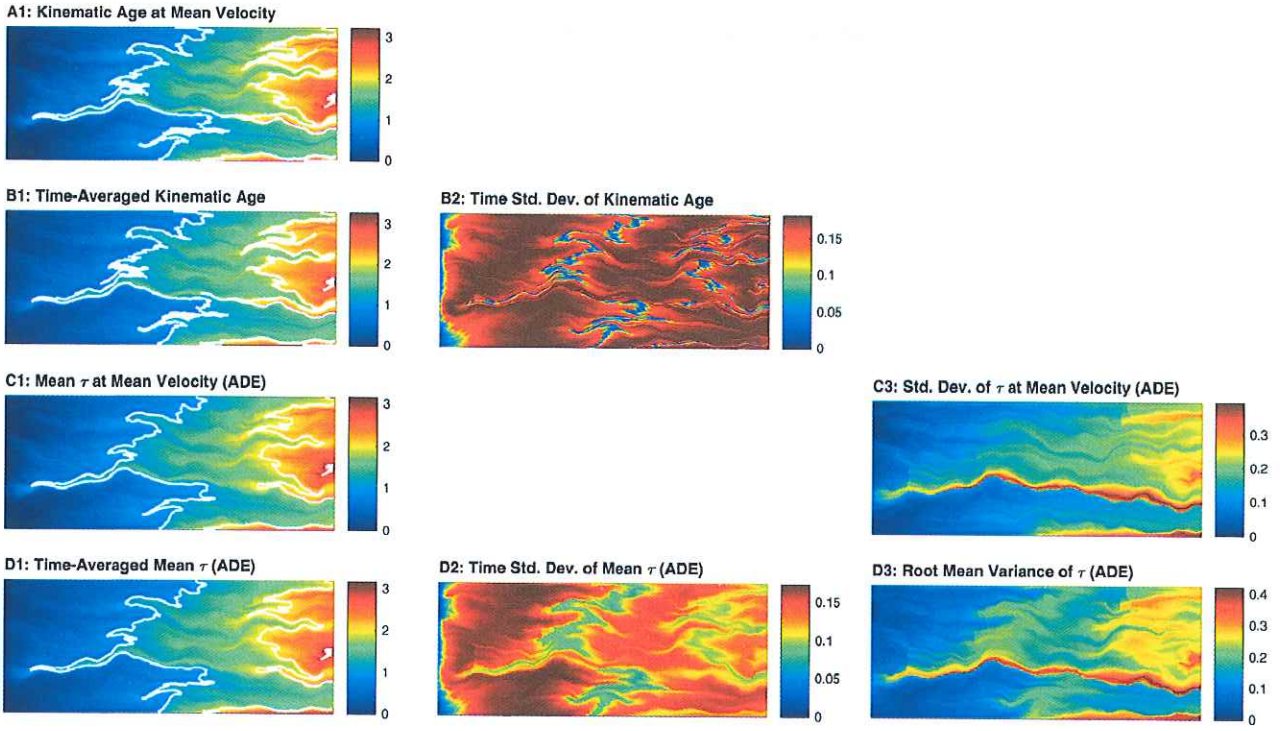

Fig. 3. Spatial distribution of travel time metrics of the four case studies in the two-dimensional domain: first row, kinematic age for steady-state flow; second row: kinematic age for transient flow (diurnal fluctuations); third row: advective-dispersive travel time for steady flow; fourth row: advective-dispersive travel time for transient flow (diurnal fluctuations). First column: time averaged local mean values; second column: time standard deviations of local mean values; third column: root time-mean variance of local travel time.

Sanz-Prat et al. (2015). In the transient case, this is overlain by an increase in the spread of local breakthrough curves at the daily mean isochrones where the uncertainty of the mean groundwater age was minimal.

4.2. Reactive system behavior in the 1-D Model

Fig. 4 shows the concentrations of the five reactive components in the one-dimensional advective-dispersive-reactive model with diurnal fluctuations of the spatially uniform velocity. All concentrations are normalized to range between zero and one: mobile-species concentrations are normalized by their respective inflow concentrations, whereas the biomass concentrations are normalized by the maximum biomass concentrations of the aerobes and denitrifiers. The surface plots (Fig. 4A, B, C, E, and F) illustrate the variability of concentration in the first two meters of the domain (representing the first two days of travel time for steady-state flow) during the last day of simulation. We have omitted the early-time behavior, when the reactive system is established, and concentrate on the "dynamic steady state", when the system response to the diurnal velocity fluctuations leads to daily repetitions of the same concentration distributions. The cycle starts with the onset of the low velocity. At low velocity, oxygen does not deeply penetrate into the domain, nitrate is consumed already at short distances to the inlet, and also the spatial profile of the organic substrate is squeezed towards the inlet. With the onset of a nine-fold velocity after 12 *h*, the fronts of mobile reactants are pushed deeper into the domain. The transition from one quasi steady state to the other takes about 5 *h*. At any given time, a clear pattern of the profiles can be observed: Close to the inlet, oxygen concentrations are so high that denitrification is inhibited; wherever oxygen has practically vanished, the nitrate concentration starts to decrease, and the spatial gradient of the substrate concentration is higher in the aerobic than in the denitrifying zone.

The time scale of fluctuations is considerably higher than the time scale of biomass decay. As a consequence, the temporal fluctuations of the biomass concentrations are strongly dampened in comparison to the fluctuations of dissolved-reactant concentrations. Wherever oxygen is present at least over some time, the concentration of aerobic bacteria reaches almost the maximum value. At $x \approx 0.5$ *m*, the aerobes disappear because oxygen does not penetrate deeper into the domain. A small secondary peak is a remnant of early-time behavior. The obligatory denitrifiers are permanently poisoned in the narrow zone where oxygen is always present and consequently the respective biomass concentration is practically zero. In the zone where oxygen is sometimes present at notable concentrations and sometimes not, the denitrifier concentration increases according to the time fraction with suitable conditions. Finally, the biomass concentration of the denitrifiers reaches a value of about 90% of the preset maximum biomass concentration in the zone where oxygen has permanently vanished.

Fig. 4D contains the ranges of all normalized concentrations as length profiles together with the time-averaged values (solid lines). Like in the other plots, the variability is only shown for the last day of simulation. Notable is the strong overlap of aerobic and obligatory denitrifying bacteria. This reflects that environmental conditions vary, sometimes preferring one type of biomass over the other, and at other times vice versa. For comparison, Fig. 4D also contains the concentrations

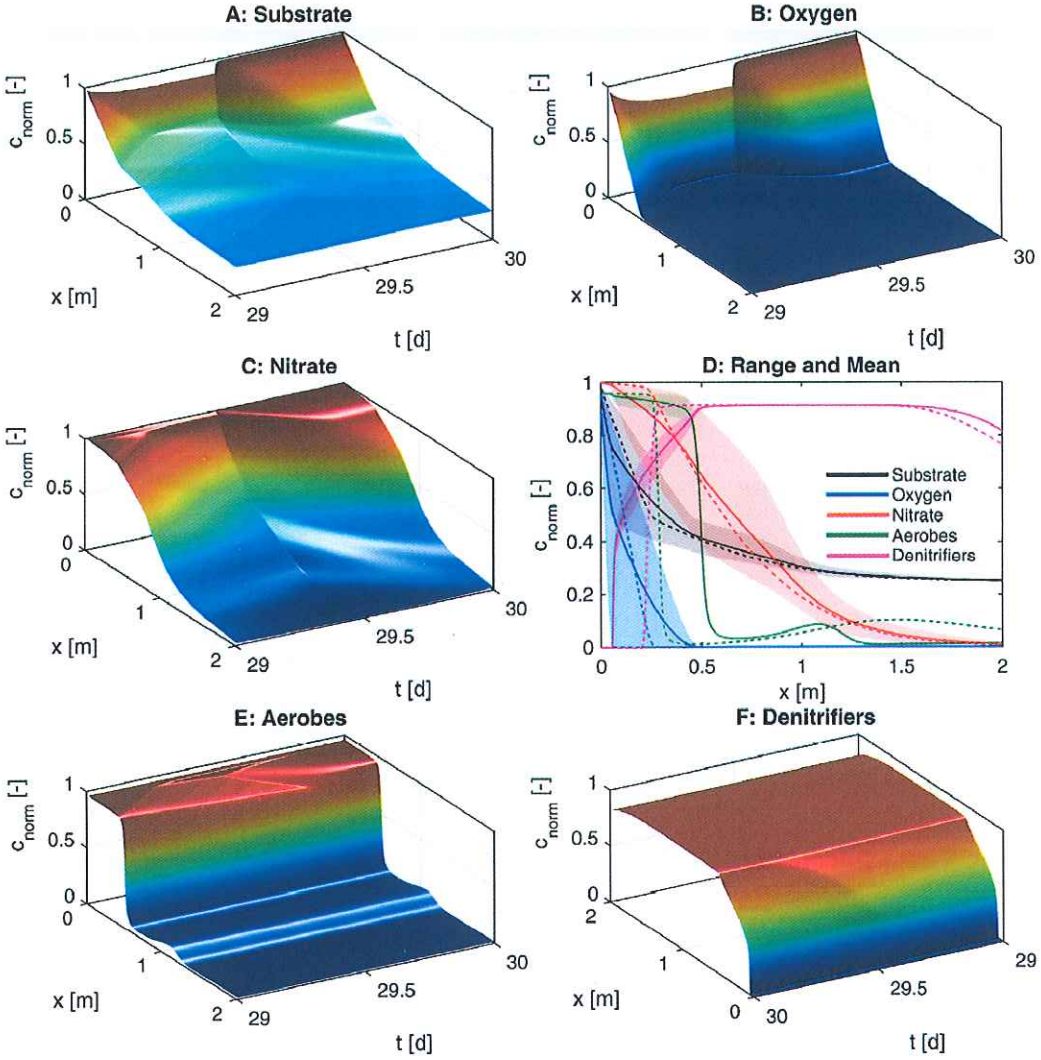

Fig. 4. Normalized concentrations of reactive compounds in the advective-dispersive one-dimensional model undergoing diurnal velocity fluctuations. A, B, C, E, and F show the normalized concentrations in the first two meters of domain at the last simulation day (F is rotated by 180°). D shows the length profiles of the reactive components in transient flow by their range (shaded areas) and mean (solid lines) in comparison to the concentration profiles at the end of the simulation time for steady-state flow (dashed lines).

of the same reactive system after 30 days of simulated times for steady-state flow conditions, shown as dashed lines. Now, the two types of bacteria hardly coincide: the aerobes penetrate only about 30 *cm*, and the denitrifiers can hardly be observed in the first 20 *cm*.

4.3. 2-D Concentration distributions of reactive components: comparison between spatially explicit and travel-time based models

Fig. 5 shows the spatial distributions of the normalized reactive-component concentrations simulated by the the spatially explicit 2-D model (left column of Fig. 5) and of the 1-D model mapped onto the 2-D domain by means of the mean travel time for steady-state flow, $\mu_{\tau_{ss}}(\mathbf{x})$ (central column of Fig. 5). The results are shown as a snapshot at the end of the simulation time, which is at a time point within the diurnal cycle when the front of oxygen has penetrated the deepest into the domain. The concentration patterns of all five reactive components are so similar that a visual inspection does not reveal the differences. The right column of Fig. 5 shows the spatial distribution of the normalized residual errors of all components as calculated by Eq. (31). The normalized residual errors of substrate and oxygen don't exceed the range of $\pm 5\%$; the error of nitrate is somewhat higher at the distinct feature where old and young water flow in parallel to each other, and the highest errors for the two bacteria concentrations are either aligned with specific isochrones or located along the already mentioned feature. At this feature, transverse dispersion leads to mixing of dissolved reactants originating from the young and old water which is not accounted for in the 1-D model. Overall, however, the error introduced by the mapping approach is small and local.

Fig. 6 further exemplifies the performance of the approach by plotting the 1-D and 2-D results as function of the mean travel time for steady-state flow $\mu_{\tau_{ss}}$. Thus, now the 2-D results

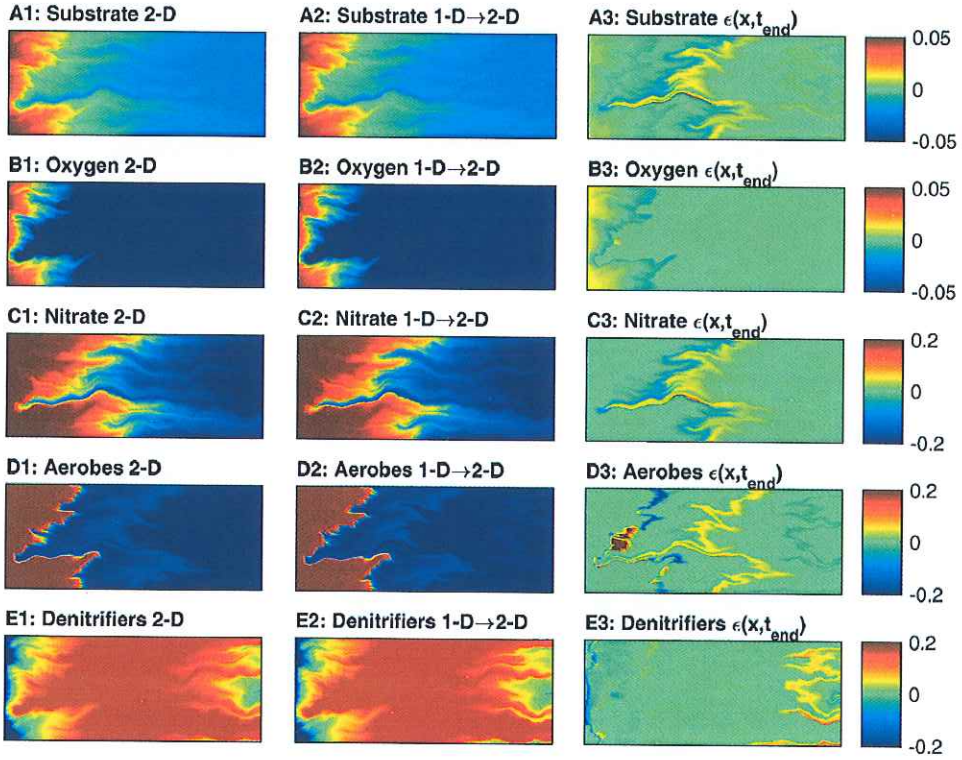

Fig. 5. Comparison between spatially explicit two-dimensional simulation results at the end of the simulation ($t_{end} = 30\,d$) and corresponding one-dimensional model results mapped onto the 2-D domain by the mean travel time at steady-state flow. All concentrations are normalized to range between zero and one. Left column: normalized concentration of the spatially explicit 2-D advective-dispersive-reactive transport model; center column: normalized concentrations of the 1-D model mapped onto the 2-D domain; right column: normalized residual error. The color axis for the left and central columns ranges from zero to one, the limits for the right column are given by the colorbars. (For interpretation of the references to color in this figure legend, the reader is referred to the web version of this article.)

are mapped into the 1-D domain. In the 2-D results, the fairly sharp front of the aerobic biomass concentration, observed in the 1-D model at $\mu_{\tau_{ss}} \approx 0.5d$, is subject to some uncertainty in the $\mu_{\tau_{ss}}$-direction causing, in conjunction with the sharp gradient, large residual errors. For the aerobic biomass, we also see a mismatch of the secondary peak which has no consequence for the overall system behavior because this peak is a remnant of early-time behavior. For nitrate and substrate we see a distinct shoulder in the 1-D results at $\mu_{\tau_{ss}} \approx 0.9d$, which is not observed in the 2-D results. This shoulder is part of the concentration pulsation illustrated in Fig. 4. In the 2-D model, heterogeneity causes additional mixing smearing the distinct shoulder. We believe that we could have obtained a better match between the 1-D and 2-D results in this part of the domain if we had used a parametrization of longitudinal mixing in the 1-D model that accounts for increasing mixing with increasing distance as done by Sanz-Prat et al. (2015) for bioreactive transport in steady-state flow.

4.4. Sensitivity analysis

We performed a sensitivity analysis to test how changing selected transport parameters affects the applicability of the travel-time models. We did this by scenario calculations, changing parameters which we believed to be most important, namely: the mean seepage velocity $\bar{v}$, the fluctuation range f

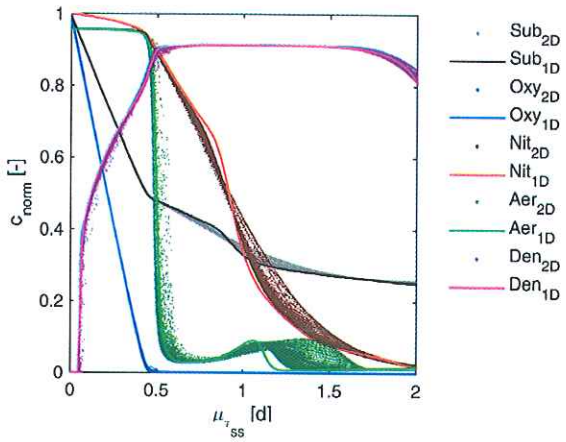

Fig. 6. Comparison of normalized reactive compound concentrations between the 2-D model or "virtual truth" and the 1-D or mean travel time model for advective-dispersive transport and transient inflow rate with respect to the mean travel time estimated at mean velocity (equivalent steady state simulation) at the last hour of day 29. Black line, substrate concentration in the 1-D model; gray dots, substrate concentration in the 2-D model; blue line, oxygen concentration in the 1-D model; blue dots, oxygen concentration in the 2-D model; red line, nitrate concentration in the 1-D model; red dots, nitrate concentration in the 2-D model; green line, aerobes concentration in the 1-D model; green dots, aerobes concentration in the 2-D model; magenta line, denitrifier concentration in the 1-D model; magenta dots, denitrifier concentration in the 2-D model. (For interpretation of the references to color in this figure legend, the reader is referred to the web version of this article.)

of velocity, the transverse dispersivity α_t, the variance of log-hydraulic conductivity σ^2_{lnK}, and a multiplication factor for all reaction rates. In all cases, we repeated the 1-D and the spatially explicit 2-D simulations (including the calculations of the mean travel time for steady-state flow, $\mu_{\tau_{ss}}(\mathbf{x})$), performed the same mapping from the 1-D models to the 2-D domain as before, computed the normalized residual errors $\varepsilon_i(\mathbf{x},t)$ according to Eq. (31), and calculated the normalized root mean-square error (NRMSE) for each compound as time-dependent metric how strongly the mapped 1-D results differed from the spatially explicit calculations:

$$NRMSE_i(t) = \sqrt{\frac{\int_\Omega \varepsilon_i^2(\mathbf{x},t)d\mathbf{x}}{\int_\Omega d\mathbf{x}}} \tag{32}$$

Fig. 7 shows the time-dependent error metric for all compounds on the last simulated day for all scenarios including the base case (bold gray line). The different line colors and patterns refer to different scenarios. Decreasing the velocity (solid black lines) or increasing all reaction rates (dotted pink lines) leads to a shrinking of the reaction zones. This makes the 2-D simulations somewhat more vulnerable to numerical dispersion, but the applicability of the mapping approach does not differ dramatically from the base case. Increasing the velocity (dashed black lines) or decreasing all reaction rates (solid pink lines) leads to an expansion of the reaction zones. Decreasing the range of temporal velocity fluctuations (solid blue lines) leads to a better agreement between the travel-time based and the spatially explicit 2-D results, whereas increasing the range of fluctuations by a factor of five (dashed blue lines) leads to an increase in the error. We expected that increasing transverse dispersion (red lines) would lead to severely stronger discrepancies because of enhanced inter-streamtube mixing, but the effects on the applicability of the approach are not dramatic. Note that in these cases the spatial distributions of both mean groundwater age and reactive-species concentrations are smoother. Finally, increasing the degree of heterogeneity (green lines) leads to more extreme differences in travel time within a cross-section, this in turn facilitates mixing of younger and older water by transverse dispersion. As expected, this leads to somewhat larger errors, but *NRMSE*-values of the bacteria concentrations, which are affected the most, remain moderate (about 10% for $\sigma^2_{lnK}=3$). Altogether, the scenario calculations show that the approach is suitable for the given reactive system and overall setup over a wide parameter range.

4.5. Comparison between diurnal and seasonal flow fluctuation in the 1-D Model

Fig. 8 shows the bacteria concentrations in the one-dimensional advective-dispersive model for diurnal (top row)

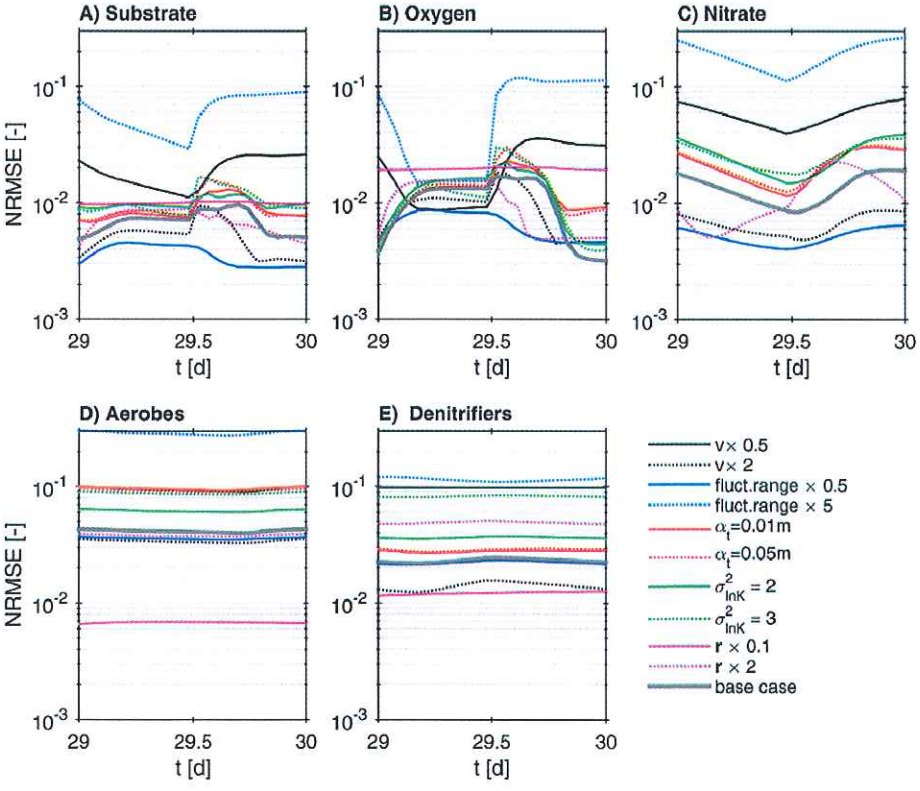

Fig. 7. Normalized root-mean square error of all compounds according to Eq. (32) as function of time on day 30 of the simulation. Titles of the subplots indicate the concentration considered. Gray line: base case; black lines: multiplication of the velocity with a constant factor (solid: 0.5, dotted: 2.0); blue lines: multiplication of the range of velocity fluctuations (solid: by 0.5, dotted: by 5.0); red lines: increase of transverse dispersivity (solid: to 0.01m, dotted: to 0.05m); green lines: increase of variance of ln(K) (solid: to 2.0, dotted: to 3.0); magenta: multiplication of all reaction rates with a constant factor (solid: 0.1, dotted: 2). (For interpretation of the references to color in this figure legend, the reader is referred to the web version of this article.)

and seasonal (bottom row) velocity fluctuations. The first column of subplots shows the aerobic bacteria, the second the denitrifying bacteria as function of space and time, and the third the correlation between the two biomass concentrations as function of time. Fig. 8 only show the first meter of the domain. As can be seen, the system with diurnal velocity fluctuations requires less than ten days to establish a more or less stable pattern. The following discussion concentrates on the dynamic steady state approached considerably later.

As discussed above, the velocity fluctuations make the oxygen-containing zone shrink and expand. In the transition zone, the conditions change from being preferable for aerobic bacteria to those preferring denitrifiers. As listed in Table A.4, the maximum specific decay coefficient of both types of biomass is 0.3/*d*, implying a characteristic time of biomass death of about 3 *d*. The time scale of diurnal fluctuations is smaller than that resulting in the already discussed overlap of aerobic and denitrifying bacteria. The presence of this overlapping zone diminishes the extent of anti-correlation between the two biomass concentrations to a value of $r_{c_{den}caer} \approx -0.7$ from day ten on (see Fig. 8C1). In case of the seasonal fluctuations, the time scale of the fluctuations is two orders of magnitude larger than the time scale of biomass death. Thus, the distribution of biomass can follow the velocity fluctuations and distinct zones with predominantly aerobic and denitrifying bacteria can be observed. As plotted in Fig. 8C2, the correlation coefficient $r_{c_{den}caer}$ assumes more negative values, even reaching almost perfect anti-correlation, in case of seasonal versus diurnal velocity fluctuations. As a consequence, the error introduced by assuming quasi steady-state conditions of reactive transport may be negligible in case of purely seasonal fluctuations, whereas the effect of flow dynamics on the time-average biomass distribution must be considered in case of diurnal fluctuations.

5. Discussion, conclusions, and practical recommendations

The presented results allow us to evaluate the validity of the hypothesis stated in Eq. (1), by which the mean travel time for steady-state flow can be used to map results of one-dimensional, non-linear bioreactive transport undergoing time-periodic fluctuations of the velocity magnitude to multi-dimensional domains subject to the same relative fluctuations of velocity. In the introduction, we have asked four questions that we may now answer:

1. How do transients in flow influence local travel-time distributions?

Both the kinematic age and the local mean travel time move back and forth in response to periodic velocity fluctuations. At points where the mean travel time equals an integer multiple of the period of fluctuations, however, the uncertainty in the mean travel time is minimal, and that of kinematic age is zero. These are the only points where artificial tracer tests or natural-tracer analysis would give univocal mean travel times. At these locations, the spread of local travel times in advective-dispersive transport exhibits a maximum.

2. How does transient flow alter biogeochemical zonation?

In our test case, time-periodic flow leads to pulsation of biogeochemical zones. At low velocity, the penetration depth of dissolved oxygen is considerably smaller than that at high velocity, leading to a transition zone in which times of aerobic degradation alter with those of denitrification. If the velocity fluctuations are on time scales smaller than those of biomass dynamics, both types of bacteria prevail in the transition zone. If the velocity fluctuations are on much larger time scales, quasi steady-state transport may be an adequate simplification, and the two types of bacteria are clearly separated in our model.

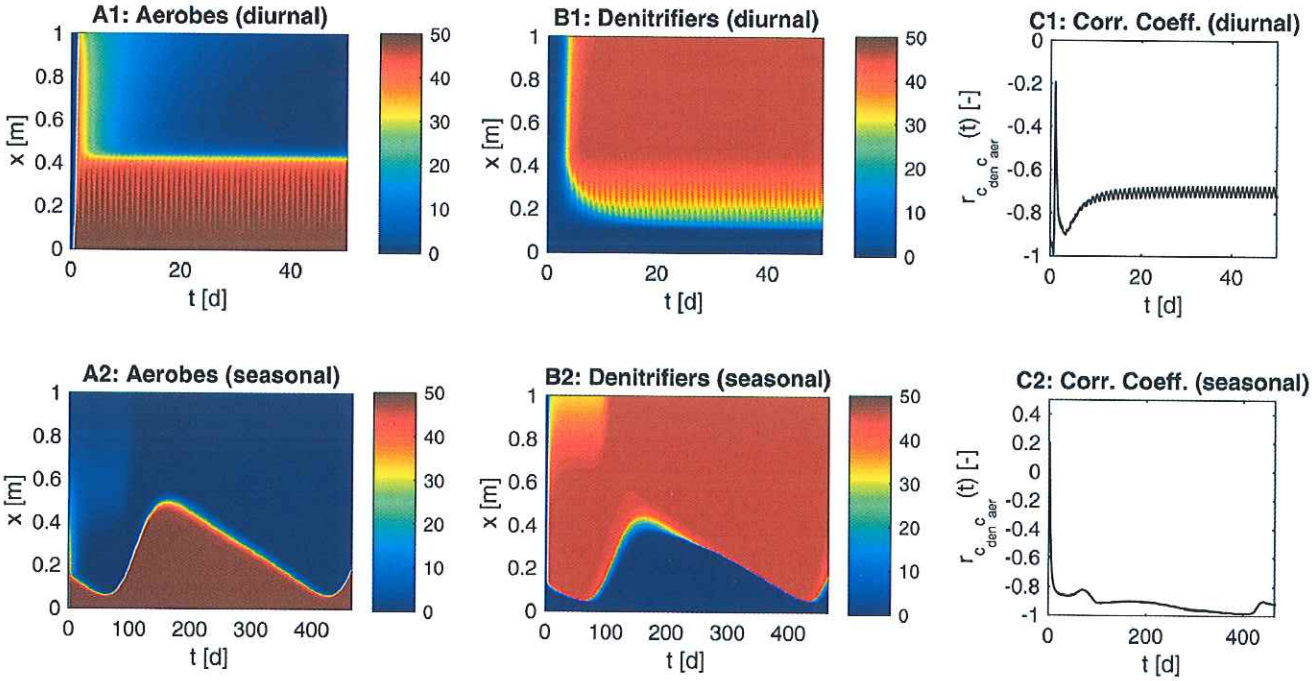

Fig. 8. Aerobic and denitrifying bacteria concentrations as function of distance and simulation time in the 1-D model for the diurnal (top row) and seasonal (bottom row) velocity fluctuations. Third column: correlation coefficient of the two biomass concentrations as function of time.

3. Which travel time or travel-time metric should be used to map travel-time based results of nonlinear (bio)reactive-transport simulations to multi-dimensional domains?

We have used the mean travel time for steady-state flow to map 1-D results to 2-D domains, because this quantity scales linearly with distance in the 1-D model if the velocity is spatially uniform. The time-averaged mean groundwater age exhibits small deviations from the linear behavior, but the two quantities appeared almost indistinguishable in the 2-D model.

4. How large is the error introduced by the mapping method?

Overall the approach of mapping 1-D results to 2-D domains by means of the mean groundwater age for steady-state flow performed excellently also for flow with periodic fluctuations of the velocity magnitude. We did not attempt optimizing the 1-D parametrization of dispersion to account for mixing enhancement by heterogeneity in the 2-D domain (Sanz-Prat et al., 2015). As a result, moving fronts were slightly more smoothed in the spatially explicit 2-D simulations than in the mapped 1-D results. We conjecture that using the kinematic age at steady-state flow as mapping variable and staying within a strictly advective description in 1-D transport would have caused more pronounced deviations between the mapped 1-D and 2-D results at moving fronts. The distribution of biomass, however, was not affected by the small mismatch of effective longitudinal mixing.

In the present study, we have assumed that the fluctuations of the flow magnitude are periodic. This is not necessarily the case in real aquifers, even though dominant diurnal and seasonal cycles are observed at many sites. Without periodicity, there are no fixed points with constant mean groundwater age. If flow is statistically stationary but not necessarily periodic, i.e., the flow magnitudes fluctuate non-periodically about a constant mean, the evaluation of an equivalent groundwater age under steady-state conditions is still possible, and the mapping procedure (using the same time fluctuations in the 1-D and multi-D models) should work similarly well as in the periodic case. In case of a pronounced trend (e.g., due to changes in water management), there is no equivalent steady state. However, as long as the spatial flow pattern does not change, the mapping could still be applied with an arbitrarily chosen steady-state flow field.

The main purpose of the present and the preceding study is to provide a conceptual simplification of modeling nonlinear multi-component reactive transport in heterogeneous domains. We have assumed that a spatially explicit representation of hydraulic conductivity exists (or that multiple realizations are provided by a Monte-Carlo approach). It is clear that the proposed travel-time models don't work in cases where reactions are controlled by transverse mixing at the macro-scale, which would be the case for a continuous point-release of a compound that reacts with compounds provided by ambient flow. We see the applications of travel-time models in cases of diffuse reactant input over large areas, e.g., agrochemical input with groundwater recharge or input of river pollutants by riverbank filtration. In the chosen set-up of our study, the reactants were mixed already in the inflow, which makes the approach less prone to effects of mixing. In replacement scenarios, in which the solution of one reactant replaces the solution of another one, the overall reaction rates are controlled by longitudinal mixing (Cirpka and Kitanidis, 2000; Luo and Cirpka, 2008, 2011). In such cases, convective-reactive models would only work if mixing is dominated by differences in the mobility of the reactants (e.g., Janssen et al., 2006).

Even in the premixed cases considered here, the mass exchange between old and new water parcels by transverse mixing can complicate the effective reactive-transport behavior. We recommend performing simulations of conservative advective-dispersive transport before setting up the reactive transport problem. In particular, we recommend analyzing breakthrough curves at individual points in control planes. If these point-related breakthrough curves show extended tailing or pronounced multiple peaks, a 1-D travel-time model based on standard advection and dispersion coupled to reactions won't be adequate, and other effective models, such as multi-porosity ad multi-permeability models may be needed (e.g., Šimunek et al., 2003). We also recommend comparing the shapes of individual breakthrough curves. If they differ dramatically, e.g., some show multiple peaks, others broad peaks, yet others long tails, whereas some look rather regular, it is difficult to imagine that a common parametrization of 1-D transport can be applied to all breakthrough curves. If the local distributions of travel time, normalized by the mean travel time, look similar in most cases, designing a nonlinear reactive transport model based on mapping a single, 1-D, travel-time model to a multi-dimensional heterogeneous domain appears reasonable. Previous findings have indicated that this may be the most difficult in domains with intermediate heterogeneity (Luo and Cirpka, 2011).

Finally, applying the approach to field sites of river-bank filtration remains challenging, We would need the mean travel time at an observation point for steady-state flow even though flow is transient. If flow remains constant for sufficiently large times, this value can be obtained by an artificial tracer test. Non-stationary analysis of natural-tracer data may be an alternative (Liao et al., 2014) but is associated with challenges of its own, because the natural tracer-data are more informative at times of hydrological events than in between so that estimation of the mean transport behavior may be biased.

Acknowledgments

This research was funded by Deutsche Forschungsgemeinschaft (DFG) in the framework of the International Research Training Group GRK 1829 "Integrated Hydrosystem Modeling", granted to the Universities of Tübingen, Hohenheim, and Waterloo. The authors also want to thank two anonymous reviewers for their comments that helped to improve the quality of the paper.

Appendix A. Bioreactive Model

The concentrations of the aerobic and denitrifying bacteria are given in moles of carbon within the biomass per volume of water, even though the biomasses are considered immobile. With the simplified elemental composition of CH_2O for dissolved organic carbon and the two types of biomass, the stoichiometries of the reactions listed in Table 1 hold. For aerobic degradation coupled to growth, we consider standard dual-Monod kinetics; biomass decay depends on the availability of an electron acceptor by introduction of Michaelis–Menten terms for oxygen

and nitrate. The effective yield Y_{eff}^{aer} of the aerobic bacteria depends on the aerobic biomass concentration c_{im}^{aer} to account for a maximum biomass concentration $c_{\max}^{aer}$, or carrying capacity. The corresponding mathematical expressions read as follows:

$$r_{growth}^{aer} = k_{aer,growth}^{max} \cdot \frac{c_m^{O_2}}{c_m^{O_2} + K_{O_2}} \cdot \frac{c_m^{DOC}}{c_m^{DOC} + K_{DOC}^{aer}} \cdot c_{im}^{aer} \tag{A.1}$$

$$r_{dec}^{aer} = k_{aer,dec}^{max} \cdot \frac{c_m^{O_2}}{c_m^{O_2} + K_{O_2}} \cdot c_{im}^{aer} \tag{A.2}$$

$$r_{dec,NO_3^-}^{aer} = k_{den,dec}^{max} \cdot \frac{c_m^{NO_3^-}}{c_m^{NO_3^-} + K_{NO_3^-}} \cdot c_{im}^{aer} \tag{A.3}$$

$$Y_{eff}^{aer} = Y_{max}^{aer} \cdot \left(1 - \frac{c_{im}^{aer}}{c_{max}^{aer}}\right) \tag{A.4}$$

leading to the reactive source-sink terms in Eqs. (A.5) & (A.6) for the aerobic biomass (r_{im}^{aer}) and dissolved oxygen ($r_m^{O_2}$):

$$r_{im}^{aer} = Y_{eff}^{aer} \cdot r_{growth}^{aer} - Y_{max}^{aer} \cdot \left(r_{dec}^{aer} + r_{dec,NO_3^-}^{aer}\right) \tag{A.5}$$

$$\begin{aligned} r_m^{O_2} = &-F_{O_2/CH_2O} \cdot \left(1 - Y_{eff}^{aer}\right) \cdot r_{growth}^{aer} \\ &- F_{O_2/CH_2O}^{growth} \cdot r_{dec}^{aer} - F_{O_2/CH_2O}^{dec} \cdot r_{dec,O_2}^{den} \end{aligned} \tag{A.6}$$

in which $F_{O_2/CH2O}$ is the stoichiometric ratio of dissolved oxygen to organic carbon for the net reaction at steady state.

The rate laws for denitrification are quite similar, but denitrification is inhibited by the presence of dissolved oxygen, which is accounted for by a non-competitive inhibition term including the inhibition constant $K_{O_2,inh}^{aer}$:

$$\begin{aligned} r_{growth}^{den} = k_{den,growth}^{max} &\cdot \frac{c_m^{NO_3^-}}{c_m^{NO_3^-} + K_{NO_3^-}} \cdot \frac{c_{DOC}}{c_{DOC} + K_{DOC}^{den}} \cdot \\ &\cdot \frac{K_{O_2,inh}^{aer}}{K_{O_2,inh}^{aer} + c_m^{O_2}} \cdot c_{im}^{den} \end{aligned} \tag{A.7}$$

$$r_{dec}^{den} = k_{den,dec}^{max} \cdot \frac{c_m^{NO_3^-}}{c_m^{NO_3^-} + K_{NO_3^-}} \cdot c_{im}^{den} \tag{A.8}$$

$$r_{dec,O_2}^{den} = k_{aer,dec}^{max} \cdot \frac{c_m^{O_2}}{c_m^{O_2} + K_{O_2}} \cdot c_{im}^{den} \tag{A.9}$$

$$Y_{eff}^{den} = Y_{max}^{den} \cdot \left(1 - \frac{c_{im}^{den}}{c_{max}^{den}}\right) \tag{A.10}$$

leading to the reactive source-sink terms in Eqs. (A.11) & (A.12) for the denitrifying biomass (r_{im}^{den}) and nitrate ($r_m^{NO_3^-}$):

$$r_{im}^{den} = Y_{eff}^{den} \cdot r_{growth}^{den} - Y_{max}^{den} \cdot \left(r_{dec}^{den} + r_{dec,O_2}^{den}\right) \tag{A.11}$$

$$\begin{aligned} r_m^{NO_3^-} = &-F_{NO_3^-/CH_2O} \cdot \left(1 - Y_{eff}^{den}\right) r_{growth}^{den} \\ &- F_{NO_3^-/CH_2O}^{growth} \cdot r_{dec}^{den} - F_{NO_3^-/CH_2O}^{dec} \cdot r_{dec,NO_3^-}^{aer} \end{aligned} \tag{A.12}$$

Finally, the reactive source/sink-term of dissolved organic carbon compiles the growth-specific reaction rate of aerobic respiration and denitrification:

$$r_m^{DOC} = -r_{growth}^{aer} - r_{growth}^{den} \tag{A.13}$$

Table A.4
Biokinetic parameters.

Symbol	Meaning	Value
$k_{aer,growth}^{max}$	Maximum specific DOC-reaction rate of aerobic bacteria under growth conditions	22.5/*d*
$k_{den,growth}^{max}$	Maximum specific DOC-reaction rate of denitrifying bacteria under growth conditions	7.5/*d*
$k_{aer,dec}^{max}$	Maximum decay rate coefficient of aerobic bacteria	0.3/*d*
$k_{den,dec}^{max}$	Maximum decay rate coefficient of denitrifying bacteria	0.3/*d*
K_{DOC}^{aer}	Monod coefficient of *DOC* in aerobic degradation	10 *μM*
K_{DOC}^{den}	Monod coefficient of *DOC* in denitrification	11.4 *μM*
K_{O_2}	Monod coefficient of dissolved oxygen in aerobic degradation	3 *μM*
$K_{NO_3^-}$	Monod coefficient of nitrate in denitrification	70 *μM*
Y_{max}^{aer}	Maximum specific yield of aerobic bacteria	0.5
Y_{max}^{den}	Maximum specific yield of denitrifying bacteria	0.5
$F_{O_2/CH2O}^{growth}$	Stoichiometric coefficient O_2 consumption for the aerobic growth	1
$F_{O_2/CH2O}^{dec}$	Stoichiometric coefficient O_2 consumption for the aerobic degradation	1
$F_{NO_3^-/CH2O}^{growth}$	Stoichiometric coefficient NO_3^- consumption for the anaerobic growth	0.8
$F_{NO_3^-/CH2O}^{dec}$	Stoichiometric coefficient NO_3^- consumption for the anaerobic degradation	0.8
c_{max}^{aer}	Maximum concentration of aerobic bacteria	50 *μM*
c_{max}^{den}	Maximum concentration of denitrifying bacteria	50 *μM*

References

Barry, D.A., Prommer, H., Miller, C.T., Engesgaard, P., Brun, A., Zheng, C., 2002. Modelling the fate of oxidisable organic contaminants in groundwater. Adv. Water Resour. 25 (8–12), 945–983.

Botter, G., Bertuzzo, E., Rinaldo, A., 2010. Transport in the hydrologic response: travel time distributions, soil moisture dynamics, and the old water paradox. Water Resour. Res. 46, W03514.

Cirpka, O.A., Kitanidis, P.K., 2000. An advective–dispersive streamtube approach for the transfer of conservative tracer data to reactive transport. Water Resour. Res. 36 (5), 1209–1220.

Cirpka, O.A., Frind, E.O., Helmig, R., 1999a. Streamline-oriented grid-generation for transport modelling in two-dimensional domains including wells. Adv. Water Resour. 22 (7), 697–710.

Cirpka, O.A., Helmig, R., Frind, E.O., 1999b. Numerical methods for reactive transport on rectangular and streamline-oriented grids. Adv. Water Resour. 22 (7), 711–728.

Cornaton, F.J., 2012. Transient water age distributions in environmental flow systems: the time-marching Laplace transform solution technique. Water Resour. Res. 48, W03524.

Cvetkovic, V., Dagan, G., 1994. Transport of kinetically sorbing solute by steady random velocity in heterogeneous porous formations. J. Fluid Mech. 265, 189–215.
Cvetkovic, V., Dagan, G., 1996. Reactive transport and immiscible flow in geological media. 2. applications. Proc. R. Soc. Lond. A 452 (1945), 303–328.
Cvetkovic, V.D., Shapiro, A.M., 1990. Mass arrival of sorptive solute in heterogeneous porous media. Water Resour. Res. 26 (9), 2057–2067.
Cvetkovic, V.D., Shapiro, A.M., Dagan, G., 1992. A solute flux approach in transport in heterogeneous formations: 2. uncertainty analysis. Water Resour. Res. 28 (5), 1377–1388.
Cvetkovic, V., Cheng, H., Wen, X.-H., 1996. Analysis of nonlinear effects on tracer migration in heterogeneous aquifers using Lagrangian travel time statistics. Water Resour. Res. 32 (6), 1671–1680.
Dagan, G., Cvetkovic, V., 1996. Reactive transport and immiscible flow in geological media. 1. general theory. Proc. R. Soc. Lond. A 452 (1945), 285–301.
Dagan, G., Nguyen, V., 1989. A comparison of travel time and concentration approaches to modelling transport by groundwater. J. Contam. Hydrol. 4, 79–91.
Dagan, G., Cvetkovic, V.D., Shapiro, A., 1992. A solute flux approach to transport in heterogeneous formations: 1. the general framework. Water Resour. Res. 28 (5), 1369–1376.
Destouni, G., Persson, K., Prieto, C., Jarsjö, J., 2010. General quantification of catchment-scale nutrient and pollutant transport through the subsurface to surface and coastal waters. Environ. Sci. Technol. 44 (6), 2048–2055.
Feyen, J., Jacques, D., Timmerman, A., Vanderborght, J., 1998. Modelling water flow and solute transport in heterogeneous soils: a review of recent approaches. J. Agric. Eng. Res. 70 (3), 231–256.
Ginn, T.R., 1999. On the distribution of multicomponent mixtures over generalized exposure time in subsurface flow and reactive transport: foundations, and formulations for groundwater age, chemical heterogeneity, and biodegradation. Water Resour. Res. 35 (5), 1395–1407.
Ginn, T.R., 2001. Stochastic-convective transport with nonlinear reactions and mixing: finite streamtube ensemble formulation for multicomponent reaction systems with intra-streamtube dispersion. J. Contam. Hydrol. 47 (1–2), 1–28.
Ginn, T.R., Simmons, C.S., Wood, B.D., 1995. Stochastic-convective transport with nonlinear reaction: biodegradation with microbial growth. Water Resour. Res. 31 (11), 2689–2700.
Ginn, T.R., Murphy, E.M., Chilakapati, A., Seeboonruang, U., 2001. Stochastic-convective transport with nonlinear reaction and mixing: application to intermediate-scale experiments in aerobic biodegradation in saturated porous media. J. Contam. Hydrol. 48 (1–2), 121–149.
Hatch, C.E., Fisher, A.T., Revenaugh, J.S., Constantz, J., Ruehl, C., 2006. Quantifying surface water-groundwater interactions using time series analysis of streambed thermal records: method development. Water Resour. Res. 42 (10), W10410.
Janssen, G., Cirpka, O.A., van der Zee, S.E.A.T.M., 2006. Stochastic analysis of nonlinear biodegradation in regimes controlled by both chromatographic and dispersive mixing. Water Resour. Res. 42 (1), W01417.
Jose, S.C., Cirpka, O.A., 2004. Measurement of mixing-controlled reactive transport in homogeneous porous media and its prediction from conservative tracer test data. Environ. Sci. Technol. 38 (7), 2089–2096.
Kaluarachchi, J.J., Cvetkovic, V., Berglund, S., 2000. Stochastic analysis of oxygen- and nitrate-based biodegradation of hydrocarbons in aquifers. J. Contam. Hydrol. 41 (3–4), 335–365.
Keery, J., Binley, A., Crook, N., Smith, J.W.N., 2007. Temporal and spatial variability of groundwater-surface water fluxes: development and application of an analytical method using temperature time series. J. Hydrol. 336 (1–2), 1–16.
Köhne, J., Köhne, S., Šimunek, J., 2009. A review of model applications for structured soils: a) water flow and tracer transport. J. Contam. Hydrol. 104, 4–35.
Liao, Z., Osenbrück, K., Cirpka, O.A., 2014. Non-stationary nonparametric inference of river-to-groundwater travel-time distributions. J. Hydrol. 519 (D), 3386–3399.
Lindgren, G.A., Destouni, G., Miller, A.V., 2004. Solute transport through the integrated groundwater-stream system of a catchment. Water Resour. Res. 40 (3), W03511.
Luo, J., 2012. Travel-time based reactive transport modeling for in situ subsurface reactor. In: Kitanidis, P.K., McCarty, P.L. (Eds.), Delivery and Mixing in the Subsurface: Processes and Design Principles for in situ RemediationSERDP ESTCP Remediation Technology vol. 4. Springer, New York, pp. 117–138 (Ch. 5).
Luo, J., Cirpka, O.A., 2008. Travel-time based descriptions of transport and mixing in heterogeneous domains. Water Resour. Res. 44 (9), W09407.
Luo, J., Cirpka, O.A., 2011. How well do mean breakthrough curves predict mixing-controlled reactive transport. Water Resour. Res. 47 (2), W02520.
MacQuarrie, K.T.B., Mayer, K.U., 2005. Reactive transport modeling in fractured rock: a state-of-the-science review. Earth Sci. Rev. 72 (3), 189–227.
Malmström, M.E., Destouni, G., Martinet, P., 2004. Modeling expected solute concentration in randomly heterogeneous flow systems with multicomponent reactions. Environ. Sci. Technol. 38 (9), 2673–2679.
Molz, F., Widdowson, M., 1988. Internal inconsistencies in dispersion-dominated models that incorporate chemical and microbial kinetics. Water Resour. Res. 24 (4), 615–619.
Painter, S., Cvetkovic, V., Mancillas, J., Pensado, O., 2008. Time domain particle tracking methods for simulating transport with retention and first-order transformation. Water Resour. Res. 44 (1), W01406.
Sanz-Prat, A., Lu, C., Finkel, M., Cirpka, O.A., 2015. On the validity of travel-time based nonlinear bioreactive transport models in steady-state flow. J. Contam. Hydrol. 175-176, 26–43.
Scheidegger, A.E., 1961. General theory of dispersion in porous media. J. Geophys. Res. 66 (10), 3273–3278.
Seeboonruang, U., Ginn, T.R., 2006. Upscaling heterogeneity in aquifer reactivity via exposure-time concept: forward model. J. Contam. Hydrol. 84 (3–4), 127–154.
Selroos, J.-O., Cvetkovic, V.D., 1992. Modeling solute advection coupled with sorption kinetics in heterogeneous formation. Water Resour. Res. 28 (5), 1271–1278.
Selroos, J.-O., Cheng, H., Painter, S., Vidstrand, P., 2013. Radionuclide transport during glacial cycles: comparison of two approaches for representing flow transients. Phys. Chem. Earth 64, 32–45.
Severino, G., De Bartolo, S., Toraldo, G., Srinivasan, G., Viswanathan, H., 2012. Travel time approach to kinetically sorbing solute by diverging radial flows through heterogeneous porous formations. Water Resour. Res. 48, W12527.
Shapiro, A.M., Cvetkovic, V.D., 1988. Stochastical analysis of solute arrival time in heterogeneous porous media. Water Resour. Res. 24 (10), 1711–1718.
Silliman, S.E., Ramirez, J., McCabe, R.L., 1995. Quantifying downflow through creek sediments using temperature time-series — one-dimensional solution incorporating measured surface-temperature. J. Hydrol. 167 (1–4), 99–119.
Simmons, C.S., 1982. A stochastic-convective transport representation of dispersion in one-dimensional porous-media systems. Water Resour. Res. 18 (4), 1193–1214.
Simmons, C.S., Ginn, T.R., Wood, B.D., 1995. Stochastic-convective transport with nonlinear reaction: mathematical framework. Water Resour. Res. 31 (11), 2675–2688.
Šimunek, J., Jarvis, N.J., van Genuchten, M.T., Gärdenäs, A., 2003. Review and comparison of models for describing non-equilibrium and preferential flow and transport in the vadose zone. J. Hydrol. 272 (1–4), 14–35.
Soltani, S.S., Cvetkovic, V., 2013. On the distribution of water age along hydrological pathways with transient flow. Water Resour. Res. 49, 1–8.
Steefel, C.I., DePaolo, D.J., Lichtner, P.C., 2005. Reactive transport modeling: an essential tool and a new research approach for the earth sciences. Earth Planet. Sci. Lett. 240 (3–4), 539–558.
van der Velde, Y., Heidbüchel, I., Lyon, S.W., Nyberg, L., Rodhe, A., Bishop, K., Troch, P.A., 2015. Consequences of mixing assumptions for time-variable travel time distributions. Hydrol. Process. 29 (16), 3460–3474.
Yabusaki, S., Steefel, C., Wood, B., 1998. Multidimensional, multicomponent, subsurface reactive transport in nonuniform velocity fields: code verification using an advective reactive streamtube approach. J. Contam. Hydrol. 30 (3–4), 299–331.

Appendix C: Third publication

Title

Effects of nonlinear reactive-transport processes in physical-geochemical heterogeneous media on the exposure time approach

Authors

Alicia Sanz-Prat, Chuanhe Lu, Richard Amos, Michael Finkel, David Blowes, Olaf A. Cirpka

Journal

Manuscript submitted to the Journal of Contaminant Hydrology

Year

2016

Highlights

- Exposure time as a good proxy of geochemical heterogeneity in nonlinear bioreactive transport in 1-D domain.
- Coupled physical-geochemical heterogeneity is defined as binary properties in a 2-D domain.
- Perform nonlinear bioreactive transport in the 2-D domain and in a homogeneous 1-D domain.
- Map 2-D exposure time by using travel time exclusively activated in reactive zones.
- Good agreement of trends and magnitudes of chemical-concentrations as function of exposure time between the 2-D and 1-D model.
- Significant reduction of computation effort with the exposure time approach when transverse mixing does not control the reactive system and reactions are strictly located.

Journal of Contaminant Hydrology 192 (2016) 35–49

Contents lists available at ScienceDirect

Journal of Contaminant Hydrology

journal homepage: www.elsevier.com/locate/jconhyd

Exposure-time based modeling of nonlinear reactive transport in porous media subject to physical and geochemical heterogeneity

Alicia Sanz-Prat [a], Chuanhe Lu [a], Richard T. Amos [b], Michael Finkel [a], David W. Blowes [c], Olaf A. Cirpka [a,*]

[a] University of Tübingen, Center for Applied Geosciences, Hölderlinstraße 12, 72074 Tübingen, Germany
[b] Institute of Environmental Science, Department of Earth Sciences, Carleton University, Ottawa, Canada
[c] Department of Earth Sciences, University of Waterloo, Waterloo, Ontario, N2L 3G1, Canada

ARTICLE INFO

Article history:
Received 27 April 2016
Received in revised form 6 June 2016
Accepted 12 June 2016
Available online 16 June 2016

Keywords:
Exposure time
Travel time
Denitrification
Bioreactive transport

ABSTRACT

Transport of reactive solutes in groundwater is affected by physical and chemical heterogeneity of the porous medium, leading to complex spatio-temporal patterns of concentrations and reaction rates. For certain cases of bioreactive transport, it could be shown that the concentrations of reactive constituents in multi-dimensional domains are approximately aligned with isochrones, that is, lines of identical travel time, provided that the chemical properties of the matrix are uniform. We extend this concept to combined physical and chemical heterogeneity by additionally considering the time that a water parcel has been exposed to reactive materials, the so-called exposure time. We simulate bioreactive transport in a one-dimensional domain as function of time and exposure time, rather than space. Subsequently, we map the concentrations to multi-dimensional heterogeneous domains by means of the mean exposure time at each location in the multi-dimensional domain. Differences in travel and exposure time at a given location are accounted for as time difference. This approximation simplifies reactive-transport simulations significantly under conditions of steady-state flow when reactions are restricted to specific locations. It is not expected to be exact in realistic applications because the underlying assumption, such as neglecting transverse mixing altogether, may not hold. We quantify the error introduced by the approximation for the hypothetical case of a two-dimensional, binary aquifer made of highly-permeable, non-reactive and low-permeable, reactive materials releasing dissolved organic matter acting as electron donor for aerobic respiration and denitrification. The kinetically controlled reactions are catalyzed by two non-competitive bacteria populations, enabling microbial growth. Even though the initial biomass concentrations were uniform, the interplay between transport, non-uniform electron-donor supply, and bio-reactions led to distinct spatial patterns of the two types of biomass at late times. Results obtained by mapping the exposure-time based results to the two-dimensional domain are compared with simulations based on the two-dimensional, spatially explicit advection-dispersion-reaction equation. Once quasi-steady state has been reached, we find a good agreement in terms of the chemical-compound concentrations between the two approaches inside the reactive zones, whereas the exposure-time based model is not able to capture reactions occurring in the zones with zero electron-donor release. We conclude that exposure-time models provide good approximations of nonlinear bio-reactive transport when transverse mixing is not the overall controlling process and all reactions are essentially restricted to distinct reactive zones.

* Corresponding author.
E-mail address: olaf.cirpka@uni-tuebingen.de (O.A. Cirpka).

http://dx.doi.org/10.1016/j.jconhyd.2016.06.002
0169-7722/

1. Introduction

Significant spatial variability of aquifer properties determines the fate of reactive components in groundwater. While the heterogeneity of physical properties (mainly hydraulic conductivity) determines the spatial structure of the groundwater flow field, the spatial variability of geochemical properties establishes different aquifer reactivities within the domain. Scheibe et al. (2006) recommended that the effects of coupled physical and biogeochemical heterogeneities should be jointly considered in reactive transport and bioremediation modeling. As tested by Cunningham and Fadel (2007) and Atchley et al. (2014), among others, both positive and negative correlations between physical and geochemical heterogeneities substantially modify the propagation and fingering of reactive fronts in porous media. The interplay between spatial variability of linear sorption (both in local equilibrium and kinetic) and hydraulic conductivity has been the subject of intensive stochastic analysis (e.g., Burr et al., 1994; Espinoza and Valocchi, 1997; Cushman et al., 1995; Cvetkovic et al., 1998). Dentz et al. (2011) analyzed kinetic dissolution-precipitation reactions in physically and chemically heterogeneous domains, highlighting that physical and chemical heterogeneity cannot be upscaled separately. Fully analytical treatment of joint physico-chemical heterogeneity in transport with nonlinear reactions, however, is inherently difficult, so that numerical simulations of such systems appear indispensable.

Most natural redox reactions in groundwater are catalyzed by microbes, which depend on particular chemical environments but also change them. Ginn et al. (2002) highlighted the need for new modeling approaches accounting for the time that a microorganism has been exposed to nutrients, the dynamics of biomass growth under changing chemical conditions, and the effects of heterogeneity on microbial populations. Likewise, Mohamed et al. (2010) observed that the mass discharge of contaminants undergoing microbial degradation is highly sensitive to chemical heterogeneity because the availability of substrates controls microbial activity. Tufenkji (2007) stressed the need of understanding the influence of physical and geochemical heterogeneity on microbial transport in porous media.

A key challenge for numerical bioreactive transport modeling in heterogeneous media is to allocate restricted computational resources: Uncertainty of the spatial distribution of aquifer properties requires multiple simulations with different parameter combinations (in the simplest version as Monte-Carlo simulations) but the computational effort for a single simulation run using multi-dimensional spatially explicit methods may be so high that it restricts the number of possible runs. In certain environmental settings, travel-time based bioreactive transport models are a feasible alternative to the traditional spatially-explicit advective-dispersive-reactive models due to the simplification of a multi-dimensional problem to a quasi one-dimensional one (see Sanz-Prat et al., 2015, 2016). The travel time $\tau(\mathbf{x})$ [T] is defined as the time that a particle needed to travel from the inlet boundary to the observation point with spatial coordinates $\mathbf{x}$ [L]. Due to dispersion, the travel time at a point is a probability density function, $p(\tau(\mathbf{x}))$, rather than a unique value, but its mean value (also denoted the mean groundwater age) and spread can easily be computed by temporal-moment generating equations (Harvey and Gorelick, 1995; Goode, 1996). The main assumption of travel-time based reactive-transport models is that reactive fronts are aligned with groundwater isochrones. This assumption holds under idealized conditions without groundwater mixing, that is, without dispersion. Also flow should be at steady state, the distribution of the reactants should be uniform across the entire inlet boundary, and the biogeochemical parameters must be uniform within the domain.

Various analyses have been based on the assumption of strictly advective transport, facilitating a Lagrangian analysis of solute transport in multi-dimensional domains (e.g., Simmons, 1982; Dagan and Nguyen, 1989; Shapiro and Cvetkovic, 1988; Dagan et al., 1992; Cvetkovic et al., 1992). Conceptually identical to the kinematic-Lagrangian framework is the assumption of transport occurring by advection only in independent stream tubes that do not interact with each other (e.g., Crane and Blunt, 1999). This framework is well suited to address reactive transport, at least in steady-state flow or if there are no reactants in an immobile phase (e.g., Dagan and Cvetkovic, 1996; Cvetkovic and Dagan, 1996; Kaluarachchi et al., 2000; Simmons et al., 1995; Diem et al., 2013). Ginn et al. (1995) simulated coupled microbial growth and non-linear reactive transport of a single solute in one-dimensional stream tubes and addressed the effects of heterogeneity by considering a distribution of velocities among individual stream tubes, meeting the travel-time distribution in the outlet of the original multi-dimensional domain. This method enables the upscaling of microbially influenced transport in heterogeneous domains without relying on Fickian macrodispersion, which has been shown to introduce artifacts in bioreactive transport already by Molz and Widdowson (1988). Stream-tube formulations considerably reduce the computational effort making Monte-Carlo simulation to analyze the effects of spatially variable physical properties on reactive transport feasible. Cirpka and Kitanidis (2000a) denoted the latter method the advective-dispersive stream-tube approach and suggested parameterizing the dispersivities of the independent stream tubes by analyzing the width of point-like measured breakthrough curves of conservative tracers (Cirpka and Kitanidis, 2000b). Ginn (2001) and Ginn et al. (2001) extended the approach by allowing longitudinal dispersive mixing within the stream tubes. Cirpka (2002) used effective longitudinal dispersion coefficients derived by linear stochastic theory (Dentz et al., 2000; Fiori and Dagan, 2000) for the within-stream-tube mixing, and the difference between ensemble and effective dispersion to parameterize the apparent velocity distribution among the independent stream tubes. In all these studies, the intrinsic rate coefficients and the initial biomass distribution were assumed to be spatially uniform. Microbial biomass, and thus the concentration of the reaction catalyst, was allowed to vary but it organized itself due to the interplay of advective (or advection-dominated) transport, reactions, and microbial dynamics (growth, decay, in some cases transport of microbes). In two preceding studies, we have analyzed the validity of travel-time based models for bioreactive transport subject to small, but non-zero transverse mixing (Sanz-Prat et al., 2015) and under the additional influence of time-period fluctuations of the magnitude of flow (Sanz-Prat et al., 2016). As a reactive

system, we considered the oxidation of dissolved organic carbon by oxygen and nitrate coupled to the growth of the catalyzing bacteria. All compounds were jointly introduced into the domain, and the rules and parameters of microbial activity were spatially uniform.

Accounting for any sort of biogeochemical heterogeneity, travel times likely do not agree with the time in which the reaction actually can take place. In addition to the travel time $\tau(\mathbf{x})$, it becomes thus necessary to consider the time over which a material has the opportunity to be processed (Oldham et al., 2013), here denoted the exposure time, $\tau_{exp}(\mathbf{x})$ [T], as this time controls the time of reaction. The exposure time was included as independent variable in a modified version of the stochastic-convective-reactive method by Seeboonruang and Ginn (2006) for linear kinetically controlled reactions. The authors used the cumulative reactivity, T_{exp}, as the total exposure time in each stream tube to solve linear reactive systems. The approach properly captured breakthrough curves of solutes based on the joint distribution function of travel time and cumulative reactivity. However, further research on coupled and nonlinear kinetically-controlled reactions was suggested. Interference of the approach by transverse mixing was excluded altogether.

Ginn (1999, 2000a, 2000b) introduced the exposure time as additional dimension in reactive-transport equations. The general equation is based on mass-balance principles and considers that the individual molecules of a solute at a given location in space and time may have experienced different times of exposure to reactive conditions. By introducing the exposure time as additional dimension, and considering that a sample is a weighted average over different exposure times, the author tried to explain inconsistencies of advective-dispersive-reactive transport in the presence significant chemical heterogeneity. While the author has applied the approach as "generalized exposure-time" concept to various problems of transport (e.g., Ginn, 2009), it comes with the key disadvantage of increasing the computational effort from 3-D or 4-D space-time to a 4-D or 5-D domain (see also the Laplace-transfrom technique to evaluate the exposure-time distribution developed by Cornaton, 2012). In the present study, we thus do not consider full exposure-time distributions at a single point in space and time, and restrict the analysis to the mean exposure time, which can be evaluated by a slightly modified version of the mean groundwater-age equation (Goode, 1996).

The hypothesis to be tested in this paper is that the concentrations of reactive constituents at each point within a domain subject to physical and chemical heterogeneity can be approximated by knowing the mean exposure time and the travel time at that location. The main objective of this paper is to identify, locate and quantify the expected errors introduced by using the exposure-time approach in nonlinear bioreactive transport affected by local dispersion. For this purpose, we compare the estimated multi-dimensional concentration and reaction rates of an equivalent spatially-explicit advective-dispersive model, acting as our reference or virtual truth. The methodology is summarized by the following steps: (1) simulation of the one-dimensional reactive transport model based on exposure time, which provides concentration/reaction rates as function of time and exposure time; (2) estimation of the spatial distribution of the mean travel and exposure times in the two-dimensional heterogeneous domain; (3) simulating two-dimensional reactive transport by the spatially-explicit model, providing the values of reference or virtual truth; (4) mapping the one-dimensional results to two-dimensional domain by using the spatial distribution of the exposure time; (5) estimation of residual errors between the 1-D mapped and the genuine 2-D results.

In the present application, the coupled physical and geochemical heterogeneity is described as a binary setting of reactive lenses embedded in a non-reactive fully saturated porous media, where the hydraulic conductivity field is negatively correlated with the reactivity. In order to restrict the analysis of mixing processes to the coupled effect of the spatial variability of physical and chemical features, the assumed flow field is at steady state (implying that the spatial distribution of the exposure time is constant in time), and all mobile reactants are introduced uniformly over the inflow boundary of the domain. We consider aerobic respiration and denitrification, coupled to biomass growth, as chemical transformations that can occur throughout the entire domain including both reactive and non-reactive zones. Reactive zones are defined by the release of dissolved organic carbon acting as the electron donor for the latter two redox reactions. Examples could be peat lenses in an otherwise sandy aquifer, or zones containing pyrite, elevated levels of biotite, or other ferrous-iron bearing minerals Thus, the distinction between "reactive" and "non-reactive" zones is in reality a distinction between zones that release electron donors and those that do not. We discuss the effects of the latter assumption by performing simulations of a simple one-dimensional test problem.

2. Theory

2.1. One-dimensional advective transport with intermittent first-order decay

We start with the simple, one-dimensional, linear case in which a solute undergoes advection and first-order decay at locations where the water parcels are exposed to a reactive material:

$$\frac{\partial c}{\partial t}+v\frac{\partial c}{\partial x}=\begin{cases}-\lambda c & \text{in reactive zones}\\ 0 & \text{elsewhere}\end{cases} \tag{1}$$

$$c(t,x=0)=c_{in}(t) \tag{2}$$

$$c(t=0,x)=0 \tag{3}$$

in which v [LT^{-1}] is the velocity, which may vary upon the spatial coordinate x [L], t [T] is time, c [ML^{-3}] is the concentration, λ [T^{-1}] is a first-order decay coefficient active in reactive zones only, and $c_{in}(t)$ [ML^{-3}] is the time series of concentration in the inflow. Applying the rules of total differentiation yields for a water parcel:

$$\frac{dc}{dt}=\begin{cases}-\lambda c & \text{in reactive zones}\\ 0 & \text{elsewhere}\end{cases}\ \text{along}\ \frac{dx}{dt}=v \tag{4}$$

subject to Eq. (2), which is a homogeneous first-order

differential equation with the solution:

$$c(t) = c(0)\exp\left(-\lambda\tau_{exp}\right) \tag{5}$$

in which $c(0)$ $[ML^{-3}]$ is the initial concentration of the individual water parcel, and τ_{exp} $[T]$ is the time that the water parcel has been within reactive zones. Considering that the water parcel observed at time t at location x has been introduced at time $t-\tau$ into the domain, the analytical solution reads as:

$$c(t,x) = c_{in}(t-\tau)\exp\left(-\lambda\tau_{exp}\right) \tag{6}$$

in which $\tau(x)$ $[T]$ and $\tau_{exp}(x)$ $[T]$ are the travel time and exposure time at location x, respectively, which can be evaluated throughout the domain by the following generating equations:

$$v\frac{\partial\tau}{\partial x} = 1 \tag{7}$$

$$v\frac{\partial\tau_{exp}}{\partial x} = \begin{cases} 1 & \text{in reactive zones} \\ 0 & \text{elsewhere} \end{cases} \tag{8}$$

$$\tau(0) = \tau_{exp}(0) = 0 \tag{9}$$

in which Eq. (7) may be interpreted as the increase of mean age along a trajectory, whereas Eq. (8) expresses that the mean exposure time only increases within reactive zones.

We now consider an equivalent domain with equivalent concentrations c_{eq} $[ML^{-3}]$, in which the non-reactive parts have been removed, whereas the boundary and initial conditions are identical:

$$\frac{\partial c_{eq}}{\partial t} + v\frac{\partial c_{eq}}{\partial\tau_{exp}} = -\lambda c \tag{10}$$

$$c_{eq}\left(t,\tau_{exp}=0\right) = c_{in}(t) \tag{11}$$

$$c_{eq}\left(t\leq 0,\tau_{exp}\right) = 0 \tag{12}$$

$$\Rightarrow c_{eq}\left(t,\tau_{exp}\right) = c_{in}\left(t-\tau_{exp}\right)\exp\left(-\lambda\tau_{exp}\right) \tag{13}$$

In the equivalent domain, there is no distinction between travel time and exposure time because the water parcels are exposed to the reactive material everywhere. We may now compare the analytical expressions of the domain with non-reactive zones, Eq. (6), with the one leaving out the reactive zones, Eq. (13). While the exponential term, $\exp(-\lambda\tau_{exp})$, is identical the inflow concentration c_{in} is to be considered at different times, namely at $t-\tau$ for the case of the domain with non-reactive zones, and at $t-\tau_{exp}$ in the system without non-reactive zones. This time offset must be considered when equating the two expressions. In doing so, the concentrations in the domain including the non-reactive zones can be computed from the equivalent concentrations in the domain leaving out the non-reactive zones by:

$$c(t,x) = c_{eq}\left(t-\tau(x)+\tau_{exp}(x),\tau_{exp}(x)\right) \tag{14}$$

Eq. (14) is at the heart of the proposed approach for slightly more complex cases of reactive transport: concentrations for a domain made of reactive and non-reactive materials are approximated by mapping concentrations from an equivalent, one-dimensional domain made only of reactive material. The key mapping variable is the mean exposure time at the location of interest, whereas the difference between travel and exposure time at that location acts as a time difference. The latter may best be explained for the case of an invading concentration front. Since the 1-D model excludes the non-reactive zones the invading front directly jumps from one reactive zone to the next, whereas in the full system with non-reactive zones the front needs extra time to move through the non-reactive zones. The time-offset of Eq. (14) accounts for this delay. Eq. (14) is exact for mixtures of solutes undergoing strictly advective transport through the reactive and non-reactive zones of the domain and reacting with each other in the reactive zones, regardless whether the reaction laws are linear or nonlinear. The key idea is to follow a water parcel containing reactive constituents that react among each other only in certain parts of the domain and measure the time that the water parcel has been exposed to the reactive material (see Seeboonruang and Ginn, 2006). In the following, we will apply the approach to cases where Eq. (14) is no longer exact because of dispersive mixing and the involvement of immobile constituents (bacteria, reactants in the matrix) in the reactions.

2.2. Proposed multi-dimensional, advective-dispersive-reactive approach

As virtual truth, we consider multi-dimensional reactive transport of multiple mobile (m: dissolved organic matter, dissolved oxygen, nitrate) and immobile (im: aerobic and denitrifying bacteria) compounds, in which the mobile compounds undergo advection with the spatially variable seepage velocity $\mathbf{v}$ $[LT^{-1}]$ and dispersive mixing with the spatially variable local dispersion tensor $\mathbf{D}$ $[L^2T^{-1}]$. The flow field is considered to be at steady state, the porosity is assumed to be spatially uniform, and the concentrations of the reactants in the inflow are assumed uniform over the inflow boundary. Then the advection-dispersion-reaction equation (ADRE) including immobile compounds reads as:

$$\frac{\partial c_m^{(i)}}{\partial t} + \mathbf{v}\cdot\nabla c_m^{(i)} - \nabla\cdot\left(\mathbf{D}\nabla c_m^{(i)}\right) = r_m^{(i)}(\mathbf{c}(\mathbf{x},t)) \tag{15}$$

$$\frac{\partial c_{im}^{(i)}}{\partial t} = r_{im}^{(i)}(\mathbf{c}(\mathbf{x},t)) \tag{16}$$

subject to spatially uniform initial conditions and:

$$\mathbf{n}\cdot\left(\mathbf{v}c_m^{(i)} - \mathbf{D}\nabla c_m^{(i)}\right) = \mathbf{n}\cdot\mathbf{v}c_{inflow}^{(i)}(t) \text{ at } \Gamma_{in} \tag{17}$$

$$\mathbf{n}\cdot\left(\mathbf{D}\nabla c_m^{(i)}\right) = 0 \text{ at } \Gamma_{out}\cup\Gamma_0 \tag{18}$$

in which $c_m^{(i)}$ $[ML^{-3}]$ is the concentration of mobile compound i, $r_m^{(i)}$ $[ML^{-3}T^{-1}]$ is the reactive source-sink term for that compound, depending on the concentration vector $\mathbf{c}(\mathbf{x},t)$ of all compounds at location $\mathbf{x}$ and time t, whereas $c_{im}^{(i)}$ and $r_{im}^{(i)}$ are the corresponding expressions for an immobile compound. $c_{inflow}^{(i)}[ML^{-3}]$ is the concentration of mobile compound i in the inflow. Γ_{in}, Γ_{out}, and Γ_0 denote inflow, outflow, and no-flow boundaries, respectively. In the given example problem, we consider the release of DOC from a seemingly infinite pool of natural organic matter (NOM) in the immobile domain. Thus, the change of immobile NOM is not considered in the model. In the given approach, we could explicitly account for inter-phase mass transfer processes. However, the distribution of DOC-releasing and non-releasing zones is considered fixed.

The equivalent one-dimensional model without non-reactive zones has been modified from Eqs. (10)–(12) to:

$$\frac{\partial c_{eq,m}^{(i)}}{\partial t}+\frac{\partial c_{eq,m}^{(i)}}{\partial \tau}_{exp}-D_\tau \frac{\partial^2 c_{eq,m}^{(i)}}{\partial \tau^2}_{exp}=r_m^{(i)}\left(\mathbf{c}_{eq}\left(\tau_{exp},t\right)\right) \tag{19}$$

$$\frac{\partial c_{eq,im}^{(i)}}{\partial t}=r_{im}^{(i)}\left(\mathbf{c}_{eq}\left(\tau_{exp},t\right)\right) \tag{20}$$

subject to the same initial conditions as for the multi-dimensional case and the boundary conditions:

$$c_{eq.m}^{(i)}-D_\tau \frac{\partial c_{eq,m}^{(i)}}{\partial \tau}_{exp}=c_{inflow}^{(i)}(t) \text{ at } \tau_{exp}=0 \tag{21}$$

$$\lim_{\tau_{exp}\to\infty}\frac{\partial c_{eq.m}^{(i)}}{\partial \tau}_{exp}=0 \ \forall t \tag{22}$$

in which $D_\tau \approx D_\ell/\|\mathbf{v}\|_2^2$ $[T]$ is a dispersion coefficient in travel/exposure-time coordinates accounting for within-stream-tube mixing, where D_ℓ $[L^2T^{-1}]$ is the longitudinal dispersion coefficient in spatial coordinates. The reaction laws $r_m^{(i)}(\mathbf{c})$ (mobile compounds) and $r_{im}^{(i)}(\mathbf{c})$ (immobile compounds) are identical for the spatially explicit multi-dimensional model and the equivalent one-dimensional model expressed in exposure times.

Due to dispersive mixing, both the travel time $\tau(\mathbf{x})$ and the exposure time $\tau_{exp}(\mathbf{x})$ at a given location are distributions rather than single values (Ginn, 1999, 2000a, 2000b): certain water molecules at time τ and location $\mathbf{x}$ have been in the domain for a longer time and experienced longer exposure to reactive materials than others. Instead of introducing the exposure time as an additional dimension for multi-dimensional transport as done by Ginn in the cited studies, we work with the mean exposure time as single qualifier, and do the same for the travel time. From this point forward, $\tau(\mathbf{x})$ denotes the mean travel time, or groundwater age, at location $\mathbf{x}$, and $\tau_{exp}(\mathbf{x})$ denotes the corresponding mean exposure time. Under steady-state flow conditions, $\tau(\mathbf{x})$ and $\tau_{exp}(\mathbf{x})$ can be computed from the groundwater-age equation (Goode, 1996) and a modified form of it by:

$$\mathbf{v}\cdot\nabla\tau-\nabla\cdot(\mathbf{D}\nabla\tau)=1 \tag{23}$$

$$\mathbf{v}\cdot\nabla\tau_{exp}-\nabla\cdot\left(\mathbf{D}\nabla\tau_{exp}\right)=\begin{cases}1 & \text{in reactive zones}\\ 0 & \text{elsewhere}\end{cases} \tag{24}$$

subject to:

$$\begin{aligned}\mathbf{n}\cdot(\mathbf{v}\tau-\mathbf{D}\nabla\tau) &= 0 \text{ at } \Gamma_{in}\\ \mathbf{n}\cdot(\mathbf{D}\nabla\tau) &= 0 \text{ at } \Gamma_{out}\cup\Gamma_0\\ \mathbf{n}\cdot\left(\mathbf{v}\tau_{exp}-\mathbf{D}\nabla\tau_{exp}\right) &= 0 \text{ at } \Gamma_{in}\\ \mathbf{n}\cdot\left(\mathbf{D}\nabla\tau_{exp}\right) &= 0 \text{ at } \Gamma_{out}\cup\Gamma_0\end{aligned} \tag{25}$$

Notice that, as a consequence of transverse dispersion, different travel and exposure times in neighboring stream tubes mix. This can lead to the counter-intuitive observation that both the mean groundwater age and the mean exposure time along a slow flow path can decrease in the longitudinal direction due to transverse exchange with stream tubes that contain younger water or have experienced less exposure, respectively. The exchange also causes a stronger increase in mean groundwater age and mean exposure time in the neighboring fast stream tubes, but the latter observation appears less counter-intuitive.

To transfer the equivalent concentrations from the exposure-time based domain to the multi-dimensional domain, we make use of the mapping expressed in Eq. (14). We do not expect that the mapping yields exact results because (1) the reactive constituents mix, (2) the equivalent model cannot switch off longitudinal dispersion if reactive sub-domains are separated by non-reactive ones, (3) the reaction laws involve immobile compounds (bacteria) that influence the reaction and are changed by it, and (4) we define zones as non-reactive even though not all reactions are inhibited therein. However, we claim that the mapping approach yields good approximations of reactive-species concentrations, and will test this by comparing spatially explicit advective-dispersive-reactive simulation results with the mapped results of the equivalent one-dimensional exposure-time based model.

3. Application to aerobic and anaerobic degradation of organic carbon released from source lenses

3.1. General setup

We conceptualize physical-geochemical heterogeneous domains as a composition of organic-matter-rich lenses within an inert porous medium. The reactive material is assumed to behave as a quasi-infinite immobile source of dissolved organic carbon (DOC). The release rate of DOC in the reactive zones is proportional to the difference between a fixed saturation concentration c_{sat}^{DOC} $[ML^{-3}]$ and the actual local concentration of DOC. This setup mimics DOC-release in peat lenses or other organic-rich inclusions of aquifers otherwise made of organic-poor sediments. It may be worth noticing that the DOC-release is the only reaction switched off in the non-reactive zones. All reactions triggered by the DOC-release (see below) can occur in the non-reactive zones if the DOC is transported thereto. In the two-dimensional application, the hydraulic-conductivity field follows the spatial pattern of reactivity: The reactive zones are assumed to exhibit a uniform low hydraulic-conductivity value,

and the matrix an equally uniform high hydraulic conductivity value, similar to peat, silt, or clay lenses embedded in sandy-loam formations (e.g., Ritzi et al., 2000). For modeling simplification, we assume a uniform and constant porosity. Dissolved oxygen, O_2, and nitrate, NO_3^-, are continuously injected through the whole inlet boundary with a uniform and constant inflow concentration. These mobile electron acceptors trigger degradation of the dissolved organic carbon. The redox reactions are catalyzed by aerobic and denitrifying bacteria, in which denitrification is non-competitively inhibited by the presence of dissolved oxygen. Initially, the microbial populations have very small biomass concentrations in the whole domain. These microbes are considered as immobile, their growth is limited by a maximum biomass concentration, or carrying capacity, ${c_{\max}}^{aer/den}$ $[ML^{-3}]$, and depends on the concentrations of the reactants by Monod kinetics. The model includes first-order biomass decay, which is relevant during large starvation periods.

In Section 3.3, we will demonstrate the system behavior for a simple one-dimensional domain comprised of alternating non-reactive and reactive zones. In Section 3.4, we consider a two-dimensional domain made of highly permeable, non-reactive zones and lowly permeable, reactive zones. The reaction parameters, initial and inflow concentrations are identical in the two applications. We test the applicability of the mapping approach in the two-dimensional application, which is more challenging because of transverse dispersive mixing.

3.2. Bioreactive system

We simulate a redox-chain triggered by dissolved oxygen and nitrate coming in contact with DOC-released from the matrix in the reactive areas. Aerobic bacteria grow on oxidation of DOC by oxygen, and denitrifying bacteria on oxidation of DOC by nitrate. The latter reaction implies two non-competing bacteria populations, where the denitrifying microbes are inhibited by the presence of dissolved oxygen (Haarstrick et al., 2001). The net biochemical reactions of aerobic respiration and denitrification are described in Table 1, in which we assume CH_2O as the chemical composition of DOC. The degradation products (carbon dioxide, water, molecular nitrogen) are not considered in the model. For the purpose of simplicity, we also neglect the release of inorganic nitrogen by ammonification of nitrogen-bearing DOC-compounds and associated nitrification of ammonium, which could be included without changing the general approach. The chemical composition of the two types of biomass is also assumed to be CH_2O. The concentrations of DOC, aerobes, and denitrifiers are all expressed in moles of carbon per volume of water.

Mathematically, the nonlinear reactive system is controlled by kinetic processes using Monod terms for aerobic degradation and denitrification. In the model, biomass decay requires the presence of electron acceptors, either dissolved oxygen or nitrate (Semprini and McCarty, 1991; Cirpka and Kitanidis, 2000c; Sanz-Prat et al., 2015). As long as oxygen is present, the biomass decay using nitrate as oxidant is inhibited in the same way as the rate law for denitrification which includes an inhibition term in the presence of dissolved oxygen with the inhibition constant ${K_{O_2,inh}}^{aer}$ $[ML^{-3}]$. This leads to the following set of reaction-rate laws:

$$r_{growth}^{aer} = k_{aer,growth}^{max} \cdot \frac{c_m^{O_2}}{c_m^{O_2} + K_{O_2}} \cdot \frac{c_m^{DOC}}{c_m^{DOC} + K_{DOC}^{aer}} \cdot c_{im}^{aer} \tag{26}$$

$$r_{dec}^{aer} = k_{aer,dec}^{max} \cdot \frac{c_m^{O_2}}{c_m^{O_2} + K_{O_2}} \cdot c_{im}^{aer} \tag{27}$$

$$r_{dec,NO_3^-}^{aer} = k_{den,dec}^{max} \cdot \frac{c_m^{NO_3^-}}{c_m^{NO_3^-} + K_{NO_3^-}} \cdot \frac{K_{O_2,inh}^{aer}}{K_{O_2,inh}^{aer} + c_m^{O_2}} \cdot c_{im}^{aer} \tag{28}$$

$$r_{growth}^{den} = k_{den,growth}^{max} \cdot \frac{c_m^{NO_3^-}}{c_m^{NO_3^-} + K_{NO_3^-}} \cdot \frac{c_m^{DOC}}{c_m^{DOC} + K_{DOC}^{den}} \cdot \frac{K_{O_2,inh}^{aer}}{K_{O_2,inh}^{aer} + c_m^{O_2}} \cdot c_{im}^{den} \tag{29}$$

$$r_{dec}^{den} = k_{den,dec}^{max} \cdot \frac{c_m^{NO_3^-}}{c_m^{NO_3^-} + K_{NO_3^-}} \cdot \frac{K_{O_2,inh}^{aer}}{K_{O_2,inh}^{aer} + c_m^{O_2}} \cdot c_{im}^{den} \tag{30}$$

$$r_{dec,O_2}^{den} = k_{aer,dec}^{max} \cdot \frac{c_m^{O_2}}{c_m^{O_2} + K_{O_2}} \cdot c_{im}^{den} \tag{31}$$

The effective yields of the aerobic and anaerobic bacteria, Y_{eff}^{aer} $[-]$ and Y_{eff}^{den} $[-]$, respectively, have maximum values of ${Y_{\max}}^{aer}$ $[-]$ and ${Y_{\max}}^{den}$ $[-]$. We consider maximum biomass concentrations, or carrying capacities, of aerobes and denitrifiers, ${c_{\max}}^{aer}$ $[ML^{-3}]$ and ${c_{\max}}^{den}$ $[ML^{-3}]$, which express the limitation of biomass growth by other factors than the availability of electron acceptors and donors. Such limitations could relate to the availability of nutrients and space, or to predation by grazers (Bajracharya et al., 2014). The effective yield of a specific biomass is reduced if the corresponding biomass concentration approaches the respective maximum biomass concentration:

$$Y_{eff}^{aer} = Y_{max}^{aer} \cdot \left(1 - \frac{c_{im}^{aer}}{c_{max}^{aer}}\right) \tag{32}$$

$$Y_{eff}^{den} = Y_{max}^{den} \cdot \left(1 - \frac{c_{im}^{den}}{c_{max}^{den}}\right) \tag{33}$$

The net reactive source-sink terms for the aerobic biomass and dissolved oxygen, r_{im}^{aer} $[ML^{-3}T^{-1}]$ and $r_m^{O_2}$ $[ML^{-3}T^{-1}]$, respectively, account for growth and decay processes and are defined by:.

$$r_{im}^{aer} = Y_{eff}^{aer} \cdot r_{growth}^{aer} - r_{dec}^{aer} - r_{dec,NO_3^-}^{aer} \tag{34}$$

Table 1
Biogeochemical reactions considered in the test case.

Net aerobic respiration	$CH_2O + O_2 \rightarrow CO_2 + H_2O$
Net denitrification	$CH_2O + \frac{4}{5}NO_3^- + \frac{4}{5}H^+ \rightarrow \frac{2}{5}N_2 + CO_2 + \frac{7}{5}H_2O$

Table 2
Biokinetic parameters.

Symbol	Meaning	Value
$k_{DOC,rel}$	Rate coefficient of DOC-release	2 d^{-1}
c_{sat}^{DOC}	Saturation concentration of dissolved organic carbon	300 μM
$k_{aer,growth}^{max}$	Maximum specific reaction rate of aerobic bacteria under growth conditions	12 d^{-1}
$k_{den,growth}^{max}$	Maximum specific DOC-reaction rate of denitrifying bacteria under growth conditions	6 d^{-1}
$k_{aer,dec}^{max}$	Maximum decay rate coefficient of aerobic bacteria	1 d^{-1}
$k_{den,dec}^{max}$	Maximum decay rate coefficient of denitrifying bacteria	1 d^{-1}
K_{DOC}^{aer}	Monod coefficient of DOC in aerobic degradation	10 μM
K_{DOC}^{den}	Monod coefficient of DOC in denitrification	11.4 μM
K_{O_2}	Monod coefficient of dissolved oxygen in aerobic degradation	3 μM
$K_{NO_3^-}$	Monod coefficient of nitrate in denitrification	70 μM
Y_{max}^{aer}	Maximum specific yield of aerobic bacteria	0.5
Y_{max}^{den}	Maximum specific yield of denitrifying bacteria	0.5
$F_{O_2/DOC}$	Stoichiometric ratio O_2/DOC in net aerobic degradation at steady state	1
$F_{NO_3^-/DOC}$	Stoichiometric ratio NO_3^-/DOC in net denitrification at steady state	0.8
c_{max}^{aer}	Maximum concentration of aerobic bacteria	500 μM_C
c_{max}^{den}	Maximum concentration of denitrifying bacteria	500 μM_C
$K_{O_2,inh}^{aer}$	Biomass inhibition coefficient of oxygen in denitrification	10 μM

$$r_m^{O_2} = -F_{O_2/DOC} \cdot \left(1 - Y_{eff}^{aer}\right) \cdot r_{growth}^{aer} - F_{O_2/DOC} \cdot \left(r_{dec}^{aer} + r_{dec,O_2}^{den}\right) \quad (35)$$

in which $F_{O_2/DOC}$ is the stoichiometric ratio of dissolved oxygen to organic carbon for the net reaction at steady state. Similar net reactive source-sink terms for the denitrifying biomass, r_{im}^{den} $[ML^{-3}T^{-1}]$ and nitrate $r_m^{NO_3^-}$ $[ML^{-3}T^{-1}]$ are given by:

$$r_{im}^{den} = Y_{eff}^{den} \cdot r_{growth}^{den} - r_{dec}^{den} - r_{dec,O_2}^{den} \quad (36)$$

$$r_m^{NO_3^-} = -F_{NO_3^-/DOC} \cdot \left(1 - Y_{eff}^{den}\right) r_{growth}^{den} - F_{NO_3^-/DOC} \cdot \left(r_{dec}^{den} + r_{dec,NO_3^-}^{aer}\right) \quad (37)$$

The release rate $r_{release}^{DOC}$ $[ML^{-3}T^{-1}]$ of dissolved organic carbon from the matrix follows a classical linear-driving force approach. The combination of the growth-specific reaction rates of aerobic respiration and denitrification, and the DOC-release comprises the total reactive source/sink strength r_m^{DOC} $[ML^{-3}T^{-1}]$ of DOC:

$$r_{release}^{DOC} = k_{DOC,rel} \cdot \left(c_{sat}^{DOC} - c_m^{DOC}\right) \quad (38)$$

$$r_m^{DOC} = r_{release}^{DOC} - r_{growth}^{aer} - r_{growth}^{den} \quad (39)$$

Table 2 lists all biokinetic parameters of the reactive system obtained from literature reviews by Sanz-Prat et al. (2015, 2016). The bioreactive transport equations are discretized in space by a cell-centered Finite Volume Method using streamline-oriented grids and upwind differentiation for advection. The resulting system of coupled non-linear ordinary differential equations is solved by the implicit Euler method using the Newton-Raphson approach for linearization. A detail description is given by Sanz-Prat et al. (2015).

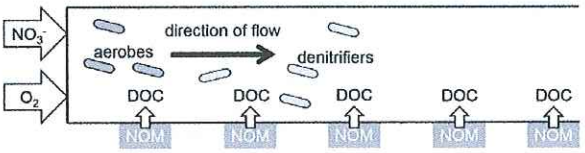

Fig. 1. Principal setup of the one-dimensional test case. NOM: natural organic matter; DOC: dissolved organic carbon.

3.3. One-dimensional test case

3.3.1. Specific setup

The purpose of the one-dimensional test case is to demonstrate the behavior of the bioreactive transport system. Fig. 1 illustrates the principal setup. The domain is made of alternating sections that release DOC and that do not. Dissolved oxygen and nitrate are introduced with the inflowing water. In the initial state, the oxygen and nitrate concentrations are zero, the concentrations of the two types of biomass are very low, and the DOC-concentration is at steady state considering DOC-release by the matrix, transport, and a zero-flux boundary condition. Table 3 contains the initial and boundary conditions of all compounds.

The length of the alternating DOC-releasing and the non-releasing sections is 0.2 m, starting with a non-reactive zone. The length of the total domain is 2 m and the cell size in the one-dimensional domain is 0.01 m. The seepage velocity is set to 1 m/d, and the dispersion coefficient to 0.01 $m^2/d = 1.167 \times 10^{-7} m^2/s$. We simulate bioreactive transport for 50 days. For comparison, a second model is set up, in which the non-reactive zones are left out.

3.3.2. Concentrations as function of space and time

Fig. 2 displays the concentrations obtained by the one-dimensional heterogeneous (left column) and homogeneous models (center column) as function of space and time. For comparison purposes, concentration values are normalized either by the inflow concentration (for dissolved oxygen and nitrate), the saturation concentration (for DOC), or the maximum biomass concentration (for both bacteria populations), respectively. Please note that the system of coordinates for the DOC-concentration, denoted "substrate", is rotated

Table 3
Initial and boundary conditions of chemical compounds.

Symbol	Meaning	Initial conc.	Inflow conc.
c_{in}^{DOC}	DOC-concentration	(*)	0 μM
$c_{in}^{O_2}$	Dissolved oxygen concentration	0 μM	250 μM
$c_{in}^{NO_3^-}$	Nitrate concentration	0 μM	100 μM
c_{in}^{tracer}	Inert tracer concentration	0 μM	100 μM
c_{im}^{aer}	Aerobic bacteria concentration	1 μM	n.a.
c_{im}^{den}	Denitrifying bacteria concentration	1 μM	n.a.

(*) Steady-state concentration distribution for the case of DOC-release without microbial activity.

about the concentration axis for better visibility. The right column of Fig. 2 shows the same concentrations as function of exposure time for the selected time points of 1 day (black), 3 days (red), 15 days (blue), and 50 days (green).

We start the discussion with the homogeneous test case (center column of Fig. 2). The initial DOC profile starts with a value of zero at the inflow boundary and then approaches exponentially the saturation concentration. The initial concentrations of the two electron acceptors are zero. At early times, dissolved oxygen and nitrate migrate into the domain. Because the initial biomass concentrations are very small, the first front of the electron acceptors behaves almost like that of a conservative tracer. The concurrent availability of DOC and oxygen triggers biomass growth of aerobic biomass, at early times throughout the domain. At that time oxygen inhibits denitrification and growth of denitrifiers. The aerobic biomass grows rather quickly and aerobic respiration leads to a decrease of the oxygen concentration with distance. Eventually, dissolved oxygen reaches a steady-state profile showing an almost linear decrease over a distance of about 0.45 m. In this zone, the aerobic bacteria reach a plateau concentration of ≈36% of the carrying capacity. The DOC also plateaus, namely to ≈12.5% of the saturation concentration. These plateaus reflect the net balance between aerobic respiration and DOC-release from the

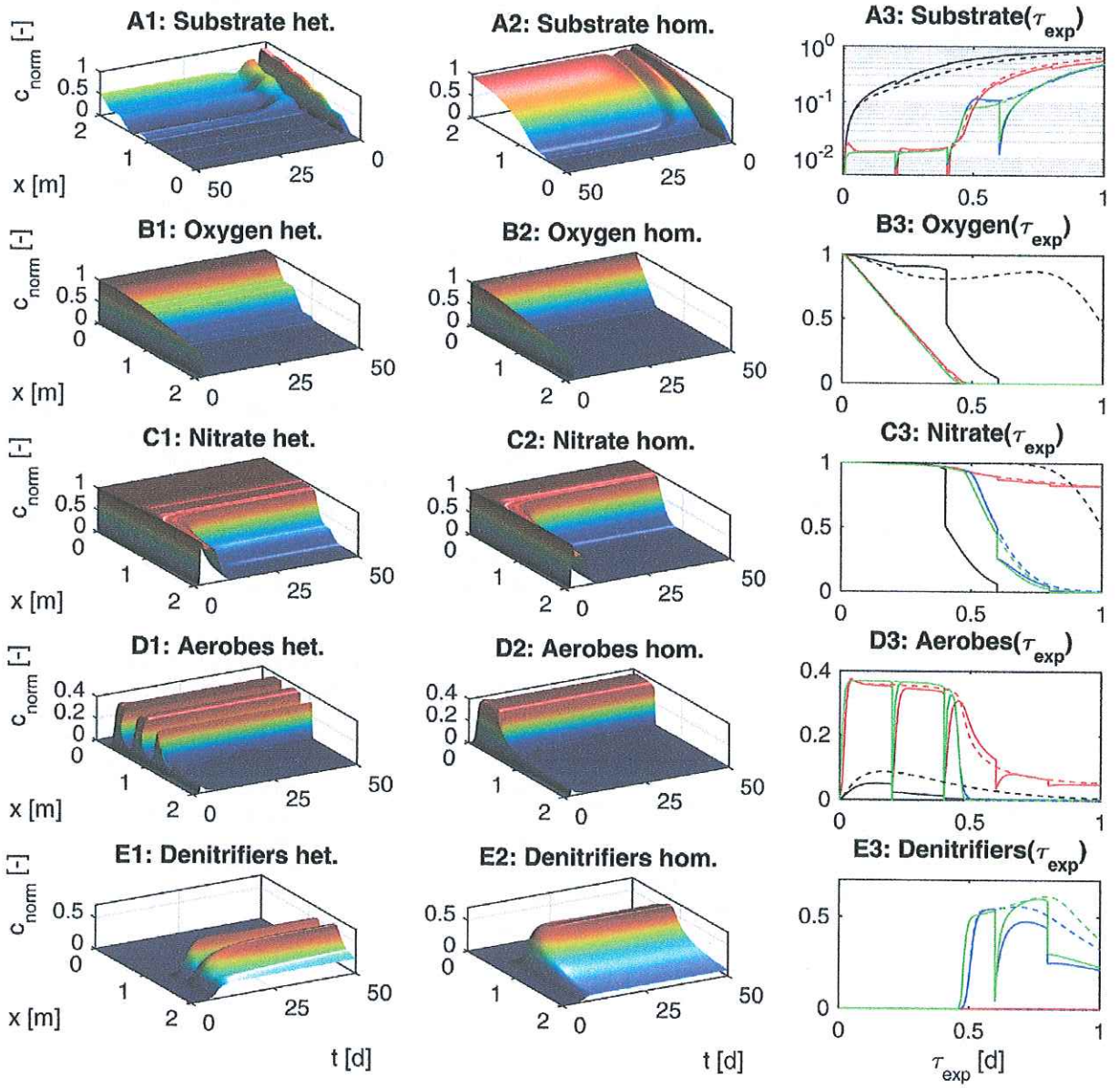

Fig. 2. Normalized concentrations of reactive species in the one-dimensional test case as function of space and time. Left column: spatio-temporal distribution for the case with alternating DOC-releasing and non-releasing sections. Center column: spatio-temporal distribution for the case with uniform DOC-release. Right column: concentration profiles as function of exposure time τ_{exp} after 1 day (black), 3 days (red), 15 days (blue), and 50 days (green) of simulation; solid lines: heterogeneous case; dashed lines: homogeneous case. In the heterogeneous case, the DOC-releasing and non-releasing zones alternate every 0.2 m. The non-releasing zones are left out in the right column. (For interpretation of the references to color in this figure legend, the reader is referred to the web version of this article.)

matrix, which could be evaluated by setting the net rates r_m^{DOC}, defined in Eq. (39), and r_{im}^{aer}, defined in Eq. (34), to zero. In a more complete model including transport of biomass, the aerobic bacteria concentration most likely would also reach a plateau value, but detachment of aerobic biomass in this zone in conjunction with attachment of these cells further downstream would lead to a less distinct lower end of the zone with high aerobic biomass.

Once oxygen has almost completely disappeared, denitrification and related growth of denitrifiers begin, eventually leading to the establishment of a new balance, namely that between DOC-release and denitrification. At steady state, the concentration of the denitrifying bacteria increases to a peak value of about 60% of the carrying capacity. Because the maximum specific reaction rate $k_{den,growth}^{max}$ of the denitrifiers is smaller than that of the aerobes $k_{aer,growth}^{max}$, the corresponding steady-state DOC-concentration is higher. Also, the Monod constant of nitrate in denitrification is considerably higher than the Monod coefficient of dissolved oxygen in aerobic respiration, leading to a dependence of the steady-state DOC-concentration on nitrate. After about 1 m, both electron acceptors are totally depleted. Without nitrate, the denitrifiers are not sustained, but their decay is also inhibited by lacking electron acceptors. Dissolved organic carbon gradually approaches its saturation concentration because of the continuous release from the matrix.

We now discuss how this pattern is changed by the alternation of DOC-releasing and non-releasing zones (left column of Fig. 2). In the initial state, the DOC-profile remains at constant values within the non-reactive zones. These steps are partially preserved after the onset of the microbial mediated reactions. The steady-state oxygen profile remains at the inflow concentration in the initial non-DOC-releasing zone, and also remains constant in the second and third ones, whereas the fourth one is beyond the penetration depth of dissolved oxygen. For nitrate, intermediate plateaus are much less obvious. The steady-state aerobic bacteria concentration in the heterogeneous domain drops to almost zero in the non-DOC-releasing zones. Without DOC-supply from the matrix and in the presence of oxygen and nitrate, the bacteria die. Directly downstream of the non-releasing zone, however, the DOC-flux originating from the "reactive" zone at steady state can sustain a remaining fraction of aerobic respiration, leading to a very slight decrease in dissolved oxygen, a consumption of DOC to about 7% of the saturation concentration, and a remaining concentration of aerobic biomass directly downstream of the DOC-releasing zone. That is, the "non-reactive" zones still permit reactions.

We have further analyzed the phenomenon of reactions in "non-reactive" zones by performing simulations with different parameter combinations (results not shown) and made the following observations:

- For model scenarios with very high (or even infinite) carrying capacity, the non-DOC-releasing zones cannot sustain aerobic biomass in the steady state. In these scenarios, the steady-state substrate concentration in the DOC-releasing zones can be computed by setting the rate of change of biomass concentration to zero. Then, the steady-state biomass concentration can be computed by considering the balance of DOC-release and consumption. Downstream of the DOC-releasing zones, the DOC value initially drops due to the presence of biomass, but it soon reaches values at which the biomass growth cannot balance its decay. At late times, this leads to a binary distribution of the aerobic biomass in the zones containing oxygen: a fairly high value in the DOC-releasing zones, and essentially zero in the non-releasing ones.
- If the carrying capacity is low, by contrast, the effective growth yield Y_{eff}^{aer} strongly depends on the actual biomass concentration c_{im}^{aer}. High biomass concentrations lead to small effective yields, which in turn leads to high steady-state DOC-concentrations. Downstream of the DOC-releasing zones, the DOC-concentration drops; however, also the biomass concentration drops, leading to a higher effective yield and thus a lower steady-state DOC-concentration.

In summary, the limitation of biomass growth in the DOC-releasing zones by factors unrelated to the electron-donor supply, leads to a higher DOC-flux entering the non-releasing zones and ultimately to the support of (low but non-zero) biomass downstream of the DOC-releasing zones. These effects are even stronger at distances where denitrification causes the DOC consumption. The DOC-flux leaving the third and fourth DOC-releasing zones at steady state is so high that significant denitrification is supported in the presumably non-reactive zones.

The third column of Fig. 2 shows the concentrations as function of the exposure time. The results for the heterogeneous test case are shown as solid lines, and those of the homogeneous case as dashed lines. These plots do not yet include the time offset proposed in the mapping of Eq. (14). The effect of the missing time offset becomes obvious for oxygen and nitrate at day one (black lines): In the homogeneous domain, the front of electron acceptors has reached larger exposure-time values than in the heterogeneous domain. At late times (blue and green profiles), the time offset does not matter because the concentrations are at steady state. When replacing space by exposure time, the agreement between the concentrations in the homogeneous (dashed lines) and heterogeneous (solid lines) at quasi-steady state (green lines) is quite good for DOC (Fig. 2A3) and excellent for dissolved oxygen (Fig. 2B3). The DOC consumption in the second and third non-DOC-releasing zone also affects the aerobic biomass in the following reactive zone (Fig. 2D3). Here, the heterogeneous model shows more or less a repetition of the pattern observed in the first reactive zone with a steady increase until the biomass concentration reaches a plateau, whereas the homogeneous model assumes a continuous plateau. For nitrogen (Fig. 2C3) the "shadow" effect of the DOC-releasing zones is the highest: There is a substantial decrease in nitrate concentrations in the fourth non-DOC-releasing zone. Interestingly, the profile of the denitrifying bacteria (Fig. 2E3) still changes from day 15 to day 50 of the simulations, leading to a closer agreement between the homogeneous and heterogeneous profiles with time.

The results of the one-dimensional test case point to a difficulty in applying the proposed exposure-time based model to the reactive system at hand: the conceptual model is based on the assumption that reactions are restricted to specific zones. The latter would be the case if the dissolved compounds would directly react with components of the immobile matrix.

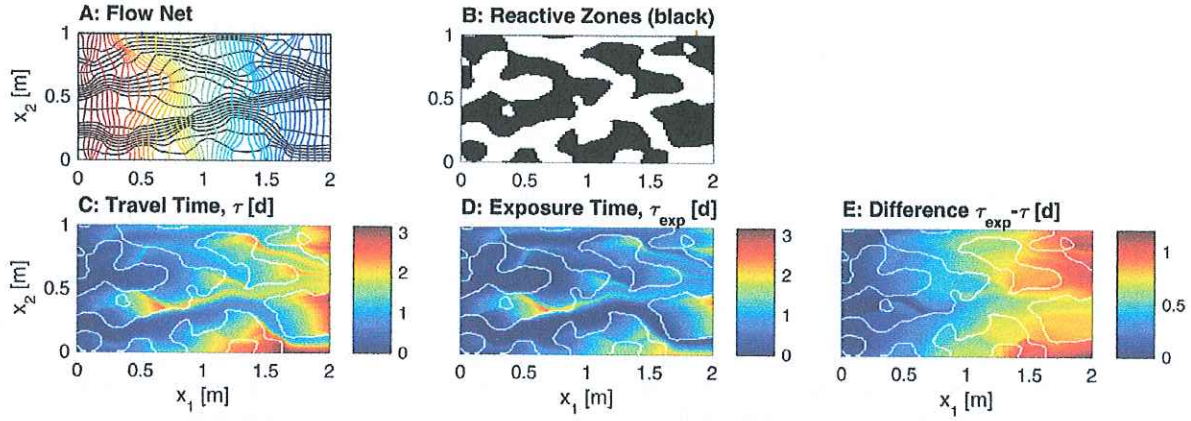

Fig. 3. A: flow net of the two-dimensional test problem (colored lines: heads; black lines: streamlines); B: spatial distribution of DOC-releasing, low-permeability aquifer materials (black) and non-DOC-releasing, high-permeability aquifer materials (white); C: spatial distribution of the mean travel time $\tau(\mathbf{x})$; D: spatial distribution of the mean exposure time $\tau_{exp}(\mathbf{x})$; E: spatial distribution of the difference between travel and exposure times. White lines in subplots C-E outline the boundaries of the reactive zones. (For interpretation of the references to color in this figure legend, the reader is referred to the web version of this article.)

In the given reactive application, however, the electron donor is released into the aqueous phase where it can react with the electron acceptors. Switching off the DOC-release eventually stalls all reactions triggered by the release, but with the chosen set of parameters, bacteria can survive directly downstream of DOC-releasing zones making the "non-reactive" zones partially reactive.

3.4. Two-dimensional test case

3.4.1. Specific setup, flow and transport model

The purpose of the two-dimensional test case is to explore the applicability and limitation of the proposed exposure-time based approach of simulating (bio)reactive transport under more realistic conditions than in the one-dimensional example. By considering physical heterogeneity, we add potential complications caused by transverse mixing. While the applicability of the approach may thus be more restricted in multi-dimensional than in one-dimensional applications, the potential benefit of the approach is also considerably higher because of the high computational effort associated with simulating multi-component reactive transport in multi-dimensional domains.

The two-dimensional domain is 2 m long and 1 m wide. The top and bottom boundaries are impermeable. The left and right boundaries of the domain are set as fixed-head boundaries, forming the inlet and outlet boundaries of the domain, respectively. The hydraulic-head difference between the in- and outlet faces is adjusted such that the mean seepage velocity is oriented from left to right with a value of 1 m/d. The distribution of the reactive and non-reactive materials is generated by defining a cut-off value for the geostatistical field of a continuous auxiliary variable. The hydraulic conductivity of the reactive inclusions is by a factor of ten smaller than that of the non-reactive matrix. Fig. 3B shows the distribution as black (reactive) and white (non-reactive) patches. Fig. 3A shows the corresponding flow net. As to be expected, flow is concentrated in the high-permeability, non-reactive parts of the domain, as indicated by the smaller distances among the streamlines.

For transport, the domain is discretized by a streamline-oriented grid of $n_{str} = 100$ stream tubes and $n_{sec} = 150$ sections (Cirpka et al., 1999). Local dispersion is calculated using the standard parameterization of Scheidegger (1961). The spatial distributions of travel times $\tau(\mathbf{x})$ and exposure times $\tau_{exp}(\mathbf{x})$ are simulated by solving the generating Eqs. (23)–(25). Conceptually, the one-dimensional exposure-time based model represents an individual stream tube, leaving out non-reactive parts of the domain. It accounts for local longitudinal dispersion equivalent to the local coefficient in the two-dimensional model, D_ℓ. The reactive system is simulated for 50 days, until reaching steady-state. Table 4 shows the values of the geometric, flow and transport parameters.

Fig. 3C depicts the spatial distribution of the mean travel time $\tau(\mathbf{x})$. The groundwater age increases over shorter

Table 4
Geometric, flow and transport parameters of the two-dimensional test case.

Symbol	Meaning	Value
Geometric parameters of the two-dimensional domain		
L	Length of the two-dimensional domain	2 m
W	Width of the two-dimensional domain	1 m
n_x	Number of cells in x-direction for flow calculation	100
n_y	Number of cells in y-direction for flow calculation	100
Δx	Cell size in x-direction for flow calculation	0.02 m
Δy	Cell size in y-direction for flow calculation	0.01 m
n_{str}	Number of stream tubes for transport	100
n_{sec}	Number of stream-tube-sections for transport	150
Discretization of exposure-time model of the one-dimensional domain		
τ_{exp}^{max}	Length of the exposure-time domain	10 d
$\Delta\tau_{exp}$	Exposure-time increment	0.01 d
Flow parameters		
K_{nrz}	Hydraulic conductivity in non-reactive zones	10^{-3}m/s
K_{rz}	Hydraulic conductivity in reactive zones	10^{-4}m/s
$\overline{q_x}$	Mean specific discharge	0.4 m/d
$\overline{v}_x$	Mean seepage velocity	1 m/d
J	Mean hydraulic gradient	$4.6 \cdot 10^{-3}$
Transport parameters		
θ	Porosity	0.4
α_ℓ	Longitudinal dispersivity (2-D)	0.01 m
α_t	Transverse dispersivity (2-D)	0.001 m
D_p	Pore diffusion coefficient	10^{-9}m^2/s

distances in zones of low velocity, which are within the reactive zones, forming a complex pattern of old- and young-water fringes. The mean travel time $\tau(\mathbf{x})$ also increases with travel distance in the non-reactive zones, but here the velocities are higher so that the increase per distance is smaller. Fig. 3D shows the distribution of the mean exposure time $\tau_{exp}(\mathbf{x})$ using the same color range as in Fig. 3C. The overall pattern is similar. However, the source-term of exposure time is zero in the non-reactive zones, leading to a deviation between $\tau(\mathbf{x})$ and $\tau_{exp}(\mathbf{x})$, depicted in Fig. 3E, that increases with travel distance. For orientation, Fig. 3C–E include the boundaries of the reactive zones as white lines.

3.4.2. Comparison between the spatially explicit and mapped results

In order to quantify the error associated with the mapping approach of Eq. (14), we perform the simulations using the spatially explicit advective-dispersive-reactive system, Eqs. (15)–(18), resulting in virtually true concentration fields $c_{2D}(\mathbf{x},t)$, and repeat the simulation in the equivalent exposure-time domain mapped to the two-dimensional domain, resulting in $c_{eq}(\tau_{exp}(\mathbf{x}),t-\tau(\mathbf{x})+\tau_{exp}(\mathbf{x}))$. The initial and boundary conditions are identical to those of the one-dimensional test case. We denote the difference between the two concentration fields as the residual error, $\varepsilon_c(\mathbf{x},t)$, to be computed for each compound. The residual errors are normalized by the inflow concentration in case of the injected electron acceptors (oxygen and nitrogen), by the maximum concentration in case of microbial biomasses (see the description of the reactive system in Section 3.2):

$$\varepsilon_c(\mathbf{x},t)=\frac{c_{2D}(\mathbf{x},t)-c_{eq}\left(\tau_{exp}(\mathbf{x}),t-\tau(\mathbf{x})+\tau_{exp}(\mathbf{x})\right)}{c_{inflow/\,max}} \tag{40}$$

We also compute residual errors of the corresponding reaction rates:

$$\varepsilon_r(\mathbf{x},t)=r(c_{2D}(\mathbf{x},t))-r\left(c_{eq}\left(\tau_{exp}(\mathbf{x}),t-\tau(\mathbf{x})+\tau_{exp}(\mathbf{x})\right)\right) \tag{41}$$

in which the mapped reaction rates $r(c_{eq}(\tau_{exp}(\mathbf{x}),t-\tau(\mathbf{x})+\tau_{exp}(\mathbf{x})))$ are set to zero in non-reactive parts of the domain. Additionally, we estimate the mean error, $ME^{(i)}$ $[ML^{-3}]$, and the root mean squared error, $RMSE^{(i)}$ $[ML^{-3}]$, of each reactive compound i in the entire domain (reactive and non-reactive

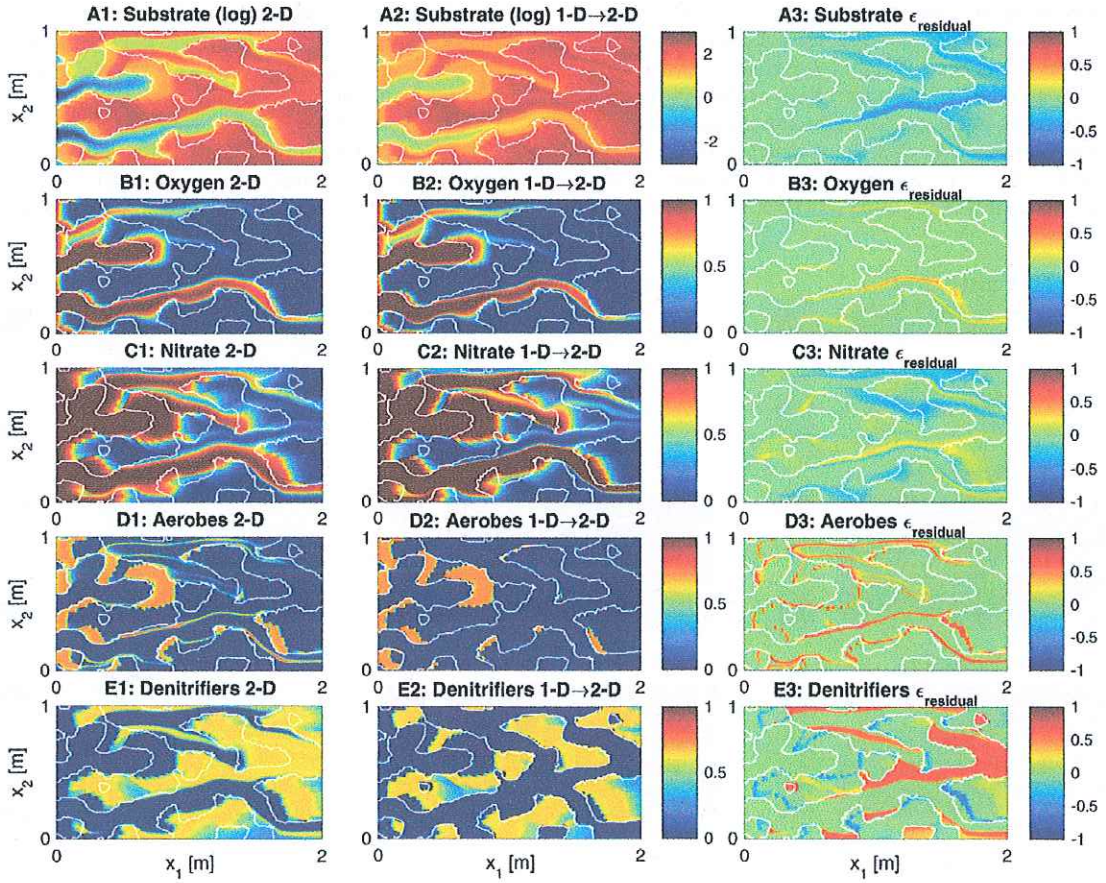

Fig. 4. Spatial distribution of the normalized concentrations of reactive-chemical compounds in the spatially-explicit two-dimensional model (left column), the exposure time one-dimensional model (center column), and their residual errors (right column) in quasi-steady state, after 50 days of simulation. The white lines indicate boundaries between the reactive and non-reactive areas. Substrate concentrations in A1 and A2 are logarithmized to the base of ten.

zones) at the end of the simulation by;

$$ME^{(i)} = \frac{\int_{\Omega} c_{2D}(\mathbf{x},t) - c_{eq}\left(\tau_{exp}(\mathbf{x}), t - \tau(\mathbf{x}) + \tau_{exp}(\mathbf{x})\right) d\mathbf{x}}{} \quad (42)$$

$$RMSE^{(i)} = \sqrt{\frac{\int_{\Omega} \left(c_{2D}(\mathbf{x},t) - c_{eq}\left(\tau_{exp}(\mathbf{x}), t - \tau(\mathbf{x}) + \tau_{exp}(\mathbf{x})\right)\right)^2 d\mathbf{x}}{LW}} \quad (43)$$

in which $\int_{\Omega} d\mathbf{x}$ denotes spatial integration over the entire domain.

3.4.3. Quasi-steady-state concentrations and reaction rates as function of space

Fig. 4 shows the spatial distributions of normalized concentrations obtained by both models and the related residual errors at the end of the simulation (50 days after start of nitrate and dissolved-oxygen injection). Note that the substrate concentrations are displayed using a logarithmic concentration-scale to improve the visualization. The left column shows the results of the spatially explicit, two-dimensional simulations, the center column shows the concentrations mapped from the exposure-time based one-dimensional model to the two-dimensional domain using the approach of Eq. (14), and the right column shows the residual errors. All concentrations are normalized as described previously. White lines in the plots outline the boundaries of the DOC-releasing zones. Note that the mapped biomass concentrations in Fig. 4D2 & E2 are set to zero in the non-reactive zones. The biomasses are the catalysts of DOC-oxidation and, to be consistent with the idea of non-reactive zones, must not exist in such zones.

To understand the patterns of concentrations in Fig. 4, one has to consider the flow net of Fig. 3A and the distribution of DOC-releasing zones shown in Fig. 4B. Without transverse dispersion, the concentration distributions within an individual stream tube would resemble the one-dimensional test case of Section 3.3: In DOC-releasing zones, the DOC-concentration remains at low values as long as dissolved oxygen is still present. Here, the oxygen concentrations are supposed to decrease approximately linear with exposure time, and the concentration of aerobic bacteria remains at a high plateau value. In reactive zones downstream of the aerobic zone, the DOC-concentration increases and denitrification sets in, leading to a decrease of nitrate concentrations and large biomass concentrations of denitrifiers. Like in the one-dimensional problem, the DOC-non-releasing zones show less remaining reactions if dissolved oxygen is still present than in the denitrifying zone.

The distribution of dissolved oxygen in the spatially resolved model shown in Fig. 4B1 follows closely the distribution of the exposure time shown in Fig. 3D, which is corroborated by an excellent agreement with the mapped concentrations plotted in Fig. 4B2. In essence, there are three fingers of oxygen-rich water penetrating deep into the domain: a very long thin finger at the bottom of the domain, a thicker finger slightly above the middle, and another thin finger at the top. These are non-reactive zones that are continuously connected to the inflow boundary so that the water has not been exposed to the DOC-releasing material at all.

Where the oxygen-rich water enters DOC-releasing zones, the DOC-concentrations remain low at first, but the concentrations of the aerobic biomass, shown in Fig. 4D1 are high. This is predicted well by the mapping approach, as can be seen in Fig.

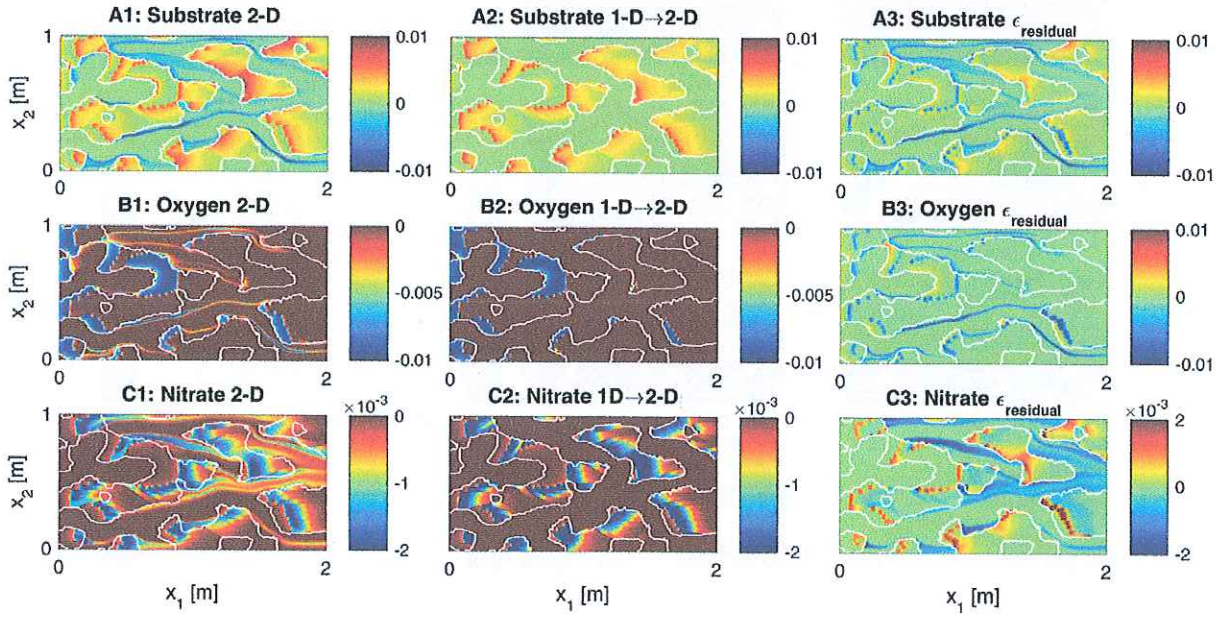

Fig. 5. Spatial distribution of the reaction rates of reactive-chemical compounds of the spatially-explicit two-dimensional model (left column), the exposure time one-dimensional model (center column), and their residual errors in % (right column) in quasi-steady state, after 50 days of simulation. The white lines indicate boundaries between the reactive and non-reactive areas.

4D2. Also, the penetration of nitrate into the areas of aerobic respiration is predicted well by the mapping approach (compare Fig. 4C1 with Fig. 4C2). As in the one-dimensional test case, the oxygen-free zones without DOC-release differ in the spatially explicit simulations (Fig. 4C1 & E1) in comparison to the mapping approach (Fig. 4C2 & E2) because of denitrifying microbial activity downstream of the DOC-releasing zones.

The third column of Fig. 3 illustrates the residual errors between the spatially explicit and the mapping approaches according to Eq. (40). Besides effects that have already been seen in the one-dimensional example, there are stripes of residual errors aligned with the direction flow. This is where old (with respect to travel and exposure time) and young groundwater flow side by side. An example is the elongated feature between $x \approx 0.65$ m, $y \approx 0.3$ m, then meandering upwards to $x \approx 1.2$ m, $y \approx 0.4$ m and coming down to $x \approx 1.6$ m, $y \approx 0.3$ m. Here, transverse exchange leads to mixing of elevated oxygen and substrate concentrations in a non-DOC-releasing zone. Such features only occur along the fringes of the above mentioned fingers.

Fig. 5 illustrates the reaction rates computed with the spatially explicit and mapped concentrations at quasi-steady state after 50 days of simulated times. The figure also include the normalized residual error according to Eq. (41) in the right column. Reaction rates within "non-reactive" zones are set to zero in the mapping results. The residual errors in the reaction rates of substrate and oxygen are dominated by the effects of transverse mixing. Because mixing facilitates the loss of both substrate and dissolved oxygen, the residual errors in the above mentioned features are negative. In contrast, the residual errors of nitrate are dominated by denitrification taking place in presumably non-reactive zones according to the mechanism already explained for the one-dimensional test case.

Table 5 lists the mean errors of all concentrations as spatially integral estimators of the bias introduced by the exposure-time concept. These values are not normalized. The observed negative values imply that the concentrations are smaller in the spatially explicit model than in the exposure-time based model. This is consistent with reactions occurring in presumably non-DOC-releasing zones that are not captured by the exposure-time based approach. Table 5 also contains the corresponding root mean squared errors.

4. Discussion and conclusions

In the present study, we have proposed a simple approach of estimating concentrations affected by multi-component reactive transport in domains subject to physical and chemical heterogeneity. The chemical heterogeneity considered is binary: there are reactive zones with identical and uniform reactive parameters, and non-reactive ones. The key point is to analyze the time that a water parcel has been exposed to reactive materials, denoted exposure time. We have proposed that concentration distributions of multiple reactive species in multi-dimensional domains can be approximated by performing simulations in one-dimensional domains omitting non-reactive zones, followed by mapping the equivalent one-dimensional results to the multi-dimensional domain using the spatial exposure-time distribution as mapping variable and accounting for the time-offset between exposure and travel time.

Table 5
Mean error (ME, μM) and root mean squared error (RMSE, μM) of the entire domain (reactive and non-reactive zone) by comparison of the multi-dimensional and the one-dimensional approaches.

Symbol	Substrate	Oxygen	Nitrate	Aerobes	Denitrifiers
ME	−25.4	−2.31	−2.96	−13.3	−9.03
RMSE	39.5	13.2	10.2	47.2	25.7

The proposed approach would be exact under the following conditions: (1) physical transport is purely advective, (2) all reactions are strictly restricted to the "reactive" zones, (3) chemical parameters of the reactive zones are uniform, (4) flow is at steady state, at least if immobile reactive species are involved. We have tested the approach under non-ideal conditions by violating the first and second conditions. Our test case involved bioreactive transport of dissolved organic carbon, released from the matrix in "reactive zones", dissolved oxygen, and nitrate, considering the microbial dynamics of aerobic and denitrifying bacteria. This application was similar to our previous studies (Sanz-Prat et al., 2015, 2016), where we also considered aerobic respiration and denitrification, but in the preceding studies all dissolved reactants had jointly been introduced into the domain.

We have applied the exposure-time concept to the case where components of the aquifer matrix act as electron donor, or source of electron donors, reducing mobile electron acceptors. The chosen example of denitrification is of high relevance to water quality in regions with intensive agriculture. However, the approach is not restricted to this scenario. In the bioremediation of petroleum hydrocarbons, the relevant mobile contaminants, such as benzene, toluene, ethybenzene, and xylene, are electron donors requiring an electron acceptor, which could be a ferric-iron bearing mineral in the matrix. Under these conditions, the exposure time would refer to the time that the water parcel was exposed to the oxidizing mineral. Conceptually more difficult to handle are systems in which redox conditions fluctuate, e.g. due to water-table fluctuations. While it may be possible to evaluate how long a water parcel has been exposed to oxic or anoxic conditions under fully transient conditions, at least if mixing is neglected, shifting of the zones complicates the spatial self-organization of the bacteria catalyzing the biogeochemical transformations.

As expected, the influence of dispersive mixing on the applicability of the proposed exposure-time based approach is similar to the one found in the previous studies using travel times: where old and young groundwater (with respect to exposure time in the given application) flows parallel to each other, transverse mixing can lead to a deviation of concentrations from what is expected by the mapping approach. If the dependence of a reactive-constituent concentration on exposure time was a strictly linear relationship, the effects of mixing would be perfectly addressed by the dispersion of exposure time included in Eq. (24). However, this is only the case for some reactants over restricted ranges of exposure time at particular times (e.g., for dissolved oxygen in steady state at early exposure times). Nonetheless, in the given example the dispersive mixing had only minor effects on the applicability of the approach. We may add that accounting for the full distribution of exposure time rather than its mean value, but

retaining the comparably simple mapping approach, would most likely not eliminate the (here small) errors introduced by mixing.

A new aspect of the current application was that not all reactions were suppressed in the non-DOC-releasing zones. Before steady-state conditions are established, substantial microbial activity can take place in "non-reactive" zones downstream of the zones, where DOC is released. This behavior could already be observed in a simple one-dimensional test case of alternating DOC-releasing and non-releasing zones. Even at steady state, DOC may be flushed into downstream "non-reactive" zones at levels sustaining biomass. This happens if biomass growth is limited by other factors than the availability of electron acceptors and donors. In our example calculation, the latter effect was of higher relevance in the parts of the aquifer where DOC was oxidized by nitrate than in the aerobic part of the aquifer. We could have constructed reactive cases where this cannot happen, e.g., because the oxidants directly react with minerals of the matrix, or because the carrying capacity is set to infinity. We believe, however, that the more complicated system behavior chosen in our example is fairly typical for many bioreactive systems.

Overall, the exposure-time based modeling approach agreed fairly well with the computationally much more expensive spatially explicit approach. Given the uncertainty of the parameters involved, we believe that computer power should be spent on uncertainty analysis of the simplified approach rather than improving the accuracy of matching the exact spatial distribution of reactants. Of course, the applicability of the approach should be tested by simple test cases, like the one-dimensional simulations presented in the current study, before addressing big-scale problems.

The simulated dynamics of the microbes was comparably simple. We have not considered the release of extracellular enzymes by the microbes to enhance the DOC-release; we have also not accounted for dormancy or transport, attachment and detachment of microbial cells. And finally, we have considered obligatory anaerobic organisms to perform the denitrification, whereas facultative anaerobic organisms may be better suited in aerobic-to-anaerobic transition zones. Reactivity was defined as an on-off process, whereas in real aquifers there may be a gradual transition between non-reactive and highly reactive zones. Temporal dynamics of the flow field were neglected. Performing fully explicit, transient simulations with the entire known complexity of the reactive system including microbial transport may always be a fall-back option. However, such simulations require many parameters, which are often highly uncertain. As a consequence, one would have to perform ensemble calculations to address the uncertainty, but the computational effort may be too high to do that. In contrast, we believe that preliminary one-dimensional simulations can be used to identify the rate-limiting processes and test conceptual simplifications. We are convinced that the supply of electron donors from the matrix is a very common rate-limiting process in aerobic respiration, denitrification, and also sulfate reduction (see the review of Wu et al., 2014, Section 4). We further believe that the microbial community adapts towards maximizing the turnover under rate-limiting conditions. After a sufficient adaptation time, details of microbial dynamics may thus become much less decisive than the electron-donor supply. Towards this end, large-scale system behavior may be simulated quite accurately with models that are even simpler than the one used here. We are in the process of deriving such simplified approaches.

Acknowledgments

This research was funded by Deutsche Forschungsgemeinschaft (DFG) in the framework of the International Research Training Group GRK 1829 "Integrated Hydrosystem Modelling" of the Universities of Tübingen, Hohenheim, and Waterloo. The authors would like to thank two anonymous reviewers and Tim Ginn for their meaningful comments helping to improve the paper.

References

Atchley, A.L., Navarre-Sitchler, K.A., Maxwell, R.M., 2014. The effects of physical and geochemical heterogeneities on hydro-geochemical transport and effective reaction rates. J. Contam. Hydrol. 165, 53–64.

Bajracharya, B.M., Lu, C., Cirpka, O., 2014. Modeling substrate-bacteria-grazer interactions coupled to substrate transport in groundwater. Water Resour. Res. 50 (5), 4149–4162.

Burr, D., Sudicky, E., Naff, R., 1994. Nonreactive and reactive solute transport in 3-dimensional heterogeneous porous media — mean displacement, plume spreading, and uncertainty. Water Resour. Res. 30 (3), 791–815.

Cirpka, O.A., 2002. Choice of dispersion coefficients in reactive transport calculations on smoothed fields. Water Resour. Res. 58 (3–4), 261–282.

Cirpka, O.A., Kitanidis, P.K., 2000a. An advective-dispersive stream tube approach for the transfer of conservative-tracer data to reactive transport. Water Resour. Res. 36 (5), 1209–1220.

Cirpka, O.A., Kitanidis, P.K., 2000b. Characterization of mixing and dilution in heterogeneous aquifers by means of local temporal moments. Water Resour. Res. 36 (5), 1221–1236.

Cirpka, O.A., Kitanidis, P.K., 2000c. Impact of biomass decay terms on the simulation of pulsed bioremediation. Ground Water 38 (2), 254–263.

Cirpka, O.A., Frind, E.O., Helmig, R., 1999. Streamline-oriented grid-generation for transport modelling in two-dimensional domains including wells. Adv. Water Resour. 22 (7), 697–710.

Cornaton, F.J., 2012. Transient water age distributions in environmental flow systems: the time-marching Laplace transform solution technique. Water Resour. Res. 48, W03524.

Crane, M.J., Blunt, M.J., 1999. Streamline-based simulation of solute transport. Water Resour. Res. 35 (10), 3061–3078.

Cunningham, J.A., Fadel, Z.J., 2007. Contaminant degradation in physically and chemically heterogeneous aquifers. J. Contam. Hydrol. 94, 293–304.

Cushman, J., Hu, B., Deng, F., 1995. Nonlocal reactive transport with physical and chemical heterogeneity — localization errors. Water Resour. Res. 31 (9), 2219–2237.

Cvetkovic, V., Dagan, G., 1996. Reactive transport and immiscible flow in geological media. 2. Applications. Proc. R. Soc. Lond. A 452 (1945), 303–328.

Cvetkovic, V., Dagan, G., Cheng, H., 1998. Contaminant transport in aquifers with spatially variable hydraulic and sorption properties. Proc. R. Soc. Lond. A Math. Phys. Sci. 454 (1976), 2173–2207.

Cvetkovic, V.D., Shapiro, A.M., Dagan, G., 1992. A solute flux approach in transport in heterogeneous formations: 2. Uncertainty analysis. Water Resour. Res. 28 (5), 1377–1388.

Dagan, G., Cvetkovic, V., 1996. Reactive transport and immiscible flow in geological media. 1. General theory. Proc. R. Soc. Lond. A 452 (1945), 285–301.

Dagan, G., Nguyen, V., 1989. A comparison of travel time and concentration approaches to modelling transport by groundwater. J. Contam. Hydrol. 4, 79–91.

Dagan, G., Cvetkovic, V.D., Shapiro, A., 1992. A solute flux approach in transport in heterogeneous formations: 1. The general framework. Water Resour. Res. 28 (5), 1369–1376.

Dentz, M., Gouze, P., Carrera, J., 2011. Effective non-local reaction kinetics for transport in physically and chemically heterogeneous media. J. Contam. Hydrol. 120-121, 222–236.

Dentz, M., Kinzelbach, H., Attinger, S., Kinzelbach, W., 2000. Temporal behavior of a solute cloud in a heterogeneous porous medium 1. Point-like injection. Water Resour. Res. 36 (12), 3591–3604.

Diem, S., Cirpka, O.A., Schirmer, M., 2013. Modeling the dynamics of oxygen consumption upon riverbank filtration by a stochastic-convective approach. J. Hydrol. 505, 352–363.

Espinoza, C., Valocchi, A.J., 1997. Stochastic analysis of one-dimensional transport of kinetically adsorbing solutes in chemically heterogeneous aquifers. Water Resour. Res. 33 (11), 2429–2445.
Fiori, A., Dagan, G., 2000. Concentration fluctuations in aquifer transport: a rigorous first-order solution and applications. J. Contam. Hydrol. 45 (1–2), 139–163.
Ginn, T.R., 1999. On the distribution of multicomponent mixtures over generalized exposure time in subsurface flow and reactive transport: foundations, and formulations for groundwater age, chemical heterogeneity, and biodegradation. Water Resour. Res. 35 (5), 1395–1407.
Ginn, T.R., 2000a. On the distribution of multicomponent mixture over generalized exposure time in subsurface flow and reactive transport: theory and formulations for residence-time-dependent sorption/desorption with memory. Water Resour. Res. 36, 2885–2893.
Ginn, T.R., 2000b. On the distribution of multicomponent mixtures over generalized exposure time in subsurface flow and reactive transport: batch and column applications involving residence-time distribution and non-Markovian reaction kinetics. Water Resour. Res. 36 (10), 2895–2903.
Ginn, T.R., 2001. Stochastic-convective transport with nonlinear reactions and mixing: finite streamtube ensemble formulation for multicomponent reaction systems with intra-streamtube dispersion. J. Contam. Hydrol. 47 (1–2), 1–28.
Ginn, T.R., 2009. Generalization of the multirate basis for time convolution to unequal forward and reverse rates and connection to reactions with memory. Water Resour. Res. 45, W12419.
Ginn, T.R., Murphy, E.M., Chilakapati, A., Seeboonruang, U., 2001. Stochastic-convective transport with nonlinear reaction and mixing: application to intermediate-scale experiments in aerobic biodegradation in saturated porous media. J. Contam. Hydrol. 48 (1–2), 121–149.
Ginn, T.R., Simmons, C.S., Wood, B.D., 1995. Stochastic-convective transport with nonlinear reaction: biodegradation with microbial growth. Water Resour. Res. 31 (11), 2689–2700.
Ginn, T.R., Wood, B.D., Nelson, K.E., Scheibe, T.D., Murphy, E.M., Clement, T.P., 2002. Processes in microbial transport in the natural subsurface. Adv. Water Resour. 25, 1017–1042.
Goode, D.J., 1996. Direct simulation of groundwater age. Water Resour. Res. 32 (2), 289–296.
Haarstrick, A., Hempel, D., Ostermann, L., Ahrens, H., Dinkler, D., 2001. Modelling of the biodegradation of organic matter in municipal landfills. Waste Manag. Res. 19, 320–331.
Harvey, C.F., Gorelick, S.M., 1995. Temporal moment-generating equations: modeling transport and mass-transfer in heterogeneous aquifers. Water Resour. Res. 31 (8), 1895–1911.
Kaluarachchi, J., Cvetkovic, V., Berglund, S., 2000. Stochastic analysis of oxygen- and nitrate-based biodegradation of hydrocarbons in aquifers. J. Contam. Hydrol. 41 (3–4), 335–365.
Mohamed, M., Hatfield, K., Hassan, A., Klammler, H., 2010. Stochastic evaluation of subsurface contaminant discharges under physical, chemical, and biological heterogeneities. Adv. Water Resour. 33, 801–812.
Molz, F., Widdowson, M., 1988. Internal inconsistencies in dispersion-dominated models that incorporate chemical and microbial kinetics. Water Resour. Res. 24 (4), 615–619.
Oldhman, C., Farrow, D., Peiffer, S., 2013. A generalized damköhler number for classifying material processing in hydrological systems. Hydrol. Earth Syst. Sci. 17, 1133–1148.
Ritzi, R., Dominic, D., Slesers, A., Reboulet, E., Telford, J., Masters, R., Klohe, C., Bogle, J., Means, B., 2000. Comparing statistical models of physical heterogeneity in buried-valley aquifers. Water Resour. Res. 36, 3179–3192.
Sanz-Prat, A., Chuanhe, L., Finkel, M., Cirpka, O.A., 2015. On the validity of travel-time based nonlinear bioreactive transport models in steady-state flow. J. Contam. Hydrol. 175-176, 26–43.
Sanz-Prat, A., Chuanhe, L., Finkel, M., Cirpka, O.A., 2016. Using travel times to simulate multi-dimensional bioreactive transport in time-periodic flows. J. Contam. Hydrol. 187, 1–17.
Scheibe, T.D., Fang, Y., Murray, C.J., Roden, E.E., Chen, J., Chien, Y.-J., Brooks, S.C., Hubbard, S.S., 2006. Transport and biogeochemical reaction of metals in a physically and chemically heterogeneous aquifer. Geosphere 2, 220–235.
Scheidegger, A.E., 1961. General theory of dispersion in porous media. J. Geophys. Res. 66 (10), 3273–3278.
Seeboonruang, U., Ginn, T.R., 2006. Upscaling heterogeneity in aquifer reactivity via exposure-time concept: forward model. J. Contam. Hydrol. 84 (3–4), 127–154.
Semprini, L., McCarty, P.L., 1991. Comparison between model simulation and field results for in-situ biorestoration of chlorinated aliphatics: Part 1. Biostimulation of methanotrophic bacteria. Ground Water 29 (3), 365–374.
Shapiro, A.M., Cvetkovic, V.D., 1988. Stochastical analysis of solute arrival time in heterogeneous porous media. Water Resour. Res. 24 (10), 1711–1718.
Simmons, C.S., 1982. A stochastic-convective transport representation of dispersion in one-dimensional porous-media systems. Water Resour. Res. 18 (4), 1193–1214.
Simmons, C.S., Ginn, T.R., Wood, B.D., 1995. Stochastic-convective transport with nonlinear reaction: mathematical framework. Water Resour. Res. 31 (11), 2675–2688.
Tufenkji, N., 2007. Modeling microbial transport in porous media: traditional approaches and recent developments. Adv. Water Resour. 30, 1455–1469.
Wu, S., Kuschk, P., Brix, H., Vymazal, J., Dong, R., 2014. Development of constructed wetlands in performance intensifications for wastewater treatment: a nitrogen and organic matter targeted review. Water Res. 57, 40–55.